

https://dspace.org/

Production of biogasoline and biojet fuel from castor oil using nano-nickel catalyst supported on carbon dots

Ntombela, Tholakele Happiness

2021
https://hdl.handle.net/10539/32964

Downloaded from a DSpace repository. https://dspace.org/

Production of biogasoline and biojet fuel from castor oil using nano-nickel catalyst supported on carbon dots.

Submitted by

Tholakele Happiness Ntombela

(1211296)

A Dissertation submitted to the Faculty of Engineering and the Built Environment, University of the Witwatersrand, Johannesburg, South Africa, in fulfilment for the degree of Master of Science.

Supervisor: Prof. Diakanua Bavon Nkazi

Co-supervisor: Dr. Manoko Maubane-Nkadimeng

Johannesburg, 2020

DECLARATION

I declare that this dissertation titled *"Production of biogasoline and biojet from castor oil using nano-nickel catalyst supported on carbon dot."* is the result of my own unaided research work, except as cited and acknowledged in the references. This dissertation has not been submitted for any degree.

Name: **Tholakele Happiness Ntombela**

Student Number: **1211296**

Signature: T.H. Ntombela …….

Date: 17/12/2020……..

DEDICATION

This work is dedicated to:

My grandmother Ms. Rose Lozizwe Shabangu

ACKNOWLEDGEMENTS

This study has been successfully completed through receiving different support from organizations and individuals. I would like to acknowledge the following individuals and organization for their contribution towards the completion of this study.

To my supervisor Prof. Diakanua Bavon Nkazi, thank you for your support and guidance that you have given me in every step of this study. Your support and commitment throughout this project has made it all possible and I am grateful. Thank you for assisting me in getting funding for this project.

To Dr. Manoko Maubane-Nkadimeng, thank you for assisting with catalyst synthesis through advising on carbon materials and different methods that can be used to synthesis my catalysts. Thank you for also helping in analysing my results and editing for my research proposal and dissertation reports.

To my grandmother Rose Shabangu, thank you for encouraging and praying for me to successfully finish this project. Thank you for always encouraging me to always go after my dreams.

I express my gratitude to Selokong Sa Dimelana (SSD) for providing with castor seeds. Thank you to Chieta and sasol for financial support for the duration of this study.

A special thanks to the following staff from the School of Chemical and Metallurgical Engineering:

- Thank you to the School of Chemical and Metallurgical Engineering workshop staff for helping with my laboratory experimental set-up. Your assistance is very much appreciated.
- Thank you to Mr. Motlatsi Phali for your assistance with GC-MS analysis, AAS analysis, and FT-IR spectrometry and for providing with lab equipment.

- Thank you to Mrs. Janet Smith for assisting with TGA, providing with lab equipment, and also for advising on which people I should talk to for analysing my samples.
- Thank you to Mrs. Petra Dinham for helping with SEM analysis.
- Thank you to Ms. Swathi Burla for helping with XRD analysis.

Thank you to the following staff from the faculty of Sciences (Schools of Chemistry, Microbiology and Physics):

- The Microscopy and Microanalysis Unit (MMU) staff for helping with TEM analysis training.
- Prof. N.J. Coville for helping with BET characterisation.
- Mr. Orlette Mkhari for assisting with preparation of C dots and giving me ideas on how to prepare my catalyst.
- Mr. Eric Morifi for assisting with GC-MS analysis.

ABSTRACT

Bio-energy resources become more interesting as alternative to produce energy and can attract investors depending on their availability as feedstock, production cost and sustainability of conversion of biomass into biofuels. This study addressed the challenges raised by the heavy reliance on petroleum fuel in South Africa, which has resulted to the crisis of energy security, greenhouse gas emissions, and heavy foreign exchange spent on imported oil. This study focuses on the production of biojet and biogasoline fuel from castor oil using hydrocracking process on a nano-nickel catalyst supported on carbon dots (C dots).

Castor oil was extracted from castor seeds obtained from Selokong Sa Dimelang (SSD) plantation using solvent extraction. The castor oil extraction parameters were optimised using RSM by varying extraction temperature, extraction time, and seed/solvent ratio to obtain maximum oil that can be extracted. The maximum oil yield obtained from SSD castor seeds was 44.8 wt. % at optimal extraction parameters of 63.3^{o}C, 3.6 h, and 0.03 g/ml of extraction temperature, extraction time and seed/solvent ratio, respectively. The compounds identified by GC/MS in the extracted oil were oleic acid, palmitic acid, undercylenic acid, methyl ricinoleate, behenic acid,tridecylenic acid and 13-hexyloxacyclotridec-10-en-2-one. The acid value, saponification value, iodine value, specific gravity, viscosity of the castor oil were determined to be 1.22, 178, 85, 0.952, and 6.6 respectively, and were found to be within ASTM standard specification values.

Different Ni/C dots catalysts were synthesized with varying Ni-loadings from 5 wt. % to 25 wt. % and calcination temperatures from 350°C to 750°C. The catalysts were characterised using AAS, TGA, BET, SEM, TEM, XRD, and FT-IR spectroscopy. 5 wt. % Ni-loading catalyst calcined at 350^{o}C showed highest thermal stability, highest BET surface area of 71.69 m^2/g, and the particles were less agglomerated compared to the catalyst produced with different Ni-loadings and calcination temperatures.

The effect of Ni-loading, calcination temperature, extraction time extraction temperature, and catalyst/oil ratio on the production of biojet and biogasoline fuel was studied. The maximum production yield of biojet was obtained to be 56 wt. % at 5 wt. % Ni-loading catalyst calcined at 350^{o}C, reaction temperature of 250^{o}C, reaction time of 1.5 h, and catalyst/oil ratio of 0.005 g/ml and the maximum production yield of biogasoline was obtained to be 36 wt. % at 5wt. % Ni-loading catalyst calcined 350^{o}C, reaction time of 350^{o}C, reaction time of 1.5 h, and catalyst/

oil ratio of 0.003 g/ml. The overall order of the reaction for the biojet and biogasoline production was investigated according to 0 to 4^{th} order and but did not fit to any reaction order for the forward reaction. Then reverse process yield of biofuel reduced was assumed. Second order rate plots best fitted both biojet and biogasoline production for the reverse reaction. The rate constant (k) was obtained from the slope of the plots. The rate constants for biojet production from 0.5-1.5 h and 1.5-2.5 h were 0.0326 and 0.007, respectively. The rate constants for biogasoline production from 0.5-1.5 h and 1.5-2.5 h were 0.0294 and 0.0206, respectively. RSM from Design Expert version 11.0.4 software was used to determine the optimum process conditions for the hydrocracking of castor oil. The optimal reaction temperature, reaction time, and catalyst/oil ratio were 350^{o}C, 1.5 h, and 0.002 g/ml and produced the maximum production of 50.51 wt. % and 33.57 wt. % of biojet and biogasoline fuel, respectively.

Table of Contents

DECLARATION ..... **ii**
DEDICATION ..... **iii**
ACKNOWLEDGEMENTS ..... **iv**
ABSTRACT ..... **vi**
List of figures and tables ..... **xi**
List of figures xi
List of tables xiii
NOMENCLATURE ..... **xiv**
Chapter 1: Research background **1**
1.1. Introduction 1
1.2. Problem statement 2
1.3. Aims and objectives 3
1.4. References 4
Chapter 2: Literature review **5**
2.1. Sources of biofuel 5
2.1.1. Sugar-containing plant crops 7
2.1.2. Starch crops 8
2.1.3. Oil seeds 8
2.2. Castor oil as the biofuel feedstock 11
2.2.1. Castor seeds pre-treatment 12
2.2.2. Castor oil extraction 14
2.2.4. Castor oil refining 19
2.3. Comparison of production routes 20
2.3.1. Catalytic hydroprocessing 20
2.3.2. Transesterification 26
2.3.3. Pyrolysis 32
2.3.4 Method selection 35
2.4. Catalyst selection 37
2.4.1. Nickel-based catalysts 38
2.4.2. Carbon materials as catalyst supports 39
2.5. Biofuel products from castor oil 40
2.5.1. Biodiesel 40
2.5.2. Biogasoline 40
2.5.3. Biojet 41

2.7. References 43
Chapter 3: Castor oil extraction 52
3.1. Introduction 52
3.2. Materials and methods 54
3.2.1. Castor cake formation method 54
3.2.2. Moisture content determination 54
3.2.3. Soxhlet extraction 55
3.2.4. Response surface methodology (RSM) 55
3.2.5. Castor oil characterization 56
3.3. Results and discussion 58
3.3.1. Moisture content determination. 58
3.3.2. Effects of operating conditions on the oil yield. 59
3.3.3. Experimental layout from RSM 60
3.3.4. Analysis of variance for the extraction of castor oil 62
3.3.5. Optimization of processing parameters for maximum oil yield 66
3.3.6. Characterization of castor oil produced 67
3.3.7. Conclusion 70
3.4. References 71
Chapter 4: Catalyst synthesis 73
4.1. Introduction 73
4.2. Materials and methods 74
4.2.1. Preparation of C dots 74
4.2.2. Synthesis of Ni/C dots catalyst 75
4.3. Catalyst characterisation techniques 76
4.3.1. Thermogravimetric analysis (TGA) 76
4.3.2. Brunauer-Emmet-Teller (BET) 76
4.3.3. X-Ray Diffraction (XRD) 76
4.3.4. Fourier Transform Infrared (FTIR) Spectrometry 76
4.3.5. Scanning Electron Microscopy (SEM) 77
4.3.6. Atomic absorption spectroscopy (AAS) 77
4.4. Results and discussion 77
4.4.1. C dots characterisation 77
4.4.2 Actual Ni-loading determination 79
4.4.3 Effect of Ni-loading on the Ni/C dots catalyst 79
4.4.4. Effect of calcination temperatures on the Ni/C dots 86

4.5. Conclusion 91
4.5. Refferences 93
Chapter 5: Hydrocracking process 95
5.1. Introduction 95
5.2. Materials and methods 95
5.3. Results and discussion 96
5.3.1. Effect of Ni-loading and calcination temperature on the production yield 97
5.3.2. Effect of reaction temperature, reaction time, and catalyst/oil ratio on the production yield 98
5.3.3. Reaction kinetics 100
5.3.4. Response surface methodology 104
5.3.4. Product characterisation 111
5.4. References 112
Chapter 6: Conclusions and recommendations 114
6.1. Conclusions 114
6.2. Recommendations 115
Appendices 117
Appendix A: Castor oil extraction 117
A.1: Effect of operating conditions on the oil yield 117
A.2: GC-MS analysis of extracted castor oil 118
Appendix B: Catalyst synthesis 120
Appendix C: Hydrocracking process 120
C.1: ANOVA analysis 120
C.2: GC-MS analysis for hydrocracked product 122

List of figures and tables

List of figures

Figure 2. 1. Leading countries based on the biofuel production in 2018 (in thousand metric tons of oil equivalent). 5
Figure 2. 2. An overview of biofuel production technology and their feedstocks. 7
Figure 2. 3. Block flow diagram of castor oil extraction. 12
Figure 2. 4. Continuous screw press. 15
Figure 2. 5. Filter press 18
Figure 2. 6. Oil refining process. 19
Figure 2. 7. Possible pathways during HDO process of triglycerides. 23
Figure 2. 8. Reactions occurring during hydrocracking. 25
Figure 2. 9. (a) Transesterification of triglyceride using methanol, (b) transesterification stages of triglycerides. 27
Figure 2. 10. Acid-catalysed transesterification mechanism of vegetable oil. 29
Figure 2. 11. The base-catalysed transesterification mechanism of vegetable oils. 30
Figure 2. 12. Reaction mechanism of triglycerides for thermal cracking 33
Figure 2.13. (a) Hydrocracking and hydrogenation products yields (%) of POM catalysts: $K_3PW_{12}O_{40}$, $K_4SiW_{12}O_{40}$, Co-POM and Ni-POM and (b) Yields (%) of hydrocracking products and hydrogenation products for 9.1 % Ni-POM supported over different supports: γ-Al_2O_3, TiO_2, SiO_2, and active C. 38
Figure 3. 1. Effect of (a) temperature (b) seed/solvent ratio, and (c) time on the oil yield from different authors 53
Figure 3. 2. Process flow of castor cake formation. 54
Figure 3. 3. Soxhlet extraction. 55
Figure 3. 4. Effect of extraction (a) temperature, (b) time, and (c) seed/solvent ratio on the oil yield. 60
Figure 3. 5. Comparison of the actual oil yield with the predicted oil yield. 64
Figure 3. 6. The 3D surface plot showing the effect of extraction temperature and seed/solvent ratio on the oil yield. 65
Figure 3. 7. 3D surface plot showing the effect of the seed/solvent ratio and extraction time on the oil yield. 65
Figure 3. 8. 3D surface plot showing the effect of extraction time and extraction temperature on the oil yield. 66
Figure 3. 9. Typical GC-MS total ionic chromatogram (TIC) of Castor oil. 67
Figure 3. 10. FTIR analysis of castor oil produced 69
Figure 4. 1. Preparation of Cdots. 74
Figure 4. 2. Synthesis of Ni/Cdots. 75
Figure 4. 3. (a) TEM image of synthesized Cdots, (b) FT-IR spectrometry of Cdots, (c) TGA plot of Cdots 78
Figure 4. 4. TGA plot of the Ni/Cdots catalyst at different Ni-loading. 80
Figure 4. 5. SEM images for Ni/Cdots catalyst at different Ni-loading. 83

Figure 4. 6. TEM images for Ni/Cdots catalyst at different nickel loading.....84
Figure 4. 7. FT-IR Spectrometry for Ni/Cdots catalyst at different catalyst loading 85
Figure 4. 8. XRD spectrum of Ni/Cdots at different Ni-loading 86
Figure 4. 9. TGA plot of Ni/Cdots catalyst at different calcination temperatures.....87
Figure 4. 10. TEM images of Ni/Cdots catalyst at different calcination temperature. 90
Figure 4. 11. FTIR spectra of Ni/Cdots catalyst at different catalyst loading. 90
Figure 4. 12. XRD spectra of Ni/Cdots catalyst at different calcination temperatures.....91

Figure 5. 1. Hydrocracking experimental setup.....96
Figure 5. 2. (a) Effect of Ni-loading on the production of bi-jet and biogasoline, and (b) Effect of calcination temperature on the production of biojet and biogasoline.....97
Figure 5. 3. (a) Effect of time on the production yield, (b) effect of catalyst/ratio on the production yield, and (d) effect of temperature on the production yield. 98
Figure 5. 4. Second order plots for the hydrocracking of castor oil. 103
Figure 5. 5. 1/Temperature versus ln(1/time) graph plots.....104
Figure 5. 6. (a) Actual production yield versus predicted production yield of biojet and (b) Actual production yield versus predicted production yield of biogasoline. 106
Figure 5. 7. 3D surface plot for (a) effect of reaction time and temperature on the biojet production yield, (b) effect of catalyst/oil ratio and reaction time on the biojet production yield, and (c) effect of catalyst/oil ratio and reaction temperature on the biojet production yield. .108
Figure 5. 8. 3D surface plot for (d) Effect of reaction time and temperature on the biogasoline production yield, (e) effect of catalyst/oil ratio and reaction temperature on the biogasoline production yield, and (f) effect of catalyst/oil ratio and reaction time on the biogasoline production yield. 108
Figure 5. 9. The optimal reaction condition for biojet and biogasoline production. 110
Figure 5. 10. Total Ion Chromatograph (TIC) for hydrocracked product.....111
Figure A. 1. GC-MS analysis spectra for the extracted castor oil. 118

List of tables

Table 2. 1. Edible and non-edible oils with their oil content. 9
Table 2. 2. Fatty acids composition of different edible oils 10
Table 2. 3. Fatty acids composition of different edible oils 11
Table 2. 4. Physicochemical characteristics of castor oil extracted from untreated and pre-treated castor seeds. 13
Table 2. 5. Physicochemical properties of castor oil obtained from mechanical pressing. 16
Table 2. 6. Physicochemical characteristics of castor oil from different oil extraction method 16
Table 2. 7. Physicochemical characteristics of oil extracted at different types solvent 18
Table 2. 8. Physicochemical characteristics of crude and refined castor oil 20
Table 2.9. Physiochemical properties of biodiesel international standards and biodiesel obtained from castor oil 40
Table 2. 10. Properties of gasoline fuel 41
Table 2. 11. Properties of Jet A, Jet A-1, Jet B, and TS-1. 42

Table 3. 1. Summary of experimental design. 56
Table 3. 2. Moisture content determination. 59
Table 3. 3. Experimental design layout using RSM. 61
Table 3. 4. Analysis of Variance (ANOVA) for extraction of castor oil from castor seeds. 62
Table 3. 5. The ANOVA results for response models. 63
Table 3. 6. Major fatty acids derived from castor oil 68
Table 3. 7. Physiochemical characteristics of castor oil. 69
Table 4. 1. AAS analysis of the catalyst at different loadings. 79
Table 4. 2. The pore size, surface area, pore volume of the Ni/Cdots catalyst at different Ni-loadings. 81
Table 4. 3. The pore size, surface area, pore volume of the Ni/Cdots catalyst at different calcination temperatures. 88
Table 5. 1. Comparison of biojet and biogasoline production yield from different researchers. 100
Table 5. 2. Biojet reaction orders 101
Table 5. 3 Biogasoline reaction orders 102
Table 5. 4. Summary of experimental design. 105
Table 5. 5. Experimental design layout. 105
Table A. 1. Effect of extraction temperature on the oil yield. 117
Table A. 2. Effect of extraction time on the oil yield. 117
Table A. 3. Effect of seed/solvent ratio on the oil yield. 117
Table A. 4. Full results data obtained from GC-MS analysis. 118
Table B. 1. Raw data from AAS analysis 120
Table C. 1. ANOVA analysis table for Biojet production 120
Table C. 2. ANOVA analysis table for Biogasoline production 121
Table C. 3. GC-MS results table for hydrocracked products 122

NOMENCLATURE

AAS:	Atomic Absorption Spectrometry
ANOVA:	Analysis Of Variance
ASTM:	American Society for Testing and Materials
BET:	Brunauer-Emmet-Teller
C dots:	Carbon dots
CHMT:	School of Chemical and Metallurgical Engineering
CO:	Carbon monoxide
CO_2:	Carbon dioxide
EU:	European Union
FAME:	Fatty Acid Methyl Ester
FFA:	Free Fatty Acid
FTIR:	Fourier Transform Infrared
GC-MS:	Gas Chromotography Mass Spectrometry
H_2:	Hydrogen gas
HDM:	Hydrodemetallization
HDN:	Hydronitrogenation
HDO:	Hydrodeoxygenation
HDS:	Hydrodesulphurization
H_2O:	Water
IEA:	International Energy Agency
LHV:	Low Heating Value
MW:	Molecular Weight

$NaBH_4$:	Sodium borohydride
Ni:	Nickel
$NiCl_2$:	Nickel Chloride
POM:	Polyoxometalate
ROM:	Research Octane Number
RSM:	Response Surface Methodology
RT:	Retention time
SDS:	Safety Data Sheets
SEM:	Scanning Electron Spectrometry
SSD:	Selokong Sa Dimelang
TEM:	Transmissiom Electron Microscopy
TGA:	Thermogravimetric Analysis
TIC:	Total Ion Chromotograpgh
US:	United States
Wt. %:	Weight Percentage
XRD:	X-ray Diffraction

Chapter 1: Research background

1.1. Introduction

The demand of clean energy from bioresources has been continuously increasing for the past decades due to the increasing population worldwide, which requires continuous supply of energy to support human activities such as agriculture, transportation, and industrialisation. Biofuels has been considered as a possible clean energy that can be used worldwide as the substitute for fossil fuels or petroleum-derived transportation fuels to help address the problem of global warming, energy cost and energy security associated with fossil fuels (Owusu and Asumadu-Sarkodie, 2016). Several studies that have been conducted in African countries suggested that African countries have the potential of producing biofuels for international and domestic use (Owusu and Asumadu-Sarkodie, 2016). South Africa has also shifted to biofuel development, in December 2006 the biofuel industrial strategy was approved and the drafted strategy was developed by the biofuels task team appointed by the cabinet in December 2005 (Department of Minerals and Energy, 2007). The biofuel industrial strategy aims at increasing the production of biofuels by using non-edible crops such as sugar cane, canola, and jastropha which will help in job creation in the energy-crop and biofuels value chain.

The production of biofuels has been increasing globally reaching 153 billion litres in 2018 (REN21, 2019). Brazil and the United States dominated the production with 69 % biofuel production combined of all the biofuels produced 2018 worldwide (REN21, 2019). Brazil and the US were followed by China 3.4 %, Germany 2.9 %, and Indonesia 2.7 % (REN21, 2019). The main biofuels produced are ethanol from sugar canes and biodiesel from fatty acid methyl esters.

The consumption of biofuels has been increasing worldwide. The sustainable development scenario (SDS) aim in tripling biofuel consumption by 2030 from 2017 (IEA. 2019). However, the production of biofuels is not growing fast enough to meet the targeted demand. Only 2.5 % annual growth is estimated over the next five years (IEA, 2019). To meet the SDS target, biofuel demand need to strongly increase from the current market. Other countries have shown the biggest acceleration of biofuel demand such as India, Latin America and China (IEA.2019). In other countries such as Mexico and South Africa the production of biofuels is still in the early stages, hence significant technology shift and market development is required (IEA, 2019).

In South Africa, researchers have been investigating different feedstocks that have potential in producing biofuels. These feedstocks includes edible oils such as vegetable oil and non-edible oils such as castor oil and waste edible oils. Edible oils has been eliminated as the possible feedstock for food security and more focus has been shifted to non-edible oils and waste edible oils since these type of oils does not compete with food security (Gui, Lee and Bhatia, 2008). This project focuses on the production of biofuel from castor oil, which is non-edible oil. Castor oil is also considered the feedstock that can be used for producing biofuel because it does not compete with the food security regulations since they are known to be poisonous as they contain ricin. Castor seeds could be a possible solution in South Africa since it can be produced locally at a larger scale and contains high oil content of about 50-60 % (Patel et al., 2016).

Various researchers have studied different methods of processing castor oil into biofuels. More work has been done on the production of biodiesel from castor oil. This project shift the focus into maximising the production of biojet and biogasoline from castor oil. Biojet and biogasoline are used for running aircraft and conventional gasoline engines, respectively. These biofuels are obtained through hydrocracking of oil into a blend short of chain of hydrocarbons. The hydrocracking process is performed in the presence of catalyst for high production yield. In this project, nano-nickel catalyst was synthesized on carbon dots as catalyst support, and the hydrocracking process was investigated by varying the operating conditions such as catalyst loading, size and calcination temperatures.

1.2. Problem statement

According to a report by the International Energy Agency (IEA), South Africa is the largest consumer of energy in Africa (IEA, 2019), with transport as the large energy sector covering about one quarter of South African energy consumption (IEA, 2019). South Africa is also classified as the world's 14th largest emitter of greenhouse gases this is because of the heavy reliance on coal (Carbon Brief, 2018). South Africa currently rely on the foreign supply of liquid fuel energy in the form of crude oil. The ZAR/USD exchange rate has been increasing for the past decades, which resulted to the increase in fuel prices (Rangasamy, 2017).

South Africa requires alternative sources that can be used to solve the crisis of energy security, greenhouse gases emissions, and heavy foreign exchange spent on imported oil. Development of biofuels has the potential on reducing South Africa's dependence on fossil fuels, imported fuels and reduce greenhouse gases emissions. The development of biofuels in South Africa will

also help in boosting rural and economic development and uplift agricultural sector and its markets (Department of Minerals and Energy, 2007).

Due to the shift in moving to biofuels as an energy source, it is very important to consider the types of biofuels required to drive the current engines available and the importance of increasing the production yield based on the demand. Biojet fuel plays a very important role in aviation fuel sector through producing fewer carbon emissions than the regular aviation fuel (Bosch *et al*., 2017). The emissions is said to be reduced by 20 % to 95 % when compared with petroleum-derived jet fuel, although the extent of reductions are still subject of much debate (Han, Elgowainy, Cai and Wang, 2013). The constant supply and production of biojet fuel will help in solving equitable economy, environmental support, and energy supply, which are the major three problems in South Africa (Winkler, 2007). The success of this project will be beneficial to South Africa since it holds the international aviation hub of O.R. Tambo and South Africa could become the clean energy market leader for Africa. Biogasoline is considered the potential renewable fuel that can be used in running spark engines (Zhao, 2010). Biogasoline can be used as the substitute for conventional crude oil based gasoline without changing the existing engines (Zhao, 2010).For continuous supply of these fuels, it is very important to investigate different factors that affect the production of these fuels.

1.3. Aims and objectives

The aims of this project are to develop nano-nickel catalyst supported on C dots and to optimize the production of biojet and biogasoline fuels from castor seed. To meet the aims of this project, the following objectives was investigated:

a) To optimize the castor oil extraction process from castor seeds using the statistical optimization tool, mechanical and solvent extraction;

b) To synthesis C dots using hydrothermal carbonization of chitosan;

c) To synthesize and study the properties of nano-nickel catalyst supported on C dots;

d) To investigate the effect of catalyst sizes, calcination temperatures, and loading amounts on the biojet and biogasoline fuels production from the extracted castor oil using hydrocracking reactor;

e) To optimize the hydrocracking process using statistical tools.

1.4. References

Bosch J., Joeng S., Hoefnagel R., Slade R., 2017. Aviation biofuels: strategically important, technically achievable, tough to deliver. *Grantham Institute Briefing paper No 23*.

Carbon Brief, 2018. The Carbon Brief Profile: South Africa. *Country Profiles*.

Department of Minerals and Energy, 2007. Biofuels Industrial Strategy of the Republic of South Africa. *Biofuels Industrial Strategy*.

Gui M., Lee K. and Bhatia S., 2008. Feasibility of edible oil vs. non-edible oil vs. waste edible oil as biodiesel feedstock. *Energy*, 33(11), pp.1646-1653.

Han, J., Elgowainy, A., Cai, H. and Wang, M., 2013. Life-cycle analysis of bio-based aviation fuels. *Bioresource Technology*, 150, pp.447-456.

IEA, 2019. South Africa Energy Outlook. *Analysis from Africa Energy Outlook 2019.*

IEA, 2019. Tracking Transport 2019.*Transport biofuels*.

Owusu, P. and Asumadu-Sarkodie, S., 2016. A review of renewable energy sources, sustainability issues and climate change mitigation. *Cogent Engineering*, 3(1).

Patel V., Dumancas G., Viswanath L., Maples R., and Subong B., 2016. Castor Oil: Properties, Uses, and Optimization of Processing Parameters in Commercial Production. *Lipid Insights*, 9, p.40-233.

Rangasamy L., 2017. The impact of petrol price movements on South African inflation. *Journal of Energy in Southern Africa*, 28(1), p.120-135.

REN21 2019.Markets and Industry Trends. *Renewables 2019 Global Status Report.*

Winkler H., 2007. Energy policies for sustainable development in South Africa. *Energy for Sustainable Development*, 11(1), pp.26-34.

Zhao, H. and Yang, C., 2010. In-cylinder studies of hybrid combustion in a direct injection single-cylinder optical engine. *International Journal of Engine Research*, 11(6), pp.515-531.

Chapter 2: Literature review

This chapter looks into the literature review associated with the production of biofuels from different possible feedstocks using different catalysts. A review study is conducted on the previous work done by researchers on the similar project. This review mainly focuses on the biofuel production, different methods used for the productions of fuels, possible types of feedstocks, and different types of catalysts than can be used. The aim of this chapter is to find the best possible method that can be used to maximise the production of biogasoline and biojet from castor oil.

2.1. Sources of biofuel

Biofuels are referred as the liquid or gaseous fuels mainly produced from biomass. The main biomass sources can be obtained from energy or agricultural crops, residues from agriculture, industries, forestry, and animal, sewage, and algae (EIA, 2018). The world contains large amount of biomass ranging from the land to oceans. Several reports estimated that the world's total biomass land reserves about 1.8 trillion tons and biomass aquatic reserves about 4 billion tons (Tursi, 2019). The total amount of biomass has the potential of producing 33, 000 EJ of world's energy; equivalent to more than 80 times of world's annual energy consumption. However, the use of these biomass sources does not show a uniform distribution around the world (Wang, 2019).

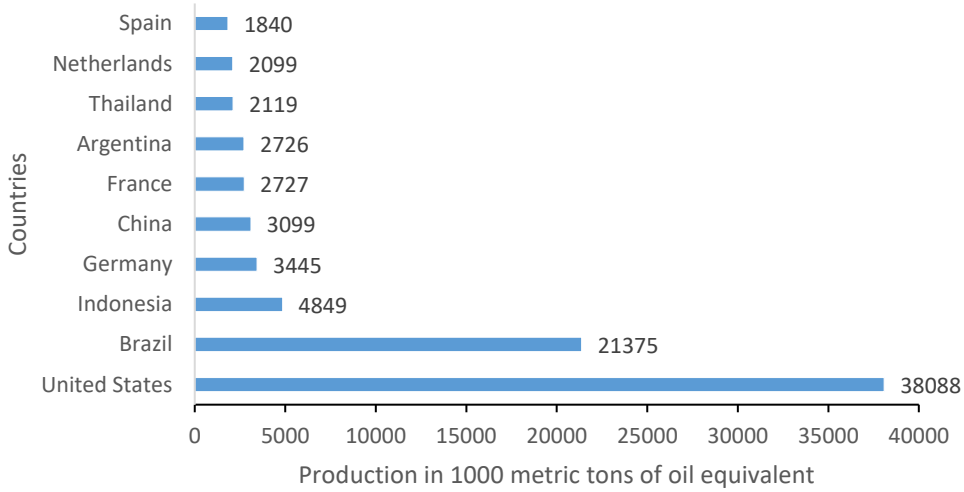


Figure 2. 1. Leading countries based on the biofuel production in 2018 (in thousand metric tons of oil equivalent) (Wang, 2019).

Based on EIA reports in 2018, United States was the leading biofuel producer in 2018; they produced about 39.9 percent of the global biofuel production (Wang, 2019). The total biomass consumption in the United States was 5196 trillion BTU in 2018(Wang, 2019). United States is followed by Brazil with the biofuel production of 22.4 million metric tons of oil equivalent (Wang, 2019). In the developing countries, the production of biofuels is still low and increasing very slow and while in developed countries the production is high and increasing very fast.

Due to the large variety of biomass sources, these sources are grouped differently based on their purpose and scope. The classifications are based on the types of biomass existing in nature and the use and application of biomass as feedstock. The different biomass groups: (1) Herbaceous biomass, (2) Aquatic biomass, (3) Wood and woody biomass, (4) Biomass mixtures, and (5) Animal and human waste biomass (Tursi, 2019).

Herbaceous biomass are obtained from plants that do not have woody stem and at the end of the growing season, they die (Tursi, 2019). These includes seeds or grains crops, and by products such as cereal straws. Aquatic biomass is considered the best possible feedstock that can be used for biofuel production since it does not compete with food crops (Tursi, 2019). Aquatic biomass can be obtained in large amounts compared to land crops. Wood and woody biomass consist of mainly lignin and carbohydrates (Tursi, 2019). They are generally materials such as roots residues, stems, or leaves of woody shrubs. Animal and human waste biomass are usually obtained from bones, human dug, meat meals, and different types of animal manure. This biomass has led into proper waste management in terms of health, pollution, and odor concerns (Tursi, 2019). Biomass mixtures belongs to the biomass groups named above in the mixed form.

The biomass sources can be converted to different energy carriers through treatment and conversion processes. The choice of production process is mainly determined by the end products, cost of the process, and the quality and quantity of biomass. Figure 2.2 shows the production routes of different biofuels from different feedstocks.

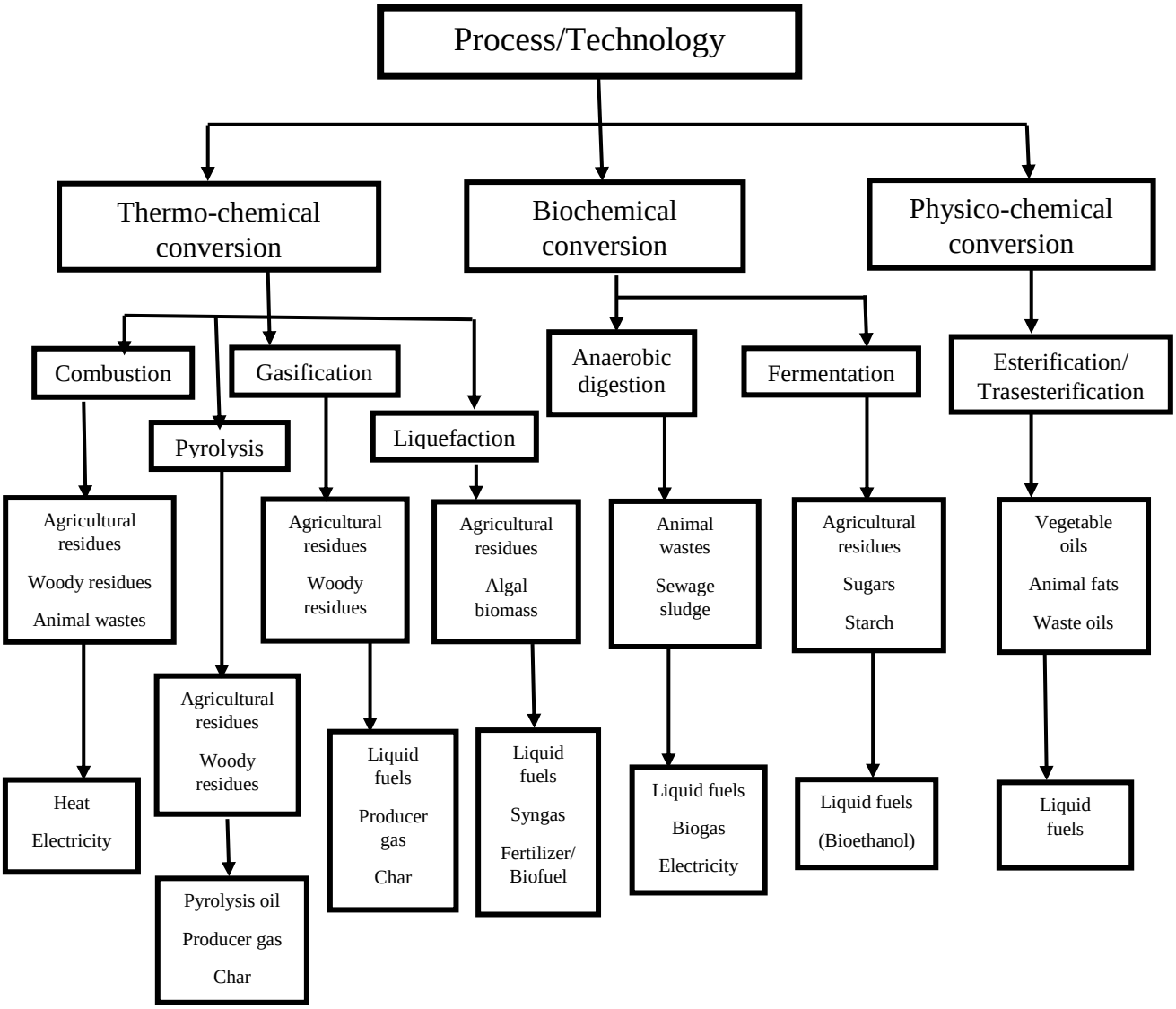


Figure 2. 2. An overview of biofuel production technology and their feedstocks (Tursi, 2019).

2.1.1. Sugar-containing plant crops

The sugar-containing plant crops include sugarcane, sugar beet, and sweet sorghum. Sugarcane has been mainly used to produce ethanol (Hinková and Bubník, 2013). It contains high concentration of sugar, which can be easily fermented to produce ethanol. The sugar stalks generally contains 10-17 % sugar, 65-75 % water, and 8-14 % ashes (Soccol *et al.*, 2016). The Sugar bagasse, which is the by-product, can be used by sugar mills to generate electricity and steam (Soccol *et al.*, 2016). The main producer of sugarcane is Brazil with about 27 % global production (Bordonal et al., 2018). Sugar beet (*B. vulgaris*) is originally from Europe and can be used for the production of ethanol. Sugar beets contains about 18 % sugar, 75 % water, and 7 % of soluble and insoluble materials (Bordonal et al., 2018). Because of the high sugar

content, they are considered for ethanol production. Sugar beets contains sugar in the form of sucrose and can be harmful to health when consumed in excess. The theoretical ethanol yield for sugar beets is 24.8-26.9 gal/ton while the theoretical yield for sugarcane is 15.5-18.6 gal/ton (Kenney and Ovard, 2013). Sweet sorghum contains about 15-23 % of fermentable carbohydrates within their stalk. It contains about 10 % of fructose, 20 % of glucose, and 70 % of sucrose and the percentage may vary due to environmental conditions (Kenney and Ovard, 2013). In some countries such as Brazil and USA, sweet sorghum has already been used to increase the production of ethanol.

2.1.2. Starch crops

Starchy crops such as corn, cassava, wheat, and barley can also be used for the production of biofuel. Corn is the most employed feedstock that has been used for the production of bioethanol (Luque, Lin and Wilson, 2011). Acid or enzymatic pre-treatment of starch materials is required to generate high content of sugar for the production of biofuel. The production of ethanol from corn is widely used in the US (Luque, Lin and Wilson, 2011). In 2014, the US used about 5 bushels of corn to produce over 13 billion gallons of ethanol fuel (Soccol *et al.,* 2016). Cassava is the shrub with tuberous roots normally used in both animal and human food (Soccol *et al.,* 2016). The world produces about 281 million tons per year of cassava and Africa contributes more than half of the global supply (Soccol *et al.,* 2016). Cassava contains high content of starch however; it is still playing a small role in the production of biofuel. From one ton of cassava with 30 % of starch content, 250 L of ethanol with 95 % purity can be produced (Soccol *et al.,* 2016).

2.1.3. Oil seeds

There are different oil seeds produced around the world that can be used for the production of biofuel. There are two types of the oil seeds; edible and non-edible oils. Edible oils includes sunflower, coconut, soya beans, and palm oils while non-edible oils includes *Jatropha curcas,* Passion seed *(Passiflora edulis),* and Pongamia (*Pongamia pinnata*). Edible oils are referred as the first generation biofuel feedstocks because they were firstly used for biofuel production (Sharma and Mudhoo, 2011). More than 95 % of the world's biodiesel is currently obtained from edible oils such as sunflower oil (13 %), rapeseed (84 %), palm oil (1 %), and others (2 %) (Gonfa Keneni and Mario Marchetti, 2017). The prices of vegetable oils has been increasing worldwide for the last few decades and this will affect the economic viability of the biofuel industries. Edible oils are also considered to be not feasible in the long term because of the

increasing gap between demands and supply (Gonfa Keneni and Mario Marchetti, 2017). Table 2.1 shows different edible oils and non-edible oils with their oil content that can be used for biofuel production.

Table 2. 1. Edible and non-edible oils with their oil content (Gonfa Keneni and Mario Marchetti, 2017).

Type of oil	**Common name**	**Species name**	**Oil content of seed/kernel**	
			Seed (wt. %)	Kernal (wt. %)
Edible	Sunflower	*Helianthus annuus*	25-35	50
	Soybean	*Glycine max*	18-20	-
	Coconut	*Cocos Nucifera L.*	63-65	63.1
	Corn	*Zea mays*	24.44	-
	Palm	*Elaeis guineensis*	30-60	-
	Rapeseed	*Brassica napus*	38-46	-
	Safflower seed	*Carthamus tinctorius*	35	-
Non-Edible	Castor	*Ricinus communis L.*	45-50	-
	Cotton seed	*Gossypium hirsutum L.*	18-25	31.42
	Jatropha	*Jastropha curcas L.*	20-60	40-60
	Jojoba	*Simmondisa chincnsis*	45-50	-
	Rubber seed	*Hevea brasiliensis*	40-60	40-50
	Polanga	*Calophyllum inophyllum*	65	22
	Neem	*Azadirachta indica*	20-30	25-45

Table 2.2 shows the average fatty acids compositions of different edible oils. The main fatty acids obtained in edible oils are linoleic acid (C18:2), oleic acid (C18:1), stearic acid (C18:0), and palmitic acid (C16:0). The composition of fatty acids in the oil greatly affected by the quality of the biofuel produced, according to Sajjadi *et al.* (2016) generally it is usually assumed that the fatty acids composition does not change during the conversion of the oil to biofuel.

Table 2. 2. Fatty acids composition of different edible oils (Gonfa Keneni and Mario Marchetti, 2017).

Source	**Fatty acids composition**								
	C14:0 Myristic acid	C16:0 Palmitic acid	C16:1 Palmiltoleic acid	C18:0 Stearic acid	C18:1 Oleic acid	C18:2 Linoleic acid	C18:3 Linolenic acid	C20:0 Arachidic acid	C22:0 Behenic acid
Soybean	-	6.14	0.09	4.11	34.30	51.17	2.23	0.17	0.41
Corn	-	-	11.67	1.85	25.16	60.60	0.48	0.24	-
Palm	0.70	36.70	0.10	6.60	46.10	8.60	0.30	0.40	0.10
Rapeseed	-	-	3.49	0.85	64.40	22.30	8.23	-	-
Safflower	-	11.07	-	4.37	12.76	69.65	0.49	0.78	0.59
Sunflower	-	16.69	-	6.66	22.70	44.13	8.97	0.62	0.63
Olive	-	11.60	1.00	3.10	75.00	7.80	0.60	0.30	0.10

Non edible oils are the promising substitutes for traditional edible oils in the production of biofuel. These oils recently got a great attention because of their availability, high oil content, and can easily grow on lands, which are not suitable for agriculture. The challenges faced with production of biofuels from edible oils can be effectively overcome by using non-edible oils. Non-edible oils generally has the greater degree of unsaturated fatty acids because it contains high number of double carbon bonds (Patil and Deng, 2009). It was reported that the increase in chain length increases the heat of combustion, cetane number, viscosity, and melting point of fatty compounds while the increase in unsaturation of the fatty acid methy esters (FAME) molecule causes the opposite effect (Patil and Deng, 2009). Thus, the physico-chemical properties of biofuel is affected by the structural fatty acid composition.

Table 2. 3. Fatty acids composition of different edible oils (Gonfa Keneni and Mario Marchetti, 2017).

Source	**Fatty acids composition**								
	C14:0 Myristic acid	C16:0 Palmitic acid	C16:1 Palmiltoleic acid	C18:0 Stearic acid	C18:1 Oleic acid	C18:2 Linoleic acid	C18:3 Linolenic acid	C20:0 Arachidic acid	C22:0 Behenic acid
Castor	-	1.00	-	-	3.00	5.00	1.00	-	-
Cotton	1.00	25.80	0.60	2.5	16.4	51.50	0.20	0.20	0.20
Jastropha	-	15.20	0.70	6.80	44.60	32.20	-	0.40	-
Jojoba	-	1.20	-	-	10.70	-	-	9.10	-
Karanja	-	11.65	-	8.9	51.59	16.46	2.65	-	-
Neem	0.2	14.9	0.1	20.6	43.9	17.9	0.4	1.6	0.3
Tobaco	0.14	8.46	-	3.38	11.24	75.5	1.14	-	-

2.2. Castor oil as the biofuel feedstock

Castor oil is the pale yellowish or colourless vegetable oil pressed from castor seeds. It is well known as the source of 18-carbon, ricinoleic acid, and a monosaturated fatty acid (Patel *et al*., 2016). Castor oil is usually used in the manufacturing of coatings, lubricants, pharmaceuticals, and skin and hair care products. Castor oil plants are mainly cultivated in Africa, India, and South America. The main countries producing castor oil is Brazil, China, and India and India is the biggest exporter of castor oil with over 90 % castor oil export while China, United States, and European Union are the biggest importers of castor oil (Patel *et al*., 2016). The world's consumption of castor oil increased by 7.32 thousand tons per year on average (Patel *et al*., 2016). The world's production of castor oil is generally considered not sufficient to meet the increasing demand.

Castor oil is one of the promising feedstock that can be used for biofuel production because it does not compete with edible oils, the cultivation process does not require high inputs, and it contains large amount of fatty acids. Castor seeds contains about 40-55 wt. % of oil which is very high compared to other commonly used oils such as sunflower: 25–35 wt. %, soybean: 15–20 wt. %, and rapeseed 38-46 wt. % (Keera, El Sabagh and Taman, 2018). The cost of cultivation for castor oil can be 25 % of the cost of cultivation for jastropha and 50 % of the cost of cultivation for rapeseed (Keera, El Sabagh and Taman, 2018).

The fuel-related properties of castor oil has been studied by researchers in pure form and as a blend with diesel fuel, primarily due to the large amount of ricinoleic acid. Berman *et al*. (2011) discovered that the methyl esters found in castor oil can be used as alternative feedstock for biodiesel when blended with diesel fuel. However, the blending level is limited to the maximum of 10% due to large amount ricinoleic acid present in the oil, which highly affect distillation temperature and biodiesel's kinematic viscosity (Berman *et al.*, 2011). Another study was done by Shojaeefard *et al*. (2013) to investigate the effects of blending diesel fuel with castor oil biodiesel on the diesel engine performance and emissions. It was obtained that the optimized blend of biodiesel-diesel proportions is 15 % blend of castor oil-biodiesel. This means that lower blends (less than 20 %) of biodiesel with diesel fuels gives acceptable engine performance and also improves the engine performance. Panwar *et al.* (2010) did similar study to those done by Shojaeefard *et al*. (2013); they performed transesterification of castor oil to methyl ester using potassium hydroxide (KOH) as catalyst. They used four-stroke, single cylinder variable compression ratio in diesel engine type to test this methyl ester. Based on their results, it was concluded that the break thermal efficiency increases and the fuel consumption is reduced with lower blends of biodiesel (Panwar *et al*. 2010).

There are different processes involved during castor oil extraction as shown Figure 2.3.

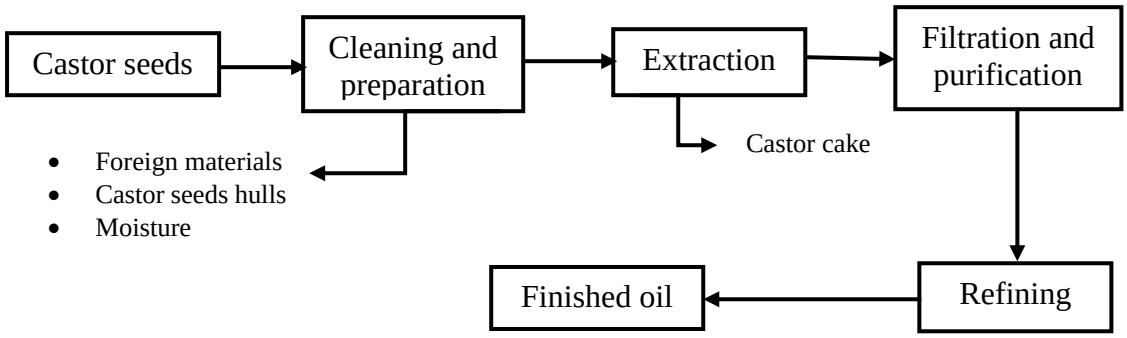


Figure 2. 3. Block flow diagram of castor oil extraction.

2.2.1. Castor seeds pre-treatment

Castor seeds goes under different processes during preparation for oil extraction. It firstly go under clearing where foreign materials and dirt are removed from castor seeds usually using hand picking. The cleaned castor seeds are then sun dried in the open for about 7 days and then further dried in oven usually at a temperature of 60^{o}C for 7 hours to reduce the moisture content in the seeds (Patel *et al*., 2016). The seeds shells are then separated from the seeds to achieve

high oil yield. Lastly, the seeds are then crushed in order to weaken or rupture the cell walls to release castor fat for extraction.

Oil yield is generally affected by the quality of the castor seeds. However, other factors such as moisture content, particle sizes of the castor seeds can be manipulated to maximise the oil yield during extraction (Patel *et al*., 2016). According to Olaniyan (2010), the oil yield and quality is normally affected by the pre-treatment stage of castor seeds prior extraction. Faugno *et al*. (2016) analysed the extraction parameters that highly affect the oil yield of mechanically pressed tobacco (*Nicotiana tabacum L*) seed oil, the results showed that preheating and high extraction temperature had a significant effect on the oil yield.

Dasari *et al.* (2014), studied the effect of pre-treatment on the properties extracted oil and oil yield by using solvent extraction. This was done by extracting oil from untreated and pre-treated castor seeds using methanol as a solvent (Dasari *et al.,* 2014). Table 2.4 shows the physicochemical properties of castor oil extracted from untreated and pre-treated castor seeds.

Table 2. 4. Physicochemical characteristics of castor oil extracted from untreated and pre-treated castor seeds (Dasari, Goud, and Vaibhav, 2014).

Property	**Oil from untreated castor seeds**	**Oil from pre-treated castor seeds**
Oil yield	54	55
Density (g/cm^3)	0.945	0.948
Specific gravity	0.960	0.963
Kinematic viscosity at 40^oC (Cst)	297	259
Acid value (mg KOH/g)	3.92	0.925
Saponification value (mg KOH/g)	168.52	171.04
Unsaponifiable matter (wt. %)	0.28	0.59
FFA (mg KOH/g)	1.96	0.462
Iodine value (gI_2,100 g)	69.74	72.86
Refractive index at 23^oC	1.477	1.475

Based on the results in Table 2.4, the pre-treatment of castor seeds resulted into the increase in saponification and iodine value and decrease in viscosity and acid value.

2.2.2. Castor oil extraction

Castor oil can be extraction from castor seeds through mechanical pressing, solvent extraction, or through the combination of mechanical pressing and solvent extraction. About 30-50 % of oil can be extracted from the castor seeds depending on the environmental conditions around the castor seeds plant, the pre-treatment procedure of the castor seeds, and the extraction method used to extract the oil (Patel *et al*., 2016).

2.2.2.1. Mechanical pressing

Mechanical pressing involves the application of pressure into the seeds using either screw or hydraulic pressing to force out the oil from the castor seeds (Patel *et al*., 2016). In this method, the oil yield is mainly enhanced by increasing the mechanical pressure. In the study of mechanical pressing of castor seeds, the main operating conditions that are mainly investigated are pressing time, operating pressure, and product bulk temperatures. According to Mwithiga and Moriasi (2007) the oil yield increases linearly with pressing time (6-12 min), operating pressure (40-80 kgf/m^2), and the increase in the bulk temperature reaching a peak at about 150^{o}C of the preheated oil seeds.

Mechanical pressing is often used to extract oil from seeds that contains oil content higher than 20 % (Sinha, Haddar, and Majumdar, 2015). This method is generally considered to have low operating cost, and produces oil with low concentration of free fatty acids and high quality light coloured oil. The oil yield of mechanical pressing is considered relatively low compared to solvent extraction, this means that large amount of oil is lest in the cake after extraction. Only about 45 % of the oil is extracted through mechanical pressing and the remaining oil can be extracted by solvent extraction (Ogunniyi, 2006).

Before extraction, the cleaned castor seeds are boiled and put through secondary drying. The purpose of cooking the castor seeds is to coagulate proteins in the seeds necessary to allow efficient extraction, and to free oil in the seeds for efficient pressing. A hydraulic press or continuous screw is used to crush the castor seeds to facilitate oil extraction (Patel *et al*., 2016). The first stage of oil extraction is called prepressing. Prepressing involves using high-pressure continuous screw press called an oil expeller (Patel *et al*., 2016).

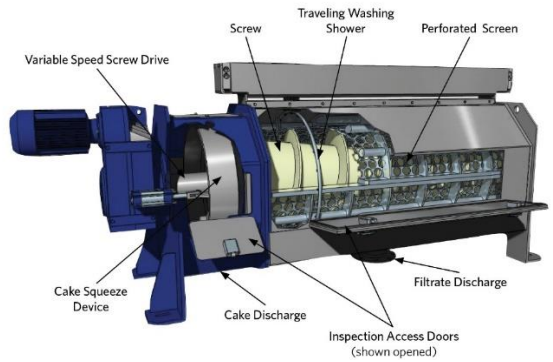


Figure 2. 4. Continuous screw press (Ishigaki usa ltd, 2020).

After extraction, the oil is collected and filtered and the filtered materials is then recycled back and combined with the fresh feed seeds further extraction. Large amount of the filtered material will then be finally ejected from the press and this material is known as castor cake. The castor cake contains about 10 % of castor oil content (Patel *et al*., 2016). The 10 % of castor oil from the castor cake can be extracted through firstly crushing it and use solvent extraction method to further extract the oil (Patel *et al*., 2016).

Higher temperatures can increase the oil yield during extraction. About 80 % of available oil in the seeds can be extracted by using high-temperature hydraulic pressing (Willems *et al*., 2008). The temperature can be controlled during extraction by circulating cold water on the mechanical presser responsible for cold pressing of the castor seeds (Patel *et al*., 2016).. The oil can be mechanically pressed by either cold-press method or hot-press method. The cold press method is carried at temperatures usually below 50^{o}C and low pressure (Patel *et al*., 2016). While hot-press method is usually carried out at very high temperature and pressure. Oil obtained from cold-press method is often preferred from the oil obtained from hot-press method because of the unfavourable effects caused by high temperatures (Patel *et al*., 2016). These unfavourable effects includes degradation of valuable oil components, decreased oxidative stability, and reduction of oil quality (Willems *et al*., 2008). The natural properties of the oil obtained from cold pressing are preserved. The attractive qualities of cold-pressed oil increases the global demand of cold pressed oil.

Yusuf *et al*. (2015) extracted castor oil using mechanical cold pressing at temperature below 45 ^{o}C from castor plant found in wet marginal lands of Katsina, Nigeria. The purified castor oil revealed the following physicochemical properties.

Table 2. 5. Physicochemical properties of castor oil obtained from mechanical pressing (Yusuf *et al*., 2015).

Property	**Value**	**ASTM standard**
pH	6.16	-
Specific gravity, 30°C	0.959	0.957 - 0.961
Refractive index, 30°C	1.472	1.476 - 1.478
Relative viscosity, 30°C	1.86	-
Acid value, mg KOH/g oil	2.07	2 (max)
Hydroxyl value, mg KOH/g oil	163.64	160 - 168
Saponification value, mg KOH/g oil	175.31	176 - 184
Iodine value (Hanus), g I_2/100 g oil	84.18	83 - 88
Peroxide value, ml/g oil	38.00	-
Cold press oil yield, %	39.43	-

The physicochemical properties indicated that the castor oil contains low peroxide value (38.00), low iodine value (84.18), low acid value (2.07), but relatively high saponification value (175.31), hydroxyl (163.64), and specific gravity (0.959). These values are within the range of ASTM standards required for industrial grade of castor oil. The peroxide value is related to the oxidation level of the oil due to hydroperoxide formation of double bonds position, iodine value measures the unsaturation level of the oil, and the acid value measures the free fatty acids content in the oil.

According to Ogunniyi, (2006), the physicochemical characteristics may differ based on the method used to extract the oil. Table 2.6 show the physicochemical characteristics of oil from different method of extraction.

Table 2. 6. Physicochemical characteristics of castor oil from different oil extraction method (Ogunniyi, 2006)

Properties	**Cold-pressed oil**	**Solvent-extracted oil**	**Dehydrated oil**
Specific gravity	0.961-0.963	0.957-0.963	0.926-0.937
Acid value	3	10	6
Iodine value (W_{ij})	82-88	80-88	125-145
Saponification value	179-185	177-182	185-188

2.2.2.2. Solvent extraction

Solvent extraction method is commonly used to extract oil from oil seeds with oil content less than 20 % such as soyabean (Patel *et al*., 2016). Solvent extraction is considered to be the most efficient method for oil extraction compared to mechanical pressing because less amount of oil is left in the cake. To maximise the amount of oil extracted from the oil it is very important to choose the best suitable solvent. There are different solvents that are commonly used for extraction such as ethanol, hexane, petroleum ether, and diethyl ether.

There are many advantages in using solvent extraction. Bhuiya *et al*. (2015) investigated on the optimization of solvent extraction and mechanical pressing method on the extraction of oil from Australian Native Beauty Leaf Seed (*Calophyllum innophyllum*) and they reported that the method which gave consistent performance and high yield is solvent extraction. However, the cost of production for solvent extraction method was found to be relatively high when compared to mechanical pressing method because of the high cost of solvent used. Muzenda *et al.* (2012) optimized the extraction of oil from castor, based on their results they concluded that the increase in extraction time enhances the extraction of oil and the solvent-solute ratio preferably 6:1 increases the extraction of oil. The quality of oil extracted is also affected by the extraction method. Ikya *et al*. (2013) investigated the quality and yield of oil extracted from solvent extraction and old traditional extraction method by comparing chemical, physical, and sensory properties of the extracted oil. They reported that the oil obtained from solvent extraction gave better quality with low flash and fire point values and low moisture content. The oil yield obtained from solvent extraction method, and old traditional method was 47.5 %, and 34.1 %, respectively. 33.2 % of oil yield was obtained by Akpan *et al*. (2006) after using solvent extraction to extract oil from castor seeds and the oil yield obtained was within the expected range from literature. Based on the results reported by different authors, it can be concluded the oil yield can be affected by the seeds variety and the type of extraction method used.

The types of solvent is also the main factor that need to be considered during solvent extraction. The type of solvent used can affect the oil yield, energy requirement, and operating cost. Danlami *et al.* (2014) investigated the extraction of castor oil using three different solvents; ethanol, petroleum-ether, and hexane. The maximum oil yields obtained from using ethanol, petroleum ether, and hexane were 59.5 %, 49.0 % and 50.9 %, respectively. Ghazali and Yasin

(2016) investigated the effect of using hexane, heptane, and ethanol solvents on the extraction of oil from *Moringa oleifera* seeds. They found out the heptane gave the maximum oil yield of 36.37 % which is higher compared to the oil yield obtained from ethanol and hexane with 18.46 %, and 33.89 %, respectively (Ghazali and Yasin, 2016). The most commonly used solvent during extraction is hexane because of its low boiling temperature and low corrosiveness.

The type of solvent can also affect the properties of the extracted oil. Table 2.7 shows the physicochemical characteristics of castor oil extracted from different solvents.

Table 2. 7. Physicochemical characteristics of oil extracted at different types solvent (Dasari, Goud, and Vaibhav, 2014).

Properties	**Hexane**	**Petroleum ether**	**Pentane**	**Ethyl acetate**	**methanol**
Density (g/cm^3)	0.976	0.944	0.937	0.925	0.948
Specific gravity	0.991	0.959	0.952	0.940	0.963
Kinematic viscosity at 40^oC (Cst)	230	288	251	207	259
Acid value (mg KOH/g)	2.71	3.08	4.4	4.7	0.925
FFA(mg KOH/g)	1.35	1.54	2.2	2.35	0.462
Saponification value (mg KOH/g)	176.33	171.15	175.11	152.87	171.04
Unsaponifiable matter (wt. %)	0.39	0.38	1.3	0.19	0.59
Iodine value (I_2/100 g)	84.93	85.55	82.53	73.21	72.86
Refractive index	1.475	1.475	1.475	1.475	1.475

After extraction, there are still unwanted materials that are remaining in the oil. These unwanted materials includes small and large size castor cake and can be removed through employing filtration systems. The equipment that is usually used for filtration is called the filter press.



Figure 2. 5. Filter press (watermark, 2020)

2.2.4. Castor oil refining

After the filtration stage, the castor oil is then sent to refining for the removal of impurities such as colloidal matter, coloring agents, phospholipids, and excess free fatty acids. The purpose of the refining stage is to facilitate the oil not to deteriorate during extended storage (Patel *et al*., 2016). The refining process includes 4 processing steps: degumming, neutralization, bleaching, and deodorization.

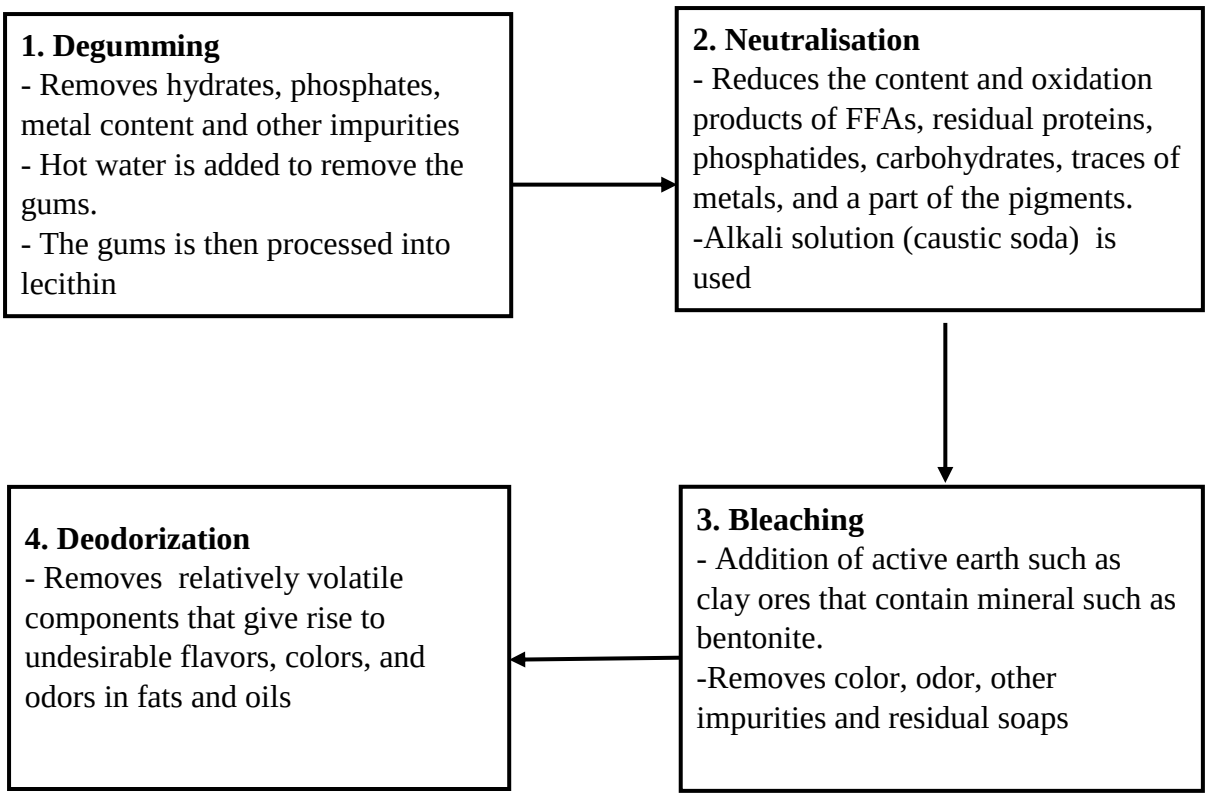


Figure 2. 6. Oil refining process (Wu *et al*., 2019).

Abdalla and Babiker, (2014) investigated the physicochemical characteristics of the crude castor oil and the refined castor oil. The results are showed in Table 2.8. Based on their results, there was no significant change on the physicochemical characteristics of both crude and refined castor oil.

Table 2. 8. Physicochemical characteristics of crude and refined castor oil (Abdalla and Babiker, 2014).

Properties	Crude oil	Refined castor oil
Specific gravity	0.963	0.960
Viscosity at 40^{o}C (Cst)	234.07	209.6
Iodine value	86.98	84.23
Acid value	1.231	0.916
Saponification value	179.33	178.56

2.3. Comparison of production routes

There are different methods used by researchers to convert castor oil into biofuel products. This section evaluates and compares three methods reported from literature: catalytic hydroprocessing, transesterification, and pyrolysis (catalytic cracking). This section aim in determining the most effective and ideal method that can be used to maximise the production of biogasoline and biojet.

2.3.1. Catalytic hydroprocessing

Catalytic hydroprocessing is one of the technology used to convert liquid biomass to biofuels. Catalytic hydroprocessing is mainly used in petrochemical industry for over a century and it is mainly used for the removal of heteroatom such as metals, sulphur, oxygen, and nitrogen, saturation of aromatics and olefins, as well as cracking and isomerisation (Treese *et al*., 2015). Catalytic hydroprocessing offers a great flexibility to the increasing demand of biofuels, as it can convert variety of liquid biomass such as animal fats, algal oils, waste cooking oil, as well as vegetable oils into biofuels with high conversion yields (Treese *et al*., 2015). To meet the numerous applications of catalytic hydroprocessing, there are different catalytic hydroprocessing units which includes hydrotreating and hydrocracking.

2.3.1.2. Hydrotreating

Hydrotreating is the process that removes unwanted impurities such as metals, sulphur, nitrogen, and oxygen by reacting with nitrogen in the presence of a catalyst (Cheremisinoff and Rosenfeld, 2009). The hydrotreating of metals, nitrogen, sulphur, and oxygen is called hydrodemetallization (HDM), hydrodenitrogenation (HDN), hydrodesulphurization (HDS), and hydrodeoxygenation (HDO), respectively. This project focuses on the production of

biofuel from castor oil. Castor oil contains large content of oxygen which must be removed during the production of biofuels. Catalytic HDO of castor oil results into production of hydrocarbon fuels with improved ignition qualities. During HDO process, the unsaturated bonds in the vegetable oil becomes saturated and oxygen is removed in the form of water at high pressure and temperature (Tran *et al*., 2014). Other researchers have reported the use of HDO process on the conversion of fats and other types of oils into biofuels. Jakkula *et al*. (2004) used vegetable oils such as sunflower, rapeseed, and canola oils, and also made use of fats in milk. Herskowirz et *al.* (2006) used both vegetable and animal oils as the feedstock, while Petri and Marker (2006) used vegetable oils and grease.

HDO process is the most effective method used to remove oxygen atoms from selected biomass-derived compounds to produce biofuels. However, this method may be quite expensive due to consumption of hydrogen and harsh reaction conditions such as operating temperature and hydrogen pressure (Jin *et al.,* 2019). To overcome these harsh reaction conditions, a highly efficient and most selective heterogeneous catalyst is required. The high cost associated with the production and purification of hydrogen is still a concern and results to high operating cost (Jin *et al*., 2019). Hydrogen is usually obtained by methane steam reforming of fossil fuels.

The vegetable oils can also undergo decarboxylation during deoxygenation process, this means that the oxygen from the feedstock is removed in the form of carbon dioxide. This process is highly influences by the reaction conditions and the nature of the catalysts (Jin *et al.,* 2019). HDO is preferably done under high hydrogen pressure and low temperatures by using molecular sieve catalysts and supported metal catalysts in sulfided or reduced form (Mortensen *et al*., 2013). Decarboxylation is favoured by catalyst supported on noble metal and HDO is favoured by sulfided or reduced catalysts. However, the sulfided catalyst results into sulphur-contaminated fuel (Mortensen *et al*., 2013).

Regarding the operating conditions of HDO, a high pressure of about 75 to 300 bar is generally used according to literature. The high pressure is normally used for enabling higher solubility of hydrogen in the oil and as a result of that increasing the availability of hydrogen closer to the catalyst (Shafaghat, Rezaei, and Ashri Wan Daud, 2015). This reduces coking in the HDO reactor and increases the rate of reaction. The reaction is also favoured by high residence time. Sulphided CoMo or NiMo supported on alumina or aluminosilicate were the first catalysts originally tested for HDO (Gupta, 2014). However, the problems regarding the catalyst arose

due to the unstableness of the catalyst supports in environment with high water content and the sulphur in the catalyst required constant re-sulfurization (Gupta, 2014). In the last few years, the use of metal catalysts on less susceptible supports such as Pd on C has been initiated.

The products obtained from HDO process contains low or no oxygen content, desired viscosity, good lubricity, and enhanced atomization (Jamil *et al.*, 2017). The process also increases the storage stability of the products (Jamil *et al.*, 2017). The main aim of doing this process is to increase the H/C ratio while simultaneously reducing the O/C ratio. The products from HDO process containing significant concentration of isomeric alkane's shows excellent low temperature properties such as cold filter plugging point and cloud point (Krár *et al.*, 2011).

It is observed that the extent of HDO process and the efficiency of the biofuel produced is affected by the nature of the feedstock and the type of catalyst used. Meller, *et al.* (2014) investigated HDO of castor oil using Pd/C and they operated under mild hydrogen pressure. They found out that heptadecane can be formed by both deoxygenation via decarbonylation, and also by hydrogenation of double bond and the hydroxyl group of methyl ricinoleate (Meller, *et al*., 2014). Krár *et al.* (2010) performed catalytic HDO of light gas oil containing 10 % sunflower oil using alumina-supported transition metal catalyst. They observed that their products contains low aromatic and sulphur content. The products also consisted carbon range of C_{15}-$C1_8$, which indicated that both HDO and decarboxylation occurred resulting to poor low temperature properties and high cetane number of the products (Krár *et al*, 2010). Šimáček *et al.* (2010) performed HDO process on the reepseed oil over different loading of Ni-Mo/alumina sulfided catalysts at temperature between 260^{o}C to 340^{o}C under hydrogen pressure of 7MPa. The product consisted carbon range of C_{17}-C_{18} of alkanes. It was observed that the alkanes increases with the increase in temperature for all the catalysts. The products produced exhibited poor cold flow properties even after adding flow modifiers when blended with mineral diesel and were also characterised by high cetane numbers (Šimáček *et al.*, 2010).

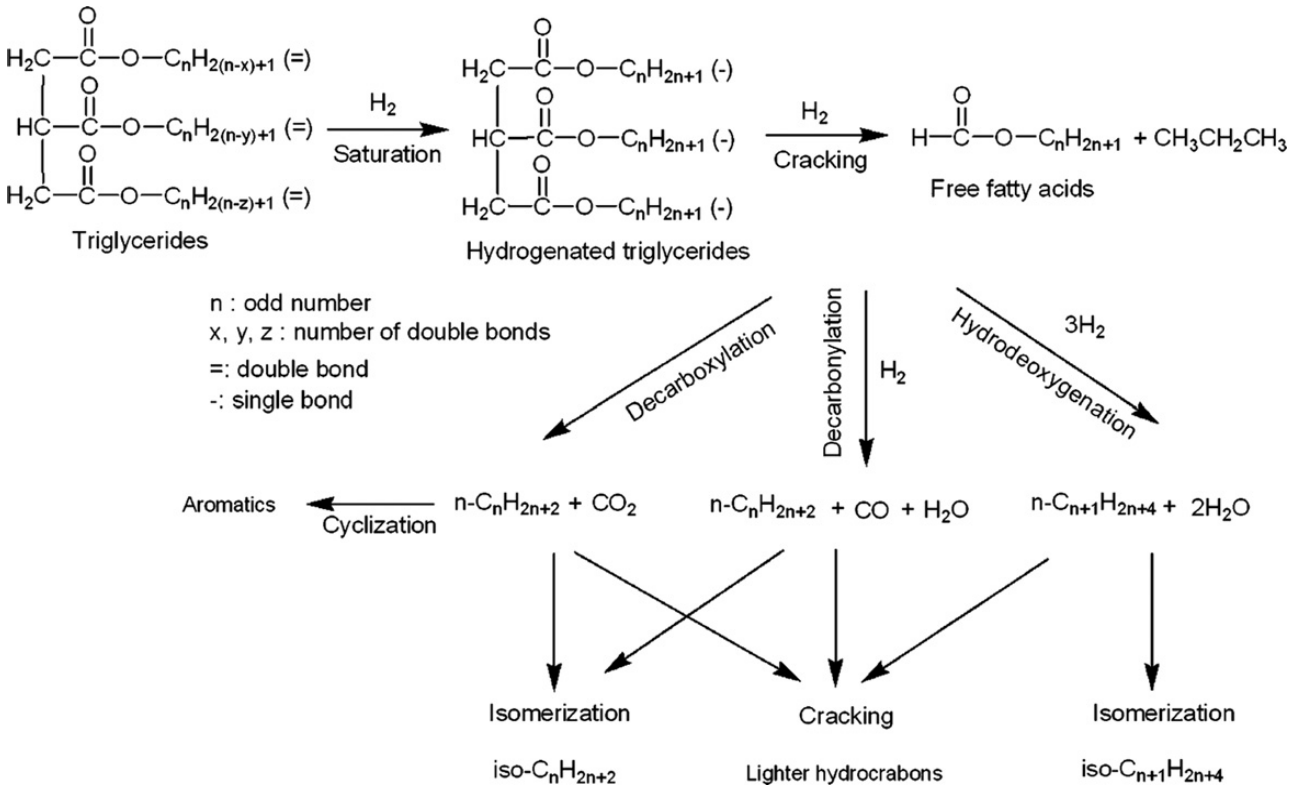


Figure 2. 7. Possible pathways during HDO process of triglycerides (Ko *et al.,* 2012).

The different processes that can be obtained during HDO of triglycerides are generalised in Figure 2.7. The HDO process can proceed to different routes such as decarboxylation, hydrocracking, and decarbonylation. The formed hydrocarbons from the HDO reaction contains chains with same number of carbons, along with propane and water (Ko *et. al.*, 2012). The routes in Figure 2.7 is influenced by the catalyst used, reaction pressure and temperature, and liquid hourly space velocity.

The removal of oxygen includes C-O bond rupture, C=O bond hydrogenation, and C-C bond cleavage. In the presence of catalyst, large hydrocarbons are selectively formed which results to C-O bond cleavage and C=O bond hydrogenation preventing the C-C bond breaking (Ko *et. al*., 2012). The routes of C-O and C-C bond cleavage and the extent of cleavage are the main factors determining the selectivity of the reaction (Ko *et al*., 2012). Gupta *et al.* (1986) studied the mechanism of associated with HDO reaction and formation of by-products and they also found that the catalysed used affect the routes of reaction and the product formation.

2.3.1.2. Hydrocracking

Hydrocracking is the process at which large hydrocarbons are broken down into simpler molecules such as kerosene or gasoline in the presence of catalyst, usually called catalytic

hydrocracking. (Speight, 2013) Hydrocracking is the severe form of hydroprocessing and purposely used for breaking C-C bonds, while drastically reducing molecular weight and produces higher yields of fuel products with about 50 % plus conversion (Speight, 2013). Hydrotreating may occur before hydrocracking for the removal of impurities such as sulphur to produce high quality cracking products.

The main difference between hydrocracking and hydrotreating is that hydrocracking generate fuels in the gasoline range through braking C-C bonds which drastically lowers the molecular weight. While, hydrotreating favours the production in the diesel range through saturating of C-C bonds and removal of hetero atoms with the number of carbon atoms still complete (De and Luque, 2014). Liu *et al.* (2015) and Usomboon *et al.* (2012) produced biogasoline and biojet from biodiesel using hydrocracking. Therefore, it is very important to produce high quality biodiesel for maximum production yield of biojet and biogasoline.

The hydrocracking products quality and yield is affected by the hydrogen pressure, operating temperature, catalyst used, and the nature of the feedstock. The operating temperature is usually selected according to the type of feedstock and catalyst used. Based on literature, the increase in temperature increases the conversion. However, the increase in temperature beyond the optimum value increases conversion but may decrease the diesel yield. This is because at higher temperatures the hydrocarbons formed breaks down into to lighter fractions resulting to low yield of diesel products (Verma *et al.,* 2018). Similar effects were observed by Hasanudin *et al*. (2019) through hydrocracking crude palm oil at temperature between 350^{o}C to 450^{o}C. The diesel yield increased before 400^{o}C and after started to decrease, while the conversion kept on increasing. The increase in hydrogen pressure increases the conversion of aromatic structures to saturated products which improves the quality of the diesel fuel, jet fuel and oil with very high viscosity index (Hasanudin *et al*., 2019). The effect of hydrogen pressure on the conversion and diesel yield is the same as the effect of temperature. Worapon *et al*. (2013) further investigated the effect of hydrogen pressure on the hydrocracking of crude palm oil by operating between 20-60 bars of hydrogen pressure. They observed that the diesel yield increased before 40 bar and then started to decrease after 40 bar. (Warapon *et al*., 2013)

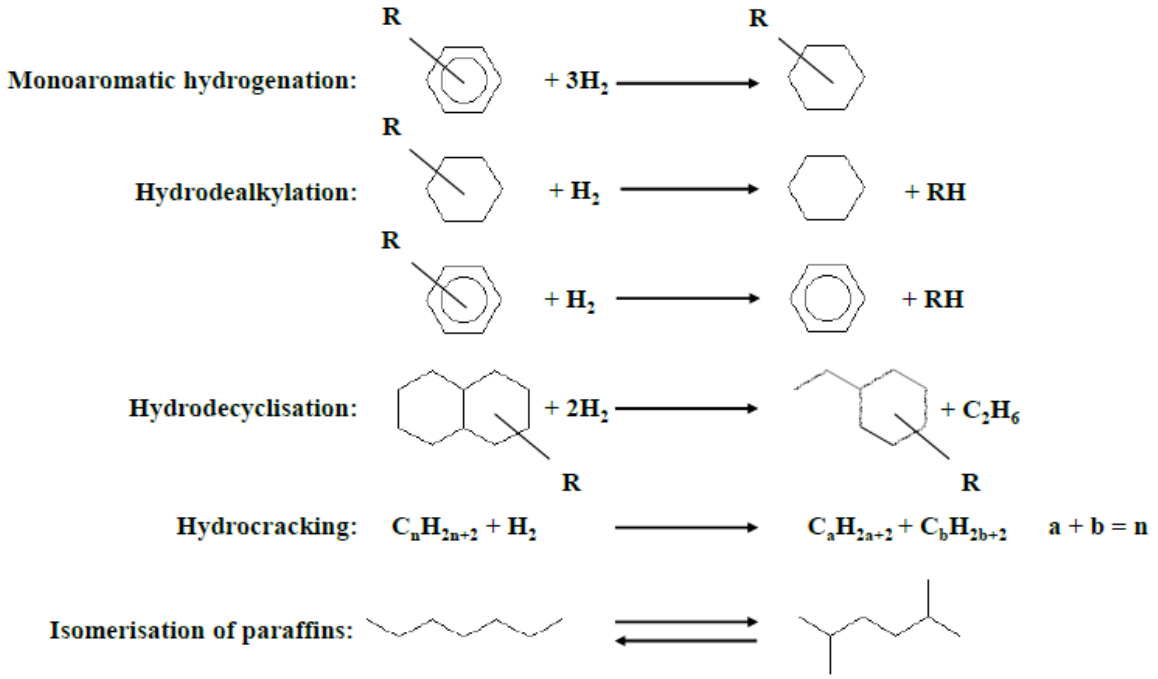


Figure 2. 8. Reactions occurring during hydrocracking (Scherzer and Gruia, 1996).

The main reactions that can occur during hydrocracking, showed in Figure 2.8 are: aromatic hydrogenation, hydrodealkylation (cracking of side chains of the cyclic compounds), hydrodecyclisation (napthene ring opening), hydrocracking of long-chain paraffins, and isomerisation of paraffins (Scherzer and Gruia, 1996).

The choice of catalyst is also important due its role in controlling the production yield, type of product, and selectivity. The main properties of are size, pore shape, surface area, metal dispersion, and acidity. According to literature, different types of porous sulfided catalyst have been used in the production of biofuels from vegetable oils. Hydrocracking reactions have two functions, a cracking function which uses catalyst usually supported on the acid support such as silica-alumina, alumina, and zeolites, and hydrogenation-dehydrogenation function using noble metals catalyst such as palladium and platinum and non-noble metals catalyst such as nickel and cobalt (Coker, 2018). Catalysts such as sulfided Ni-Mo, Co-Mo, and Ni-W supported on acidic supports such as silica-alumina and crystalline acidic support such as hierarchical mesoporous zeolites have been successfully used for hydrocracking (Coker, 2018). The ratio between bifunctional catalysts are regulated to achieve the highest product quality, selectivity, stability, and activity.

The hydrocracked products from vegetable oils contains hydrocarbons compounds such as aromatics, iso-paraffin, n-paraffin, and cylo-paraffin and other product such as ketones, esters,

carboxylic acids, alcohols, and aldehydes can also be found in the products. Kim *et al.* (2014) produced diesel range hydrocarbon by deoxygenating soybean oil at hydrogen pressure of 9.2 MPa and temperature of 400^{o}C using sulfided NiMoSx catalyst and the product contained 3.2 % of aromatics (C_{17}-C_{18}). Marlinda *et al*. (2016) produced high content gasoline range hydrocarbons and about 2.9 % of aromatics through hydrocracking of Cerbera manghaa oil at hydrogen pressure of 15 bar and temperature of 350^{o}C using Co-Ni/HZSM-5 catalyst. Pinto *et al*. (2013) obtained about 50 % of aromatics through hydrogenation of rapeseed oil at hydrogen pressure of 1.10 MPa and temperature of 400^{o}C using cobalt and molybdenum catalyst. Verma *et al*. (2015) produced kerosene range hydrocarbons through hydrocracking of jastropha oil using sulfided NiW and NiMo catalysts supported of hierarchical mesoporous SAPO-11. Non-edible oils are castor oil are recommended as the potential feedstock for the production of biofuels via hydrocracking.

2.3.2. Transesterification

Transesterification is the process that transforms ester into another when a raw renewable oil such as vegetable oil is reacted with primary or secondary monohydric aliphatic alcohols having 1-8 carbon atoms such as methanol in the presence of a catalyst to give biodiesel, methyl ester, with glycerol as a by-products (Musa, 2016). Ethanol and methanol are commonly used alcohols as reactants because of their availability and low cost. Transesterification is widely used in reducing the viscosity of vegetable oil and conversion of triglyceride into esters (Musa, 2016).

Transesterification is one of the reversible reactions and excess alcohol is used to shift the equilibrium towards the formation of esters and glycerol. The glycerol formed settles down the bottom of the reaction vessel and can be sold to the relevant markets (Suib, 2013). During transesterification of triglyceride with alcohol, diglycerides and monoglycerides are formed as the intermediates products (Suib, 2013). Triglyceride firstly reacts with alcohol to produce fatty acid ester and diglyceride. The diglyceride further reacts with alcohol to produce another fatty acid ester and a monoglyceride. Finally, the monoglyceride reacts with alcohol to produce glycerol and fatty acid ester (Suib, 2013). The three consecutive transesterification reactions are shown in Figure 2.9.

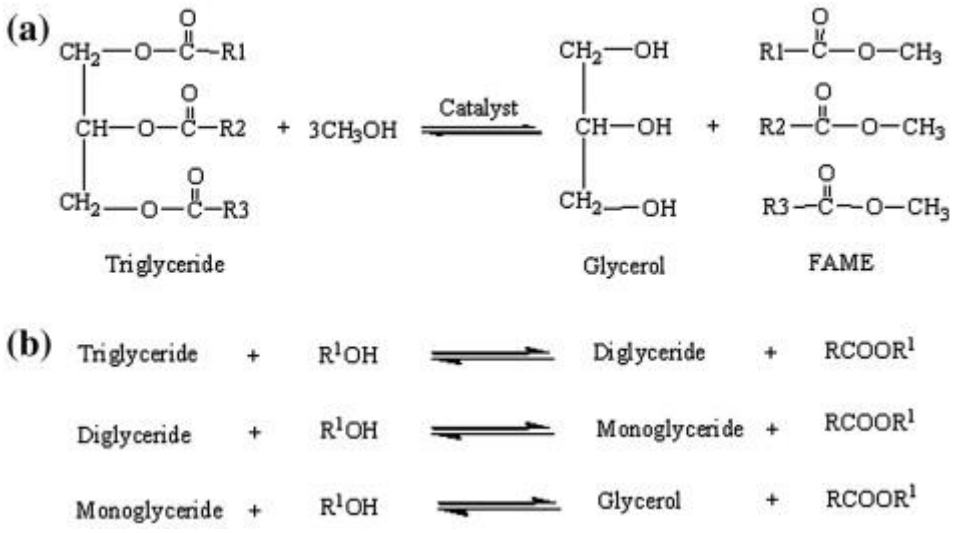


Figure 2. 9. (a) Transesterification of triglyceride using methanol, (b) transesterification stages of triglycerides (Suib, 2013).

Transesterification process can be done by catalytic, non-catalytic, and enzymatic transesterification (Suib, 2013). Non-catalytic transesterification is not preferred due to supercritical conditions required such as high temperature and pressure which is not economically feasible. Hence, catalytic transesterification is more commonly used for biofuel production (Suib, 2013).

There are different factors affecting the transesterification process such as temperature, type of catalyst, purity of the reactant, alcohol/vegetable oil molar ratio, and free fatty acids. These factors was discussed below based on the type of catalysed used.

2.3.2.1. *Acidic-catalysed transesterification*

BrØnsted acids preferably sulfonic acid and sulphuric acid are used during acidic-catalysed transesterification. Temperatures above 100^{o}C with duration of more than 3 hours are commonly used operating conditions to reach the complete conversion (Schuchardt, Sercheli and Vargas, 1998). However, the reactions are very slow with very high yields. Goff *et al.* (2004) performed acidic-catalysed transesterification on soyabean oil using nitric, acetic, formic, hydrochloric, and sulphuric acid at temperatures of 100^{o}C and 120^{o}C and only sulphuric acid was effective. About >99 wt. % was obtained by using 0.5 wt. % of sulphuric acid at 100^{o}C in 8 hours.

One of the main factors that affects transesterification is the molar ratio of alcohol/vegetable oil. An excess amount of alcohol favours the formation of the products however very high

amount of alcohol can also results into difficulties on the recovery of glycerol. It is very important to control and maintain the alcohol/vegetable oil molar ratio during transesterification.

The alcohol/vegetable oil molar ratio is one of the main factors that influences the transesterification. An excess of the alcohol favours the formation of the products. On the other hand, an excessive amount of alcohol makes the recovery of the glycerol difficult, so that the ideal alcohol/oil ratio has to be established empirically, considering each individual process (Suib, 2013). The reaction rates can be increased by increasing the amount of catalyst. About 1-5 wt. % of sulphuric acid concentrations is used in most academic studies (Suib, 2013). Canakci and Van Gerpen (1990), investigated the effects of different amount of sulphuric acid from 1-5 wt. % and the yield increases from 72.7-95.0 % (Canakci and Van Gerpen, 1990).

Homogenous acid catalysed reaction is said to be very slower than the homogeneous base catalysed reaction. However, acid-catalysed transesterification does contain very strong and important advantage when compared with base-catalysed transesterification. Acid-catalysed transesterification is not greatly affected by the presence of free fatty acids in the feedstock. As the results, low cost feedstocks associated with high free fatty acid concentrations can be successfully used in the production of biodiesel. A two-step esterification process was proposed in converting free fatty acid to fatty acid methyl ester, by using acid-catalysed process followed by base-catalysed process (Schuchardt, Sercheli and Vargas, 1998).

The mechanism of the acid-catalysed transesterification of monoglyceride is shown in Figure 2.10 and can be extended to diglycerides and triglycerides. According to this mechanism, carbocation II with water present in the reaction mixture results to formation of carboxylic acids (Schuchardt, Sercheli and Vargas, 1998). As the results, acid-catalysed transesterification must be performed in the absence of water to avoid the reduction of alkyl esters yield due to the competitive formation of carboxylic acids.

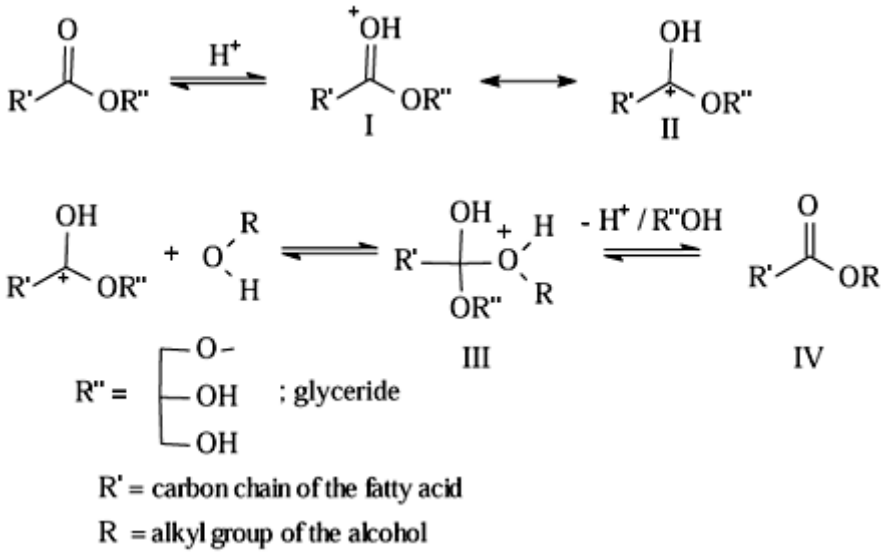


Figure 2. 10. Acid-catalysed transesterification mechanism of vegetable oil (Schuchardt, Sercheli and Vargas, 1998).

2.3.2.2. Base-catalysed transesterification

Base catalyst such as alkaline metal alkoxides, hydroxides, and sodium or potassium carbonates are commonly used during base-catalysed transesterification. The advantage of using base-catalysed transesterification is that the reaction very faster and the catalyst is less corrosive (Schuchardt, Sercheli and Vargas, 1998). Yusup and Khani (2010), performed base-catalysed transesterification using crude rubber seed oil with methanol/oil molar ratio of 9/1 and 2 wt. % of potassium hydroxide at 55^{o}C. After 5 hours, the production yield exceeded 98 % with biodiesel quality matching with international standards.

The mechanism of the base-catalysed transesterification generally involves for steps as shown in Figure 2.11. In the first step. Alcohol reacts with base to produce alkoxide and the protonated catalyst. In the second step, the alkoxide produced is the nucleophillic attacked at the carbonyl group of the triglyceride, which results in the formation of intermediate tetrahedral. In the third step, there is the production of the corresponding anion of diglyceride and alkyl ester. The final step involves the regenerating of the active species through deprotonating the catalyst to allow the reaction with the second molecule of the alcohol, which then start another catalytic cycle.

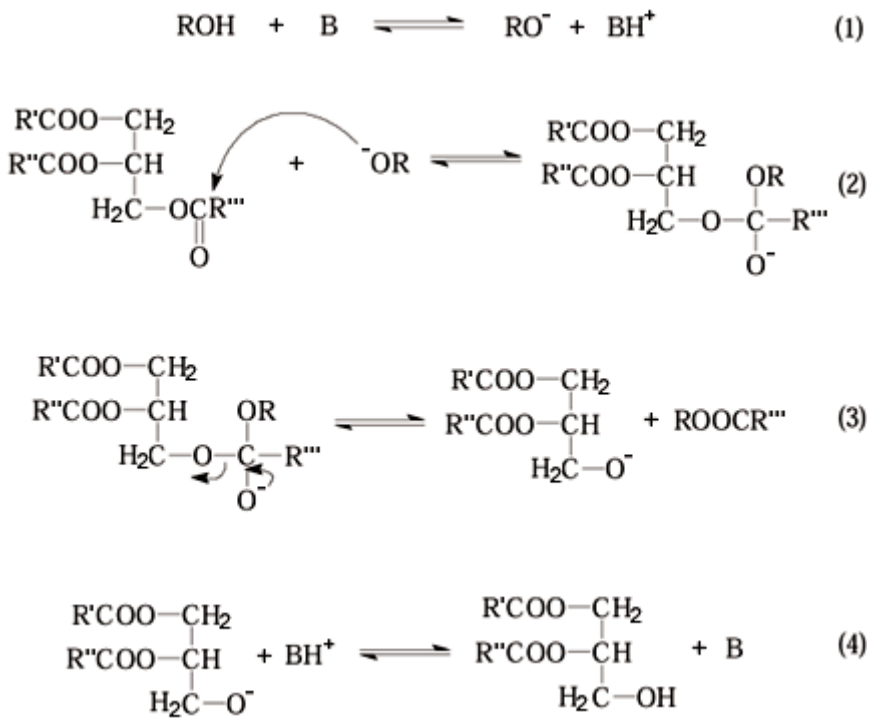


Figure 2. 11. The base-catalysed transesterification mechanism of vegetable oils (Schuchardt, Sercheli and Vargas, 1998).

2.3.2.3. Lipase-catalysed transesterification

Lipase-catalysed transesterification is also known as enzyme-catalysed transesterification. Lipase is an important enzyme catalyst that is commonly used for transesterification and esterification to produce methyl esters (Schuchardt, Sercheli and Vargas, 1998). Enzymatic reactions are very attractive due to their mild reaction conditions, reuse of the catalyst, simplify the separation of products, ability to produce high quality product (Schuchardt, Sercheli and Vargas, 1998). However, they do not give high conversion and reaction rate as compared to chemical catalyst.

Enzyme-catalysed transesterification processes are not yet commercially developed. New studies have been reported on the process in recent articles and patents. In these studies, common aspects in optimising the reaction conditions such as temperature, solvent, temperature, and the type of microorganism which generates the enzyme has been investigated in order to suitable conditions for industrial applications. More than 98 % conversion of oil to methyl esters can be obtained through stepwise addition of methanol by reusing the immobilized enzyme more than 50 times (Schuchardt, Sercheli and Vargas, 1998). Kim *et al*. (2007) performed lipase-catalysed transesterification of soybean oil using ethyl acetate, an

alternative acyl acceptor. They obtained about 63.3 % of biodiesel by using ethyl acetate/oil molar ratio of 6/1 with 8 wt. % of immobilized lipase based at temperature of 70^{o}C and stirring speed of 600 rpm.

2.3.2.4. Heterogeneous-catalysed transesterification.

Heterogeneous catalyst are also used in the production of biodiesel and they provide advantages that includes their ability give high quality of products, they are reusable, environmental friendly, and they can be used under continuous processes (Schuchardt, Sercheli and Vargas, 1998). The use of heterogeneous catalyst also makes it easier for final product separation and does not require washing step for crude ester. This catalyst is not affected by the presence of free fatty acids and water, they can be designed to produce higher selectivity, activity, and longer catalyst lifetimes (Schuchardt, Sercheli and Vargas, 1998). In literature, different number of acid and base heterogeneous catalyst has been used in the production of biodiesel.

Karmee *et al.* (2004) studied transesterification of Pongamia oil using ZnO, Hβ-Zeolite, and Montmorillonite K-10 as catalyst (11.5 wt. % of oil) at 120^{o}C with methanol/oil molar ratio of 10/1 to produce biodieel. The highest conversion of 83% was obtained from ZnO catalyst, while low conversions of 59 % and 47 % was obtained from Hβ-Zeolite and Montmorillonite K-10 catalyst, respectively (Karmee *et al.*, 2004). Wang and Jehng (2011) studied transesterification of soybean oil to produce biodiesel by using sodium aluminate as heterogeneous catalyst. About 82.0-93.9 % of methyl ester yield was obtained by using methanol/oil ratio of 12/1, 1.5 wt. % of catalyst at reflux temperature of methanol for reaction time varying from 10 to 60 min (Wang and Jehng, 2011). The catalytic durability tests indicated small decrease in activity by repeating the transesterification reaction for three times. Akbar *et al.* (2009), developed Na/SiO solid catalyst for transesterification of Jatropha oil for the production of biodiesel. About 99 % conversion was obtained by using methanol/oil molar ratio of 15/1 with catalyst amount of 6 wt. % at the reflux temperature of methanol (Akbar *et al.*, 2009). High activity of the catalysed was observed under mild conditions and relatively short reaction time of 45 min.

2.3.2.5. Non-catalysed transesterification

This type of transesterification process occur in the absence of catalyst. As the results, supercritical conditions such as high temperature and pressure is required. This method was developed due to challenges presented by biocatalysts and chemical catalyst (Schuchardt, Sercheli and Vargas, 1998). The reaction of non-catalysed transesterification is very slow and

gives very low yield. Hence, supercritical conditions are required to increase the reaction rate, production yields, and easier separation of products (Schuchardt, Sercheli and Vargas, 1998). Due to the supercritical conditions required, this method is energy intensive and highly costly.

2.3.3. Pyrolysis

Pyrolysis of triglyceride to produce biodiesel is not well established but it is becoming an increasing popular option in producing biofuels from biomass. More research has been done on the production of diesel from transesterification rather than on pyrolysis. There are significant advantages of pyrolysis process over transesterification including feedstock flexibility, low processing costs, and compatibility with infrastructure (Stumborg, Wong and Hogan, 1996). Pyrolysis of triglycerides can occur with and without catalyst. The pyrolysis process with and without catalyst is called thermal cracking and catalytic cracking, respectively. Pyrolysis in the presence of catalyst is commonly used.

2.3.3.1. Thermal cracking

Thermal cracking or pyrolysis is one of the promising technology that can be used in the production of biofuels from biomass. More studies has been done researchers to determine the reaction conditions, reaction products, and elucidate thermal decomposition pathways of thermal hydrocracking using different feedstocks. These studies include work done by Egloff and Morrell (1932) on the cracking of cottonseed oil operating at 445-485^{o}C and under the pressure of 0.93-1.3 MPa and they produced 57-60 % of gasoline rage hydrocarbons.

The thermal cracking process have been typically operated at temperatures ranging from 300-500^{o}C in a batch reactor under atmospheric pressure (Tsuji, Hasegawa and Masuda, 2003). Vegetable oils such as sunflower, safflower, soybean, palm oil, canola oil, used cooking oil, and castor oil have been used as the feedstock. Lima *et al*. (2004) studied the thermal cracking process of palm tree, soybean, and castor oil at temperatures ranging from 350-400^{o}C. Palm oil products contained largest heavy fraction and higher percentage of saturated fatty acids (Lima *et al*., 2004). Hydrocarbons and oxygenated organic compounds such as alkanes, alkenes, and carboxylic acids were formed. Alencar *et al*. (1983) studied the thermal cracking of palm oils, piqui, and babbassu at temperatures ranging from 300-500^{o}C under atmospheric pressure and main products formed were alkanes and 1-alkenes.

Most thermal cracking studies are done in batch reactors for research purposes. However, batch processes can be a problem in larger scale operations since they require frequent clean-up and

feeding of feedstocks after each run. Idem *et al.* (1996) used flow type reactor over fixed bed of inert materials to study the thermal cracking of canola oil at temperature range from 300-500^{o}C. About 54-100 % conversions were obtained and these conversions were highly affected by operating conditions. The main products formed were C_2-C_4 of olefins, C_5 of hydrocarbons, C_6 aliphatic hydrocarbons, and aromatics (Idem *et al*, 1996). Most of the feedstocks that have been studied are edible however; waste cooking oil can also be used. Dandik and Aksoy (1999) studied thermal cracking of waste cooking oil using fractionating pyrolysis ractor at temperature of 400-420^{o}C for about 180 min. The main products contained C_5-C_{17} of hydrocarbons containing aromatics, paraffins, cycloparaffins, olefins, and cycloolefins (Dandik and Aksoy, 1999).

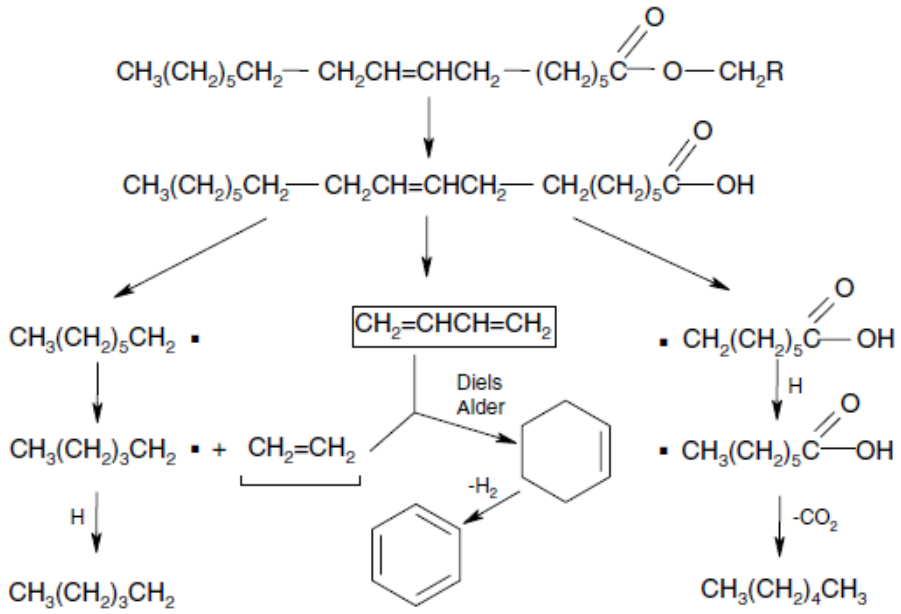


Figure 2. 12. Reaction mechanism of triglycerides for thermal cracking (Maher and Bressler, 2007).

There have been studies conducted on the reaction mechanism of triglycerides for thermal cracking, showed in Figure 2.12. This reaction mechanism was developed by Schwab *et al.*, (1988) to account for carboxylic acids, aromatics, alkadienes, alkanes, and alkenes formed during thermal cracking of unsaturated triglycerides. The formation of alkanes and alkenes are caused by the triglyceride cleavage of an RCCO radical generation. The C-C double bond cleavage is caused by the unsaturated sites of the triglycerides and this cleavage is a dominant reaction (Maher and Bressler, 2007). The degree of unsaturation of the triglyceride plays an important role in the cracking behaviour. For example, C_1-C_5 hydrocarbons can be produced through decomposition of oxygenated compounds (Maher and Bressler, 2007).

Thermal cracking products obtained from vegetable oils have thermal efficiency that is the same to diesel and can be potentially used as diesel substitute. Pyrolysis oil contains high water content which causes ignition problem and the problem can be solved further upgrading of the bio-oils. The products formed may be corrosive which is not ideal for direct usage in an engine. Lima, *et al.* (2004) investigated thermal cracking of soybean, palm tree, and castor oils. Deoxygenated and enriched hydrocarbon diesel-like fuel was produced through catalytically upgrading the soybean-derived bio-oil using HZSM-5 zeolite at 400^{o}C.

2.3.3.2. Catalytic cracking

Catalytic cracking is another alternative method that is used for upgrading triglycerides to produce biofuels. In this type of cracking, a catalyst is used to overcome the problem of high temperatures associated with thermal cracking. The use of catalyst also improves the total yield of the total products and considered cheaper due to less energy consumption. The catalytic products of vegetable oils mainly contains hydrocarbons of gasoline range consisting carboxylic acids, ketones, aldehydes, paraffins, cycloparaffins, and olefins (Taufiqurrahmi and Bhatia, 2011).

The concept of catalytic cracking is the same as thermal cracking, the only difference is that catalytic cracking requires the presence of catalyst to produce more of the desired products. The catalyst is not consumed during cracking, however, frequent renewal of the catalyst is required due to fouling by coke and metals lay-down on the catalyst and the timing of the catalyst renewal usually depends on feedstock and fouling (Taufiqurrahmi and Bhatia, 2011). Catalytic fouling is an issue during catalytic cracking. To minimise this issue, different pretreatment options have been developed such as hydrotreating or mild hydrocracking to present the excessive coking in the fluid catalytic cracking unit, deasphalting to prevent excessive coking on catalyst surfaces, demetallization to remove metals such as iron, vanadium, and nickel to catalyst deactivation and fouling, and the use of short operating time (Taufiqurrahmi and Bhatia, 2011).

Catalyst cracking is normally performed under solid acid catalyst such as zeolites and aluminosilicates. Zeolites have attractive properties such as high thermal stability, high acidity and high selectivity for the production of gasoline (Weitkamp, 1999). HZSM-5 is the most commonly used and most effective zeolites for cracking of triglycerides due to its high selectivity towards aromatic hydrocarbons (Weitkamp, 1999). Bhatia and Zabidi (1970) employed HZSM-5, HBeta and USY zeolites to study the cracking of palm oils in a fixed-bed

reactor at 350-450^{o}C under atmospheric pressure. About 99 %, 82 %, and 53 % conversion was obtained with gasoline selectivity of 28 %, 22 %, and 7 % from HZSM-5, HBeta and USY zeolites, respectively (Bhatia and Zabidi, 1970). The selectivity of gasoline increases to 40% when the mesoporous materials such as MCM-41 are employed because of the suppressed production of gaseous products (Bhatia and Zabidi, 1970). MCM-41 and SBA-15 are commonly used mesoporous catalyst due to their high selectivity on the formation of diesel fractions (Weitkamp, 1999). The degree of acidity of the mesopourous catalyst affects the production yield, low acidity results to high coke formation and lower gaseous products (Weitkamp, 1999). Ooi *et al.* (2004) studied the performance of MCM-41/BETA on the waste palm oil to produce hydrocarbons. About 35 % of maximum gasoline yield was obtained at 40 wt. % of Al-MCM-41 and Si/Al was used as the composite catalyst to prevent pre-cracking of the bulky molecule on the MCM-41 layer (Ooi *et al*., 2004).

2.3.4 Method selection

There are three types of production routes discussed in this section; hydroprocessing, transesterification, and pyrolysis. From these three types of production routes, only one suitable method must be chosen for the production of biogasoline and biojet from castor oil. The method is chosen based on the complexity of the process, operating conditions, type of catalyst, operating cost, production yield, quality products, and type of feedstock.

Transesterification consist of homogenous, heterogeneous, enzymatic, and non-catalysed transesterification. The chemical catalysis (homogenous and heterogeneous) transesterification produces very high conversion and the reaction conditions can be controlled to give the desired production yield. The cost of production is cheap and the methanol produced can be recycled (Schuchardt, Sercheli and Vargas, 1998). However, the process and the later disposal process is complex and the reaction temperature is relatively high. The waste water produced by process pollutes the environment and the methanol recycle stream requires installation which increases the cost (Schuchardt, Sercheli and Vargas, 1998). The enzymatic transesterification requires moderate reaction conditions, small amount of methanol, and have no pollution to the environment. Enzymatic transesterification do not give high conversion and reaction rate as compared to chemical catalysis and the chemicals that exist in the process may be poisonous to the enzyme resulting to catalyst deactivation (Schuchardt, Sercheli and Vargas, 1998). Non-catalysed transesterification is friendly to the environment and can be easily

controlled. However, it requires very high temperature and pressure which leads to high production cost and waste energy.

Pyrolysis is also one of the production routes that can be used to produce biofuels. Pyrolysis can be done in the present of the catalyst (catalytic cracking) and in the absence of the catalyst (thermal cracking). The catalytic cracking method is more preferred than thermal cracking because it does not require intensive operating conditions (high temperature). There are significant advantages of pyrolysis process over transesterification including feedstock flexibility, low processing costs, and compatibility with infrastructure (Stumborg, Wong and Hogan, 1996). There is also a reduction of water volume during pyrolysis due to the high operating temperature. The pyrolysis process is very complex and requires high investment and operating costs. The flue gases produced during pyrolysis need to be further treated by installing air purification unit (Stumborg, Wong and Hogan, 1996). The waste ashes produced are regarded dangerous and requires disposal.

Hydroprocessing removes atoms such as sulphur, oxygen and nitrogen to convert triglyceride molecules into paraffinic hydrocarbons. Hydroprocessing of biomass has currently gained so much attention compared to other production routes. This is because the hydroprocessed fuel chemical composition is very close to the mineral diesel fuel and hence it can meet the automotive industries requirement better than the diesel obtained from transesterification (Treese *et al*., 2015). The capital and operating cost of hydroprocessing is low and the process can be efficiently used at low temperatures. Hydroprocessing has also advantages in terms of the flexibility of feedstock because the process can utilize low quality feeds such as waste cooking oil, animal fats, and vegetable oils (Treese *et al*., 2015). The main products of hydroprocessing of vegetable oils consist mostly of paraffinic hydrocarbons, which are mostly suitable for application in combustion engine. The separation stage of the by-products produced from the process is not as complex as in the transesterification.

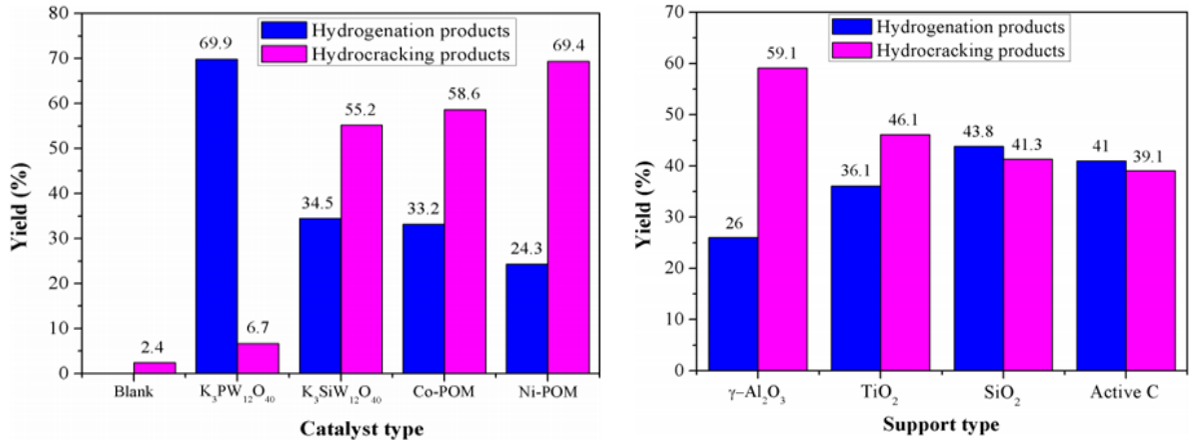
Therefore, hydroprocessing is considered to be the best method that can be used in this project for the production of biogasoline and biojet from castor oil. Hydrocracking method was used for cracking castor oil into biofuels in the presence of catalyst. Hydrocracking is the ideal method that can used because it can simultaneously produce high quality biojet and biogasoline by only using one catalyst and this method is flexible in the selectivity between light and middle distillates.

2.4. Catalyst selection

Catalyst selection is one of the main problems during hydrocracking process. It is very important that the catalyst used is highly selective to the desired catalyst. Amorphous and zeolite type of catalyst are commonly used for hydrocracking. Amorphous catalyst are primarily silica-alumina and their acidity and pore structures can be controlled to give the high yield of middle distillates (Ali, Tatsumi and Masuda, 2002). Zeolites type catalyst are aluminosilicate structure and they have high catalytic activity with strong acidity but they have low selectivity for middle distillates. Zeolites catalyst are mostly used by industries (Ali, Tatsumi and Masuda, 2002).

The hydrocracking catalyst contains two types of active sites; acidic sites and metal sites. The acidic sites is responsible for cracking the C-C bonds of the high molecular weight hydrocarbons and isomerization while the metal sites is responsible for hydrogenation and dehydrogenation (Coker, 2018). Catalyst such as CoMo, NiMo, and NiW are commonly used catalyst and they are usually supported by zeolite, ammonia, and alumina (Coker, 2018). Nickel based catalysts are mostly used currently because of its high catalytic activity on the hydrocracking of sulphur free heavy hydrocarbons (Coker, 2018). It was also found that the selectivity of this catalyst is highly dependent on the type of support materials and the dispersion of the metal in the supports.

Meller *et al. (*2016) investigated hydrocracking of castor oil using different bifunctional polyoxometalate (POM) catalyst to determine the most selective catalyst. The results are shown in Figure 2.13.



(a) (b)

Figure 2.13. (a) Hydrocracking and hydrogenation products yields (%) of POM catalysts: $K_3PW_{12}O_{40}$, $K_4SiW_{12}O_{40}$, Co-POM and Ni-POM and (b) Yields (%) of hydrocracking products and hydrogenation products for 9.1 % Ni-POM supported over different supports: γ-Al_2O_3, TiO_2, SiO_2, and active C (Meller *et al.*, 2016).

Ni-POM was found to be the most effective POM catalyst in the hydrocracking of castor oil compared to the other catalyst used. The silicon heteroatom POM catalyst is more effective when compared to phosphorus POM catalyst. $K_4SiW_{12}O_{40}$ produced high hydrocracking products yield than $K_3PW_{12}O_{40}$. The most suitable catalyst Ni-POM was then incorporated with different supports to increase the activity of the catalyst during castor oil hydrocracking. Four different of support were used to determine the most suitable support that can be used with Ni-POM. Ni-POM/Al2O3 catalyst gave the higher yield of hydrocracking products.

From the results obtained by Meller *et al.* (2016), we then can conclude that the catalyst type used during hydrocracking highly affects the production yield as well as the type of catalyst support used. Therefore, it is very important to select the most suitable catalyst and catalyst support based on your feedstock to maximise the production yield.

2.4.1. Nickel-based catalysts

Nickel-based catalysts are the most frequently used catalysts during organic synthesis and in large number of industrial processes ad this is because of their ability of withstand reaction conditions and their high activity (De, Zhang, Luque and Yan, 2016). One of the main characteristics of nickel catalyst are its ability to absorb large amount of hydrogen, which therefore increases the efficiency of the reaction (De, Zhang, Luque and Yan, 2016). Nickel catalyst is considered to be cheap and efficient relative to other competing materials. Zeolites are widely used as the catalyst support in the hydrocracking process because they highly improve the catalyst selectivity, activity and stability (Ali, Tatsumi and Masuda, 2002).

Suwannasom *et al.* (2016) investigated the hydrocracking of palm oil using Ni-Mo catalyst supported over HY zeolites to produce jet fuels. Under the optimum conditions, about 36.60 % of jet fuel products were produced at temperature of 418.85^{o}C, reaction time of 119.37 min, and catalyst weight of 3.16 wt. % (Suwannasom *et al.*, 2016). Sotelo-Boyás *et al.* (2011) studied the hydrocracking of rapeseed oil using Pt/H-Y zeolite, Pt/HZSM-5 and sulfided NiMo/γ- Al_2O_3 catalyst for the production of diesel. Ni-Mo/γ- Al_2O_3 gave the highest conversion to liquid hydrocrabons in the boiling range of diesel fraction over a temperature range of 300-400^{o}C, reaction time of 1-6 h, and hydrogen pressure of 5-11MPa (Sotelo-Boyás *et al.*, 2011). Mampuru *et al*. (2019) studied the hydrocracking of waste cooking oil using bi-functional Ni-Mo/alumina catalyst to produce biogasoline. The maximum production of 59.50 wt. % of biogasoline was obtained at reaction temperature of 250^{o}C, 5 wt. % of nickel calcinated at 300^{o}C, and reaction time of 1 h (Mampuru *et al*., 2019). Al-Muttaqii *et al*. (2019) studied the hydrocracking of coconut oil using Ni-Fe/HZSM-5 catalyst in a batch reactor at three reaction temperatures (350, 375, and 400^{o}C). The highest production yield was obtained at 400^{o}C with 39.24 % and 18.4 % of n-parrafin and biogasoline, respectively (Al-Muttaqii *et al*., 2019).

2.4.2. Carbon materials as catalyst supports

Carbon materials plays an important role as a catalyst support during enzymatic and chemical biomass transformation because of their large specific surface area, relative inertness, excellent conductivity, and high porosity (Lam and Luong, 2014). Carbon materials can be prepared from residual biomass, which make them more attractive because of the reduction of carbon dioxide released to the atmosphere (Lam and Luong, 2014). The catalytic activity of metallic nanoparticles and enzymes can be improved by decorating with carbon materials. Metal and enzymatic catalyst supported on carbon materials have more significant advantages when compared to oxide materials (Lam and Luong, 2014). The carbon materials includes carbon dots, carbon onions, carbon nanotubes, grapheme, and carbon monoliths can be used as catalyst support (Lam and Luong, 2014).

Less work has been done on using carbon materials as support for hydrocracking process of vegetable oils. This project focuses on the hydrocracking of castor oil using nickel nanoparticles supported on carbon dot to determine the activity and selectivity of both nickel and carbon on the production of biojet and biogasoline.

2.5. Biofuel products from castor oil

The main biofuel products than can be produced from hydrocracking of castor oil are biodiesel, biogasoline, and biojet. More work has been done on maximising the production of biodiesel and not biojet and biogasoline.

2.5.1. Biodiesel

Biodiesel is the form of diesel fuel derived from biomass. It is one of the most employed biofuels that is often used for partial replacement of petroleum based diesel fuel. Biodiesel has gained more attention due to its fuel properties and compatibility (Demirbaş, 2008). These properties includes renewable, non-toxic, essentially free of sulphur and aromatics, excellent lubricity, and higher biodegradability than fossil fuels (Demirbaş, 2008). Biodiesel is environmentally friendly and can be used in any diesel engine without replacing the current design technology. Biodiesel is mostly used as blend with diesel and the blending promote cleaner emission with whiter smoke and less soot particles (Demirbaş, 2008). Biodiesel can be easily produced from castor oil. The summary of physiochemical properties of biodiesel from castor and commercial aviation fuel is shown in Table 2.9.

Table 2.9. Physiochemical properties of biodiesel international standards and biodiesel obtained from castor oil (Kandaramath Hari, Yaakob and Binitha, 2015).

Specification	**ASTM D1655**	**DEF STAN 91-91**	**Biodiesel from castor oil (B100)**
Density at 15°C, g/cm^3	0.775-0.840	0.775-0.840	0.924 - 0.9268
Viscosity at -20°C, mm^2/s	Max 8.0	Max 8.0	15.98
Acid no., mg KOH/g	0.100	0.015	0.220 – 1.87
Flash point, °C	Min 38	Min 38	165 – 186.5
Heat of combustion, Mj/kg	Min 42.8	Min 42.8	35.86 - 37.9
Freezing point, °C	Max -40	Max -47	
Sulfur, wt. %	0.3	0.3	0.01

2.5.2. Biogasoline

Biogasoline is a liquid fuel obtained from biomass that is used for spark-ignition engines (Zhao, 2010). Biogasoline produced from castor oil is fully compatible with petroleum gasoline. However, the performance of biogasoline in spark ignition engines is still tested by researchers

(Zhao, 2010). Biojet and biogasoline are produced by further converting biodiesel through cracking or transesterification.

Gasoline contains homogenous mixture of lightweight hydrocarbons with carbon range of C_5-C_{10}. This mixture of hydrocarbons contains alkanes (paraffins), alkenes (olefins), and cyclo-alkanes (naphthenes) (Qi and Lee, 2014). Properties such as volatility and knocking resistance are the most important properties of gasoline fuels, whereas properties such as surface tension, viscosity, and ignition tendency are important fuel properties for diesel fuel (Qi and Lee, 2014). The properties of gasoline fuel are shown in Figure 2.10.

Table 2. 10. Properties of gasoline fuel (Qi and Lee, 2014).

Properties	**Gasoline**
Chemical formula	C_5-C_{10}
Molecular weight	95-120
LHV (MJ/kg)	42.8
Density (kg/m^3)	0.742
Boiling point (^{o}C at 1 atm)	25-215
Flash point (^{o}C at 1 atm)	-40
Auto-ignition temperature (^{o}C)	~300
Latent heat of evaporation (KJ/kg)	380-500
Reid vapour pressure (KPa)	60-90
Octane number: RON	90
MON	81-89
Composition (C,H,and O) (wt. %)	86,14,0

2.5.3. Biojet

Biojet is the type of aviation fuel obtained from biomass used in aircraft powered by gas-turbine engines. Jet fuel is sometimes called kerosene and they contain carbon range of C_9-C_{16} with boiling range of 150-290^{o}C (Shelton, 1979). Jet A and Jet A-1 are the most commonly used fuels commercial aviation fuels produced to a standardized international specification. Jet B is another commonly used jet fuel in civilian turbine-engine. Jet B fuel is rarely used because of it lighter composition which makes it more dangerous to handle, except in very cold climates because they enhance cold-weather performance (Shelton, 1979). TS-1 is also another type of jet fuel used for enhancing cold-weather performance and made to Russian standard GOST

10227 (Shelton, 1979). TS-1 has very low freezing point and is highly volatile when compared to Jet A-1.

Table 2. 11. Properties of Jet A, Jet A-1, Jet B, and TS-1 (Shelton, 1979).

Fuel	**Jet A**	**Jet A-1**	**TS-1**	**Jet B**
Specification	ASTM D 1655	DEF STAN 91-91	GOST 10277	CGSB-3.22
Acidity, mg KOH/g	0.10	0.015	0.7	0.10
Aromatics, % vol.max	25	25	22 (%mass)	25
Sulfur, %mass	0.30	0.30	0.25	0.40
Vapor pressure, kPa,max	-	-	-	21
Flash point, ^{o}C, min	38	38	28	-
Density, 15^{o}C, kg/m^{3}	775-840	775-840	Min 774@20^{o}C	750-801
Freezing point , ^{o}C, min	-40	-47	-50	-51
Viscosity, -20^{o}C, mm^{2}/sec,max	8	8	8	-
Heat of combustion, MJ/kg, min	42.8	42.8	42.9	42.8
Smoke point, mm, min	18	19	25	3.0
Napthalenes, vol%, max	3	3	-	3

2.7. References

Abdalla, and Babiker. 2014. Extraction, Refining and Characterization of Sudanese Castor Seed Oil. *Journal of Chemical Engineering*, 2, p.1-8.

Akbar E., Binitha N., Yaakob Z., Kamarudin S., and Salimon J., 2009. Preparation of Na doped SiO2 solid catalysts by the sol-gel method for the production of biodiesel from jatropha oil. *Green Chemistry*, 11(11), p.1862-2001.

Akpan U.G., Jimoh A., and Mohammed A.D., 2006. Extraction, characterization and modification of castor seed oil. *Leonardo Journal of Sciences*, 8, pp.43-52.

Ali M., Tatsumi T., and Masuda, T., 2002. Development of heavy oil hydrocracking catalysts using amorphous silica-alumina and zeolites as catalyst supports. *Applied Catalysis A: General*, 233(1-2), pp.77-90.

Al-Muttaqii M., Kurniawansyah F., Prajitno D., and Roesyadi, A., 2019. Hydrocracking of Coconut Oil over Ni-Fe/HZSM-5 Catalyst to Produce Hydrocarbon Biofuel. *Indonesian Journal of Chemistry*, 19(2), p.319.

Berman P, Nizri S, Wiesman Z., 2011. Castor oil biodiesel and its blends as alternative fuel. *Biomass Bioenergy*, 35(7):pp.2861–2866.

Bhatia F., and M. Zabidi, N., 1970. Catalytic Cracking of Palm Oil over Zeolite Catalysts: Statistical Approach. *IIUM Engineering Journal*, 2(1), p.60-156.

Bhuiya M.M.K., Rasul, M.G., Khan M.M.K, Ashwath N., Azad A.K., and Mofijur M. 2015. Optimization of oil extraction process from Australian Native Beauty Leaf Seed. (Calophyllum innophyllum). *7th International Conference on Applied Energy-ICAE2015. Energy Procedia*, 75: pp.56-61.

Bordonal R., Carvalho J., Lal R., de Figueiredo E., de Oliveira B. and La Scala N., 2018. Sustainability of sugarcane production in Brazil. A review. *Agronomy for Sustainable Development*, 38(2): pp.123-205.

Cheremisinoff N., and Rosenfeld P., 2009. *Best Practices in the Petroleum Industry $C*. Reino Unido: William Andrew.

Coker A., 2018. *Petroleum Refining Design and Applications Handbook*. 1st ed. Hoboken: John Wiley and Sons, Inc.

Dandik L., and Aksoy H.A., 1999. Effect of catalyst on the pyrolysis of used oil carried out in a fractionating pyrolysis reactor. *Renew. Energy, 16,* pp.1007–1010.

Danlami J.M., Arsad A., Zaini M.A.A., and Sulaiman H., 2014. A comparative study of various oil extraction techniques from plants. *Reviews in Chemical Engineering,* 30(6): pp.605-626.

Dasari, Swaroopa and Goud, Vaibhav, 2014. Effect of pre-treatment on solvents extraction and physico-chemical properties of castor seed oil. *Journal of Renewable and Sustainable Energy*, 10(6): pp.805-967.

Demirbaş A., 2008. Biodiesel: a realistic alternative for diesel engines. *Focus on Catalysts*, 2008(12), p.8-45.

De S., and Luque R., 2014. Upgrading of waste oils into transportation fuels using hydrotreating technologies. Biofuel Research Journal, 4(1), pp. 107-109.

De S., Zhang J., Luque R., and Yan N., 2016. Ni-based bimetallic heterogeneous catalysts for energy and environmental applications. *Energy & Environmental Science*, 9(11), pp.3314-3347.

EIA, 2018. Biomass-Energy Explained, Your Guide To Understanding Energy. Independent Energy & Statistics.

Egloff G., and Morrell J., 1932. The Cracking of Cottonseed Oil. *Industrial & Engineering Chemistry*, 24(12), pp.1426-1427.

Faugno, S., Del Piano, L., Crimaldi, M., Ricciardiello, G. and Sannino, M., 2016. Mechanical oil extraction of Nicotiana tabacum L. seeds: analysis of main extraction parameters on oil yield. *Journal of Agricultural Engineering*, 47(3), pp.142-147.

Ghazali Q., and Yasin N., 2016. The effect of organic solvent, temperature and mixing time on the production of oil from Moringa oleiferaseeds. *IOP Conference Series: Earth and Environmental Science*, 36, p.012053.

Goff M., Bauer N., Lopes S., Sutterlin W., and Suppes, G., 2004. Acid-catalyzed alcoholysis of soybean oil. *Journal of the American Oil Chemists' Society*, 81(4), pp.415-420.

Gonfa Keneni Y., and Mario Marchetti J., 2017. Oil extraction from plant seeds for biodiesel production. *AIMS Energy*, 5(2), pp.316-340.

Gupta V., Prasad K., Bakshi M., and Langar P., 1986. Improving the nutritive value of groundnut shells through fungal cultivation. *Agricultural Wastes*, 16(3), pp.161-169.

Gupta V., 2014. *Bioenergy Research*. Waltham, MA: Elsevier.

Herskowirz M., Landau M., Reizner I., Kaliya M., 2006. Production of Diesel Fuel from Vegetable and Animal Oils. U.S. *Patent Application US2006207166*.

Hinková A. and Bubník Z., 2013. Sugar beet as a raw material for bioethanol production. *Czech Journal of Food Sciences*, 19(6), pp.224-234.

Hasanudin H., Rachmat A., Said M., and Wijaya, K., 2019. Kinetic Model of Crude Palm Oil Hydrocracking over Ni/Mo ZrO2–Pillared Bentonite Catalyst. *Periodica Polytechnica Chemical Engineering*, 64(2), pp.238-247.

Idem R.O., Katikaneni S.P.R., and Bakhshi, N.N, 1996. Thermal cracking of canola oil: Reaction products in the presence and absence of steam. *Energy Fuels, 10*, pp.1150–1162.

Ikya J.K., Umenger L.N., and Iorbee A., 2013. Effects of extraction methods on the yield and quality characteristics of oils from shea nut. *Journal of Food Resource Science*, 2, pp.1-12.

ISHIGAKI USA LTD. 2020. *SCREW PRESS ISGK-A - ISHIGAKI USA LTD*.

Jakkula J., Niemi V., Nikkonen J., Purola V.M., Myllyoja J., Aalto P., Lehtonen J., and Alopaeus V., 2004. Process for producing a hydrocarbon component of biological origin. *US7232935B2, 20030905*.

Jamil F., Al-Muhatseb A., Al-Haj L., Al-Hinai M., and Baawain M., 2017. Phoenix Dactylifera Kernel Oil Used As Potential Source for Synthesizing Jet Fuel and Green Diesel. *Energy Procedia*, 118, pp.35-39.

Jin W., Pastor-Pérez L., Shen D., Sepúlveda-Escribano A., Gu S. and Ramirez Reina T., 2019. Catalytic Upgrading of Biomass Model Compounds: Novel Approaches and Lessons Learnt from Traditional Hydrodeoxygenation – A Review. *ChemCatChem*, 11(3), pp.924-960.

Kandaramath Hari, T., Yaakob Z., and Binitha N., 2015. Aviation biofuel from renewable resources: Routes, opportunities and challenges. *Renewable and Sustainable Energy Reviews*, 42, pp.1234-1244.

Karmee S., Mahesh P., Ravi R., and Chadha, A., 2004. Kinetic study of the base-catalyzed transesterification of monoglycerides from pongamia oil. *Journal of the American Oil Chemists' Society*, 81(5), pp.425-430.

Keera S., El Sabagh S. and Taman A., 2018. Castor oil biodiesel production and optimization. *Egyptian Journal of Petroleum*, 27(4), pp.979-984.

Kenney K. and Ovard L., 2013. Advanced feedstocks for advanced biofuels: transforming biomass to feedstocks. *Biofuels*, 4(1), pp.1-3.

Kim S., Jung S., Park Y. and Park K., 2007. Lipase catalyzed transesterification of soybean oil using ethyl acetate, an alternative acyl acceptor. *Biotechnology and Bioprocess Engineering*, 12(4), pp.441-445.

Kim S.K., Han J.Y., Lee H., Yum T., Kim Y., and Kim J., 2014. Production of Renewable Diesel via Catalytic Deoxygenation of Natural Triglycerides: Comprehensive Understanding of Reaction Intermediates and Hydrocarbons. *Applied Energy*, 116, pp.199-205.

Ko C., Park S., Jeon J., Suh D., Jeong K., and Park Y., 2012. Upgrading of biofuel by the catalytic deoxygenation of biomass. *Korean Journal of Chemical Engineering*, 29(12), pp.1657-1665.

Krár M., Kovács, S., Kalló D, and Hancsók, J., 2010. Fuel purpose hydrotreating of sunflower oil on CoMo/Al2O3 catalyst. *Bioresource Technology*, 101(23), pp.9287-9293.

Krár, Márton and Kasza, Tamás and Kovács, Sándorand Kalló, Dénes and Hancsók, Jenő, 2011. Bio gas oils with improved low temperature properties. *Fuel Processing Technology*. 92, pp.886–892.

Lam E., and Luong, J., 2014. Carbon Materials as Catalyst Supports and Catalysts in the Transformation of Biomass to Fuels and Chemicals. *ACS Catalysis*, 4(10), pp.3393-3410.

Lima D.G., Soares V.C.D., Ribeiro E.B., Carvalho D.A., Cardoso E.C.V., and Rassi F.C., 2004. Diesel-like fuel obtained by pyrolysis of vegetable oils. *Journal of Analytical and Applied Pyrolysis*, 71, pp.987–996.

Liu S., Zhu Q., Guan Q., He L., and Li, W., 2015. Bio-aviation fuel production from hydroprocessing castor oil promoted by the nickel-based bifunctional catalysts. *Bioresource Technology*, 183, pp.93-100.

Luque, R., 2011. *Handbook of biofuels production*. Oxford [u.a.]: Woodhead.

Maher K., and Bressler D., 2007. Pyrolysis of triglyceride materials for the production of renewable fuels and chemicals. *Bioresource Technology*, 98(12), pp.2351-2368.

Mampuru, M., Nkazi, D. and Mukaya, H., 2019. Hydrocracking of waste cooking oil into biogasoline in the presence of a bi-functional Ni-Mo/alumina catalyst. *Energy Sources, Part A: Recovery, Utilization, and Environmental Effects*, 42(20), pp.2564-2575.

Marlinda L., Al-Muttaqii M., Roesyadi A., and Danawati, H.P., 2016. Production of Biofuel by Hydrocracking of Cerbera Manghas Oil Using Co-Ni/HZSM-5 Catalyst: Effect of Reaction Temperature. J. Pure App. *Chem. Res*., 5(3), pp.189-195.

Meller E., Gutkin V., Aizenshtat Z., and Sasson Y., 2016. Catalytic Hydrocracking - Hydrogenation of Castor Oil Fatty Acid Methyl Esters over Nickel Substituted Polyoxometalate Catalyst. *ChemistrySelect*, 1(20), pp.6396-6405.

Meller E., Green U., Aizenshtat Z., and Sasson Y., 2014. Catalytic deoxygenation of castor oil over Pd/C for the production of cost effective biofuel. *Fuel*, 133, pp.89-95.

Mortensen P., Grunwaldt J., Jensen P. and Jensen A., 2013. Screening of Catalysts for Hydrodeoxygenation of Phenol as a Model Compound for Bio-oil. *ACS Catalysis*, 3(8), pp.1774-1785.

Musa I., 2016. The effects of alcohol to oil molar ratios and the type of alcohol on biodiesel production using transesterification process. *Egyptian Journal of Petroleum*, 25(1), pp.21-31.

Muzenda E., Kabuba J., Mdletye P., and Belaid M., 2012. Optimization of process parameters for castor oil production. *Proceedings of the World Congress on Engineering 2012 Vol. III WCE 2012*, July, 4-6, 2012, London, U.K.

Mwithiga G., and Morias L., 2007. A Study of Yield Characteristics during Mechanical Oil Extraction of Preheated and Ground Soybeans. *Journal of Applied Sciences Research*, 3(10): pp.1146-1151.

M.W. WATERMARK, 2020. *M.W. Watermark Filter Press*

Ogunniyi D.S., 2006. Castor Oil: a vital industrial raw material. *Bioresource Technology*, 97:pp.1086 – 1091.

Olaniyan A., 2010. Effect of Extraction Conditions on the Yield and Quality of Oil from Castor Bean. *Journal of Cereals and Oilseeds*, 1 (2), pp.24-33.

Ooi Y., Zakaria R., Mohamed A. and Bhatia S., 2004. Synthesis of composite material MCM-41/Beta and its catalytic performance in waste used palm oil cracking. *Applied Catalysis A: General*, 274(1-2), pp.15-23.

Panwar N., Shrirame H., Rathore N., Jindal S., Kurchania A., 2013. Performance evaluation of a diesel engine fueled with methyl ester of castor seed oil. *Appl Therm Eng*, 30(2–3), pp245–249.

Patel V., Dumancas G., Viswanath L., Maples R. and Subong B., 2016. Castor Oil: Properties, Uses, and Optimization of Processing Parameters in Commercial Production. *Lipid Insights*, 9, p.LPI.S40233.

Patil, P. and Deng, S., 2009. Optimization of biodiesel production from edible and non-edible vegetable oils. *Fuel*, 88(7), pp.1302-1306.

Petri J.A., Marker T.L., 2006. Production of diesel fuel from biorenewable feedstocks. *US7511181B2, 20080225*.

Pinto F., Martins M., Gonçalves M., Costa P., Gulyurtlu I., Alves A., and Mendes B., 2013.Hydrogenation of Rapeseed Oil for Production of Liquid Bio-Chemicals. *Applied Energy*, 102, pp.272-282.

Qi D., and Lee C., 2014. Combustion and emissions behaviour for ethanol–gasoline-blended fuels in a multipoint electronic fuel injection engine. *International Journal of Sustainable Energy*, 35(4), pp.323-338.

Sajjadi B., Raman A., Arandiyan H., 2016. A comprehensive review on properties of edible and non-edible vegetable oil-based biodiesel: composition, specifications and prediction models. *Renew Sust Energ Rev* 63: pp.62‑92.

Scherzer J., and Gruia A., 1996. *Hydrocracking Science and Technology*. New York: MARCEL DEKKER, INC.

Schuchardt U., Sercheli R., and Vargas R., 1998. Transesterification of vegetable oils: a review. *Journal of the Brazilian Chemical Society*, 9(3), pp.501-607.

Shafaghat H., Rezaei P., and Ashri Wan Daud W., 2015. Effective parameters on selective catalytic hydrodeoxygenation of phenolic compounds of pyrolysis bio-oil to high-value hydrocarbons. *RSC Advances*, 5(126), pp.103999-104042.

Shelton E., 1979. *Aviation Turbine Fuels, 1978*. Bartlesville, OK: Bartlesville Energy Technology Center, U.S. Dept. of Energy.

Shojaeefard M., Etgahni M., Meisami F., Barari A., 2013. Experimental investigation on performance and exhaust emissions of castor oil biodiesel from a diesel engine. *Environ Technol*, 34(13–16): pp.2019–2026.

Šimáček P., Kubička, D. Šebor, G., and Pospíšil, M., 2010. Fuel properties of hydroprocessed rapeseed oil. *Fuel*, 89(3), pp.611-615.

Sinha L.K., Haddar S., and Majumdar G.C., 2015. Effect of operating parameter on mechanical expression of solvent-soaked soybean grits. *Journal of Food Science and Technology*, 52(5): pp.2942-2949.

Soccol C., Brar S., Faulds C. and Ramos L., 2016. *GREEN FUELS TECHNOLOGY: BIOFUELS*. Switzerland: SPRINGER.

Sotelo-Boyás R., Liu Y., and Minowa T., 2011. Renewable Diesel Production from the Hydrotreating of Rapeseed Oil with Pt/Zeolite and NiMo/Al2O3Catalysts. *Industrial & Engineering Chemistry Research*, 50(5), pp.2791-2799.

Speight J., 2013. *Heavy and Extra-Heavy Oil Upgrading Technologies*. Oxford, UK: Gulf Professional Pub.

Stumborg M., Wong A. and Hogan, E., 1996. Hydroprocessed vegetable oils for diesel fuel improvement. *Bioresource Technology*, 56(1), pp.13-18.

Suib S., 2013. New developments in zeolite science and technology edited by studies in surface science and catalysis. *Journal of Catalysis*, 106(1), p.327.

Suwannasom P., Kham-or P. and Ruangviriyachai C., 2016. Jet fuel production from palm oil by catalytic hydrocracking using a Ni–Mo/HY catalyst. *Energy Sources, Part A: Recovery, Utilization, and Environmental Effects*, 38(23), pp.3549-3556.

Taufiqurrahmi N., and Bhatia S., 2011. Catalytic cracking of edible and non-edible oils for the production of biofuels. *Energy Environ. Sci.*, 4(1), pp. 1087-1112.

Tran N., Uemura Y., Chowdhury S., and Ramli A., 2014. A Review of Bio-Oil Upgrading by Catalytic Hydrodeoxygenation. *Applied Mechanics and Materials*, 625, pp.255-258.

Treese S., Pujadó P., Jones D., Treese S., Pujadó P., Jones D., LLC, P. and Company), U., 2015. Handbook of Petroleum Processing*: Hydrocracking in Petroleum Processing*. SPRINGER.

Tsuji T., Hasegawa K., and Masuda T., 2003. Thermal cracking of oils from waste plastics. *Journal of Material Cycles and Waste Management*, 5(2), pp.102-106.

Usomboon N., Santikunaporn M., and Butnar, S., 2012. Biogasoline Production from Bio-Diesel via Catalytic Cracking Reaction on Platinum Zeolite Catalyst. *GMSARN International Journal*, 6:pp. 17-22.

Verma D., Rana B.S., Kumar R., Sibi M.G., and Sinh, A.K., 2015. Diesel and Aviation Kerosene with Desired Aromatics from Hydroprocessing of Jatropha Oil over Hydrogenation Catalysts Supported on Hierarchical Mesoporous SAPO-11. *Applied Catalysis A: General*, 490, pp.108-116.

Verma P., Zare A., Jafari M., Bodisco T., Rainey T., Ristovski Z., and Brown R., 2018. Diesel engine performance and emissions with fuels derived from waste tyres. *Scientific Reports*, 8(1), pp.201-222.

Wang Y., and Jehng J., 2011, Hydrotalcite-like compounds containing transition metals as solid base catalysts for transesterification, *Chemical Engineering Journal*, 175, pp.548-554.

Wang T., 2019. Global biofuel production by select country 2018. Statista.

Weitkamp, J., 1999. *Catalysis and Zeolites*. Berlin: Springer.

Willems, Paul and Kuipers, Norbert and Haan, A.B., 2008. Hydraulic pressing of oilseeds: Experimental determination and modeling of yield and pressing rates. *Journal of Food Engineering*, 89: pp.8-16.

Wu Y., Zhou R., Wang Z., Wang B., Yang Y., Ju X.,and He R., 2019. The effect of refining process on the physicochemical properties and micronutrients of rapeseed oils. *PLOS ONE*, 14(3), p.e0212879.

Yusuf A.K., P.A.P. Mamza P.A.P., Ahmed A.S., and Agunwa4 U., 2015. Extraction and characterisation of castor seed oil from ricinus communis linn. *International Journal of Science, Environment and Technology*, 4(5): pp.1392 – 1404.

Yusup S. and Khan M., 2010. Base catalyzed transesterification of acid treated vegetable oil blend for biodiesel production. *Biomass and Bioenergy*, 34(10), pp.1500-1504.

Zhao H., 2010. *Advanced Direct Injection Combustion Engine Technologies And Development*. Boca Raton: CRC Press.

Chapter 3: Castor oil extraction

This chapter is about producing castor oil from castor seeds using solvent extraction optimised by using response surface methodology (RSM) and further characterising the produced oil to determine whether the produced castor oil meet the specification standard.

3.1. Introduction

The use of oil seeds for industrial application has been increasing in the last three decades. The use of edible oil has been increasing and more research associated with edible oil has been done. More research has now shifted to the use of non-edible oil because of food competition associated with edible oils. Castor oil is one of the non-edible oil that can be used for different industrial application such as in manufacturing of biofuel, paints, inks, soaps, and lubricants (Mubofu, 2016). Castor seeds grows well in warm climate conditions but not at temperatures above 38^{o}C (Patel *et al*., 2016). They can be widely produced in Africa especially in tropical summer rainfall areas.

Castor oil can be extracted from castor seeds using different methods such as mechanical pressing, solvent extraction, and supercritical fluid extraction (Nde and Foncha, 2020). Solvent extraction is commonly used because it is simple and easy to run. For successful solvent extraction, parameters such as time, temperature, type and amount of solvent, and the quality of feedstocks need to be extensively studied. To optimise these parameters, RSM has been described as the most suitable and easy method (Khuri, 2017). Solvents such as ethanol, hexane, and petroleum ether are used, the most suitable solvent must be determined. Hexane is commonly used due its low boiling point. (Ibrahim and Zaini, 2018).

Different researchers studied the effects of time, temperature and see/solvent ratio on the oil yield and their findings are shown in Figure 3.1. These parameters are described as the major parameters that affects oil yield during solvent extraction (Khuri, 2017).

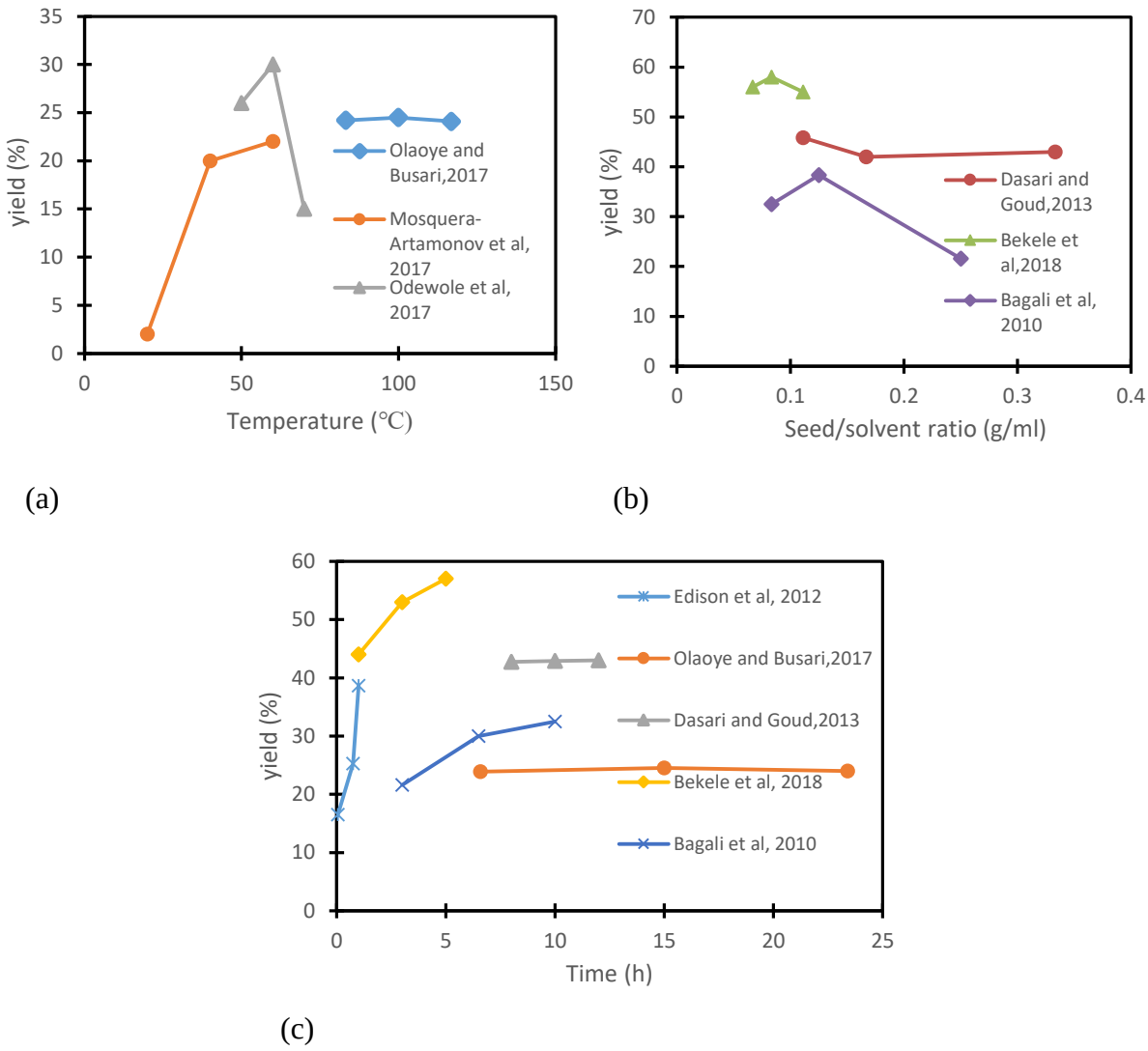


Figure 3. 1. Effect of (a) temperature (b) seed/solvent ratio, and (c) time on the oil yield from different authors

The increase in oil yield with the increase in extraction temperature has been observed from different researchers in Figure 3.1 (a) until optimum temperature is reached. Mosquera-Artamonov *et al*. (2017) observed that the oil yield increased up to and Odewole *et al.* (2017) observed that after 60^{o}C, the oil yield start to decrease. Olaoye and Busari (2017) studied the effect of temperature from 83-116^{o}C and the effect not highly significant. It is very important to determine the optimum extraction temperature for maximum extraction of oil.

Different trends was observed on the effects of seed/solvent ratio on the oil yield. Bagali *et al*. (2010), and Bekele *et al.* (2018) observed that oil yield increase until optimum seed/solvent ratio is reached. Different oil yield were obtained and this is because the oil were extracted at different extraction time and were obtained from different places. Bekele *et al.* (2018) obtained

the castor seeds from Ethiopia and Bagali *et al.* (2010) from India. The conditions at which the castor seeds plant were grown affect the quality and quantity of the oil extracted.

Based on the results observed from different researchers, it can then be concluded that the extraction parameters requires optimization for maximum extraction of oil. It is very important to extensively study these parameters for different kinds of oil seeds. This study focuses on the optimization of extraction of castor seeds obtained from SSD.

3.2. Materials and methods

3.2.1. Castor cake formation method

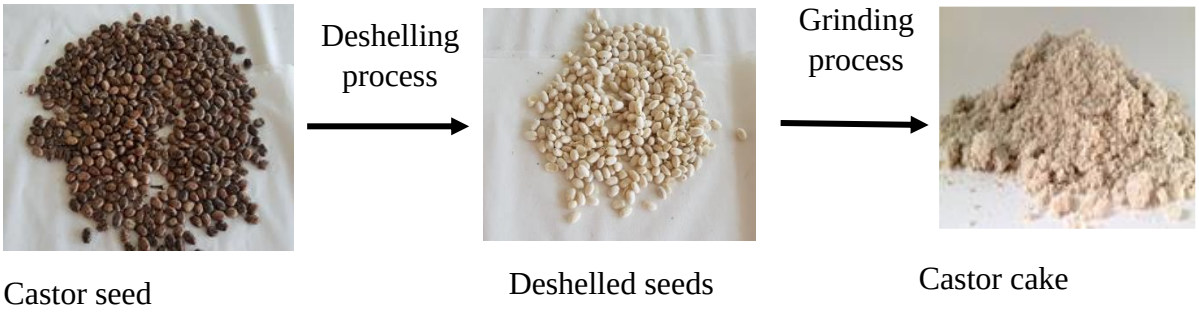


Figure 3. 2. Process flow of castor cake formation.

Before deshelling the castor seeds, the castor seeds were firstly exposed to the sun for 4-5 days to remove moisture and then taken to the oven for further removal of moisture for 6-7 hours at 80^{o}C (Gupta, Antil and Narwal, 2004). After the seeds were dried, the seeds shell were then removed using winnowing tray. Mortar and pestle was used to grind the deshelled seeds to form castor cake.

3.2.2. Moisture content determination

60 g of castor cake was placed into the oven at a temperature of 80^{o}C. After every 2 h interval, the castor cake was taken out of the oven and cooled for 20 minutes in the desiccator before weighing it. This procedure was repeated until the constant weight of castor cake was obtained. The following equation was used to determine the percentage of moisture content.

$$\%moisture\ content = \frac{w_1 - w_2}{w_1} \times 100 \qquad (3.1.)$$

Where, w_1 is the original weight of the castor cake before drying and w_2 is the weight of the castor cake after drying. The weight of moisture content is given by $w_1 - w_2$.

3.2.3. Soxhlet extraction

Soxhlet extraction was used to extract oil from the castor cake. Hexane was used as the solvent for extraction. The following set-up was used.

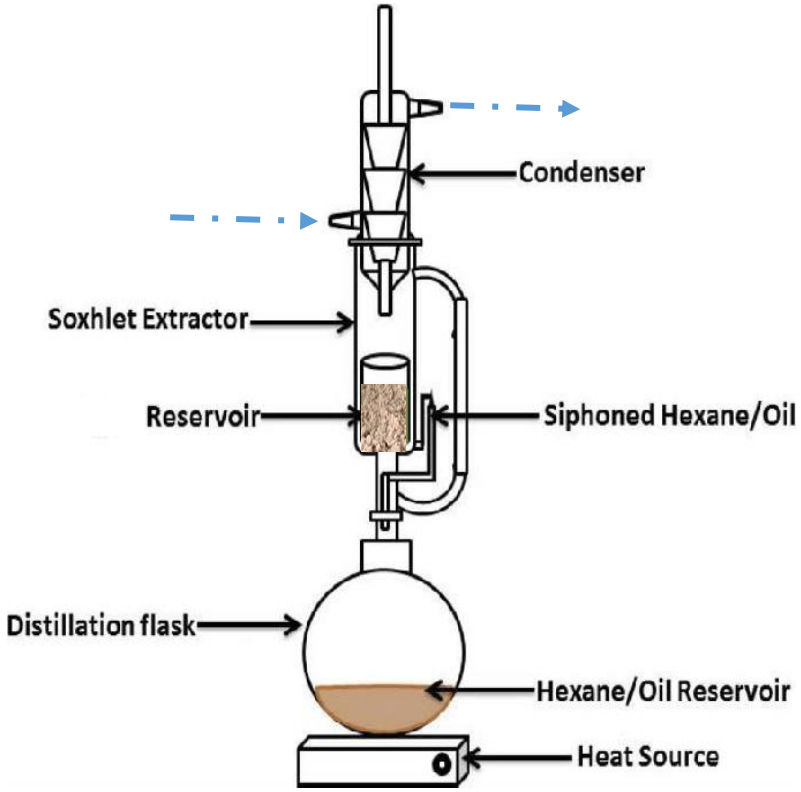


Figure 3. 3. Soxhlet extraction (Tulashie and Salifu, 2017).

The experiment was done by varying three factors which are seed/solvent ratio, extraction time, and extraction temperature. To determine the optimal conditions, the extraction was operated at temperature ranging 60-70^{o}C, extraction time from 2-6 h, and seed/solvent ratio between 0.04-0.08 g/mL. The basis of selecting the ranges of these parameters was well established. The response Surface Methodology (RSM) has been used.

3.2.4. Response surface methodology (RSM)

RSM from Design Expert version 11.0.4 software was used to determine the optimum process conditions for the extraction of oil from the castor cake. Center composite design from RSM was used for optimisation which consist of 2^{k} factorial points (Ven *et al*., 2002). Extraction time, temperature, and seed/solvent ratio were classified as independent variables and oil yield as dependent variable. The software generated 20 experimental runs based on the number of independent and dependent variables inserted.

Three different levels shown in Figure 3.1 were determine and inserted into the software. The socon order polynomial equation in Equation 3.2 was used to investigate the relationship between the depedent and independent variables.

$$Y = \beta_O + \sum_{i=1}^{k} \beta_i X_i + \sum_{i=1}^{k} \beta_{ii} {X_i}^2 \pm \sum_{i=1}^{k-1} \sum_{j=i+1}^{k} \beta_{ij} X_i X_j \quad (3.2)$$

Where, Y is the response oil yield, β is the constant coefficient, and X is the coded value of the independent variables (Dawood and Li, 2013).

Table 3. 1. Summary of experimental design.

			Level		
Factor	**Name**	**Unit**	**-1**	**0**	**1**
A	Seed/solvent ratio	g/mL	0.04	0.06	0.08
B	Extraction temperature	^oC	60	65	70
C	Extraction time	h	2	4	6

The experimental runs were generated from the software. The oil extracted was separated from hexane using rotavapor. The actual oil was then weighed to find the oil yield percentage. The experimental oil yield was calculated using the following equation.

$$Oil\ yield\ (\%) = \frac{mass\ of\ oil\ extracted\ (g)}{mass\ of\ castor\ cake\ (g)} \times 100 \quad (3.3)$$

3.2.5. Castor oil characterization

The physiochemical characteristics of the extracted castor oil was determined by following the method reported by Bagali *et al*., 2010. Gas chromatography-mass spectroscopy (GC-MS) was used to analyse the type of fatty acids present in oil. Fourier-transform infrared spectroscopy (FTIR) was used to determine the dominating functional group in the castor oil.

3.2.5.1. Physiochemical characteristics

Acid value, Saponification value, viscosity, iodine value. Specific gravity, and pH value of the castor oil extracted were determined.

3.2.5.1.1. Acid value

To determine the acid value of castor oil, about 10 g of oil was added into a 250 mL conical flask. 25 mL of ethanol was mixed with 25 mL of diethyl ether in a 250 mL beaker and the

moisture were then added to the conical flask with oil. Few drops of phenolphthalein was then added to the mixture. The final mixture was then titrated using 0.1 M NaOH through consisted shaking to the end point. The dark pink colour was observed. The acid value was then determined using the following equation.

$$\text{Acid value} = \left(\frac{V_O}{W_O} \times 2.82 \times 100\right) \times 2 \quad (3.4)$$

Where, V_O is the volume of 0.1 M NaOH, $W_o$is the sample weight. The free fatty acid (FFA) is given by $\frac{V_O}{W_O} \times 2.82 \times 100$.

3.2.5.1.2. Saponification value

2 g of oil and 25 mL of ethanol potassium hydroxide was mixed together and then boiled using reflux condenser for 60 min under constant stirring. After boiling, few drops of phenolphthalein was added to the warm solution. The solution was then titrated with 0.5 HCl to the end point until the pink colour of phenolphthalein disappeared. The same procedure was used for blank and the sample. The saponification value was determined using the following equation.

$$\text{Saponification value} = \frac{56.1N\left(\frac{V_O}{V_I}\right)}{m} \quad (3.5)$$

Where, V_O is the volume of the solution used for blank test, V_I is the volume of the solution for determination, N is the actual normality of the HCl, and m is mass of the sample

3.2.5.1.3. Iodine value

0.4 g of oil was mixed with 20 mL of carbon tetra chloride in 250 mL conical flask. 25 ml of Dam's reagent was then added to the mixture using a pipette. The mixture was stirred for 20 minutes and then placed into the dark for 2 hours 30 minutes. 20 ml of potassium iodide was diluted in 125 mL of water and then added to the moisture. The solution was titrated with 0.1M with sodium-thiosulphate until the yellow colour disappeared. The same procedure was conducted for blank test and the sample. The iodine value was determined using the following equation.

$$\text{Iodine value} = \frac{12.69C\frac{V_1}{V_2}}{m} \quad (3.6)$$

Where, C is the concentration of sodium thiosulphate, m is the mass of the sample, V_1 is the volume of sodium thiosulphate used for blank, and V_2 is the volume of the sodium thiosulphate used foe sample.

3.2.5.1.4. Specific gravity

A bottle was cleaned and dried and weighed to give Wo. The bottle was then filled with oil and weighed again to give W_1. The bottle was then washed again, dried, filled with water, and weighed to give W_2. The specific gravity was then calculated using the following equation.

$$\text{Specific gravity} = \frac{W_1 - W_O}{W_2 - W_O} = \frac{mass\ of\ the\ substance}{mass\ of\ an\ equal\ volume\ of\ water} \quad (3.7)$$

3.2.5.1.5. Viscosity

The viscometer was used to determine the viscosity of the oil. The oil was injected to the viscometer and the viscometer was then placed into bath with constant temperature of 29ºC and the sample was placed for about 10 min to allow the sample to reach 29ºC. The suction force was then applied to draw the sample slightly. The time at which the sample was flowing from the upper mark to the lower mark was recorded.

3.2.5.1.6. pH Value

The pH electrode was used to determine the pH of the oil. About 2 g of oil was mixed with 15 mL of warm distilled water in the beaker and slowly stirred. It was then cooled to 25ºC and the electrode standardised with buffer solution was immersed into the solution and the pH value was recorded.

3.2.5.2. GC-MS analysis

The GC-MS analysis of the castor oil produced was performed to determine the major acids present in the oil. The analysis was performed on a Leco GCxGC-TOF Low resolution mass spectrometer.

3.3. Results and discussion

3.3.1. Moisture content determination.

The moisture content determination is described as the loss of weight when the material is heated. The sample weight is taken prior and after heating until a steady-state weight is reached. The castor seeds moisture content was determined by weighing the sample for every 2 hour interval. Equation 3.1 was used to calculate the moisture content.

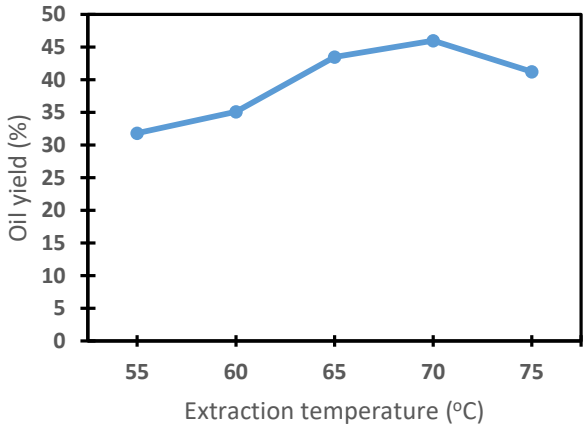
Table 3. 2. Moisture content determination.

Time (hours)	Weight (g)
0	60
2	58.1
4	57.7
6	57.5
8	57.3
10	57.3

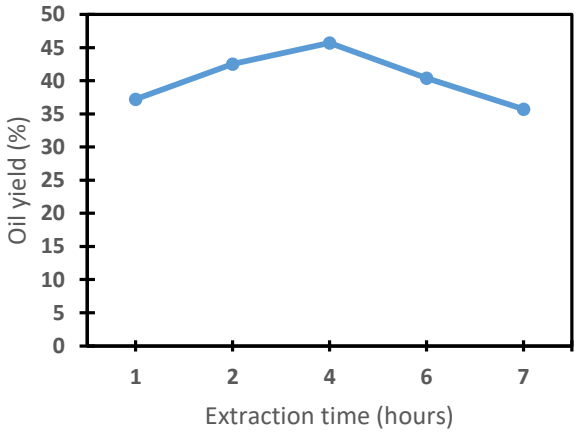
The moisture content was found to be 4.5 % after 6 runs. The value obtained is within the range reported in literature of 1.84-5.40 % (Omari, et al., 2015), (Akpan, et al., 2006), (Muzenda, et al., 2012). Moisture content has the large impact on the storage life of the seeds. Therefore, it is very important to determine the moisture content to make appropriate precise prediction of the feasible storage life of each accession (Omari, et al., 2015).

3.3.2. Effects of operating conditions on the oil yield.

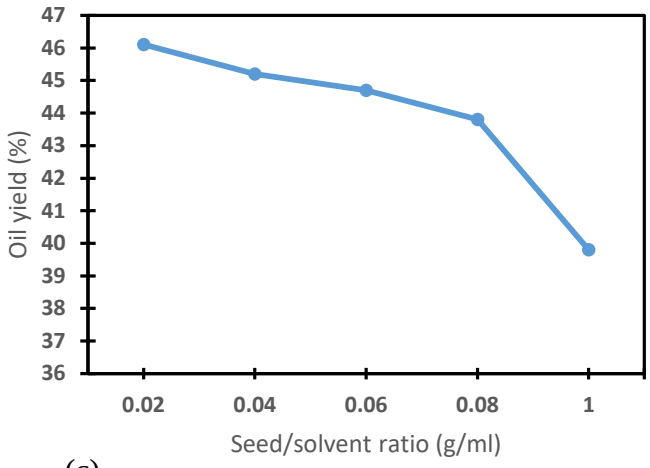
Figure 3.4 shows the effect of extraction time, temperature, and seed/solvent ratio on the oil yield.



(a)



(b)



(c)

Figure 3. 4. Effect of extraction (a) temperature, (b) time, and (c) seed/solvent ratio on the oil yield.

The preliminary solvent extraction was carried out before optimization to determine the behaviour oil yield at different extraction time, temperature and see/solvent ratio on the oil yield. The effect of temperature was investigated within the range of 55-65^{o}C at constant seed/solvent ratio and time of 0.06 g/mL and 4 h, respectively. It was observed that the oil yield increases with the increase in temperature and the maximum oil yield of 46 % was obtained at 70^{o}C. Similar trend was observed by Mosquera-Artamonov *et al*. (2017) and they obtained the maximum oil yield of 22 % at 60^{o}C. The effect of extraction time was studies at constant seed/solvent ratio and temperature of 0.06 g/mL and 65^{o}C, respectively. The increase in oil yield was observed from 1-4 hours and thereafter the yield start to decrease. Similar trend was observed by Oniya *et al.* (2017), the oil yield started with the increase and after 5 hours it then started to decrease. The effect of seed/solvent ratio was studied at the constant time and temperature of 4 h and 65^{o}C. It was observed that the oil yield decreases with the increase in seed/solvent ratio. Similar trend was also observed by Dasari and Goud, (2013).

3.3.3. Experimental layout from RSM

The experimental oil yield values with the predicted oil yield values generated by the model are presented in Table 3.2. The values obtained are different which indicates that the parameters investigated have the impact on the oil yield. It was also observed that the predicted oil yield values are closer to the experimental oil yield.

Table 3. 3. Experimental design layout using RSM.

Std	Run	A:Seed/solvent ratio (g/mL)	B:Extraction temperature (ºC)	C:Extraction time (hour)	Response experimental oil yield (%)	Predicted oil yield (%)
6	1	0.08	60	6	33.90	33.40
18	2	0.06	65	4	44.70	43.64
14	3	0.06	65	6	40.40	42.40
1	4	0.04	60	2	36.50	36.68
9	5	0.04	60	4	45.20	45.84
7	6	0.04	70	6	45.10	44.63
4	7	0.08	70	2	40.90	41.78
5	8	0.04	60	6	37.90	37.04
8	9	0.08	70	6	45.50	45.34
20	10	0.06	65	4	43.50	43.64
10	11	0.08	65	4	43.80	43.10
19	12	0.06	65	4	40.10	43.64
15	13	0.06	65	4	44.90	43.64
13	14	0.06	65	2	42.50	40.44
2	15	0.08	60	2	30.00	30.49
12	16	0.06	70	4	46.01	45.24
16	17	0.06	65	4	42.80	43.64
17	18	0.06	65	4	45.70	43.64
3	19	0.04	70	2	43.10	43.62
11	20	0.06	60	4	35.10	36.80

46.01 % was obtained as the maximum oil yield at extraction temperature, time, and seed/solvent ratio of 70^{o}C, 5 h, and 0.06 g/mL. The maximum yield obtained is slightly higher than 45.8 % obtained by Dasari and Goud (2013) and lower than 50.9 % obtained by Danlami *et.al* (2015). The difference in the maximum oil yield may be caused by the condition at which

the experiment was carried and the environmental conditions at which the castor seeds were grown.

3.3.4. Analysis of variance for the extraction of castor oil

The oil yield was statistically analyzed using analysis of variance (ANOVA) and the ANOVA results are indicated in Table 3.4. There are different models that can be obtained from the analysis such as linear model or quadratic model. In this analysis, quadratic model of oil yield was obtained. This model was used to study the relationship between the independent variables A, B, C (seed/solvent ratio, extraction temperature, and extraction time) and the response oil yield. The coded quadratic equation is shown below:

$$Y = 43.64 - 1.37A + 4.72B + 0.98C + 1.09AB + 0.6375AC + 0.1625BC + 0.8255A^2 - -3.12B^2 - 2.22C^2 \quad (3.8)$$

Where, Y represents response variable oil yield measured in %.

Table 3. 4. Analysis of Variance (ANOVA) for extraction of castor oil from castor seeds.

Source	**Sum of Squares**	**df**	**Mean Square**	**F-value**	**p-value**	
Model	356.15	9	39.57	11.99	0.0003	significant
A-Seed/solvent ratio	18.77	1	18.77	5.69	0.0383	
B-Extraction temperature	222.88	1	222.88	67.56	< 0.0001	
C-Extraction time	9.60	1	9.60	2.91	0.1188	
AB	9.46	1	9.46	2.87	0.1212	
AC	3.25	1	3.25	0.9855	0.3443	
BC	0.2113	1	0.2113	0.0640	0.8054	
A^2	1.87	1	1.87	0.5679	0.4684	
B^2	26.76	1	26.76	8.11	0.0173	
C^2	13.61	1	13.61	4.12	0.0697	
Residual	32.99	10	3.30			
Lack of Fit	12.78	5	2.56	0.6326	0.6862	not significant
Pure Error	20.21	5	4.04			
Cor Total	389.14	19				

ANOVA was used to evaluate the significance of the model and it was found to be significance based on the model F-value of 11.999 and p-value of 0.0003 which implies that the model best fitted to the experimental data. P-values less than 0.0500 indicate model terms are significant (Hinkelmann, 2012). In this case A, B, B^2 were found to be significant model terms. This means that seed/solvent ratio, extraction temperature, and extraction temperature squared has the greater effect on the oil yield. Values greater than 0.1000 indicate the model terms are not significant (Hinkelmann, 2012). If there are many insignificant model terms (not counting those required to support hierarchy), model reduction may improve the model. The Lack of Fit F-value of 0.63 implies the Lack of Fit is not significant relative to the pure error (Hinkelmann, 2012). The Adequate precision in Table 3.1 which measures the signal to noise rato was found to be 11.95 and ratio greater than 4 is desirable. Therefore, the model generated can be used to navigate the design space of the experiment.

Table 3. 5. The ANOVA results for response models.

Response	R^2	Adj.R^2	Pred.R^2	Adeq. precision	Std. Dev.	Mean	C.V.%
Oil yield	0.9152	0.8389	0.6783	11.95	1.82	41.38	4.39

The actual oil yield values from the experimental data were compared with the predicted oil yield values generated by the model using Equation 3.8 and the comparison graph is shown in Figure 3.5. According to Goos and Gilmour (2013), the predicated values and actual values must be 90 % closer to each other before the model can be used for optimization.

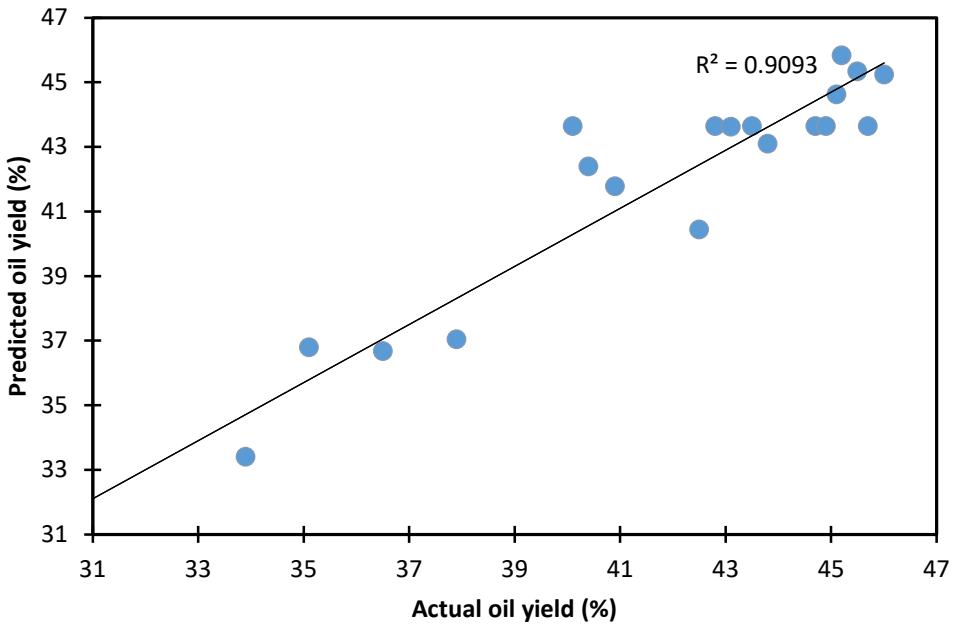


Figure 3. 5. Comparison of the actual oil yield with the predicted oil yield.

The R2 value was found to be 91 % which means that the model can be used for predicting the oil yield without doing the actual experiment with only 9 % deviation. The precision and reliability of the model is good.

3.3.4.1. Analyzing the 3D surface of oil yield generated by RSM

3.3.4.1.1. Effect of extraction temperature and seed/solvent ratio on the oil yield.

From the model, a 3D surface plot was generated to study the effect of seed/solvent ratio and extraction temperature on the oil yield. This 3D surface plot also depicts the relation between seed/solvent ratio and extraction temperature.

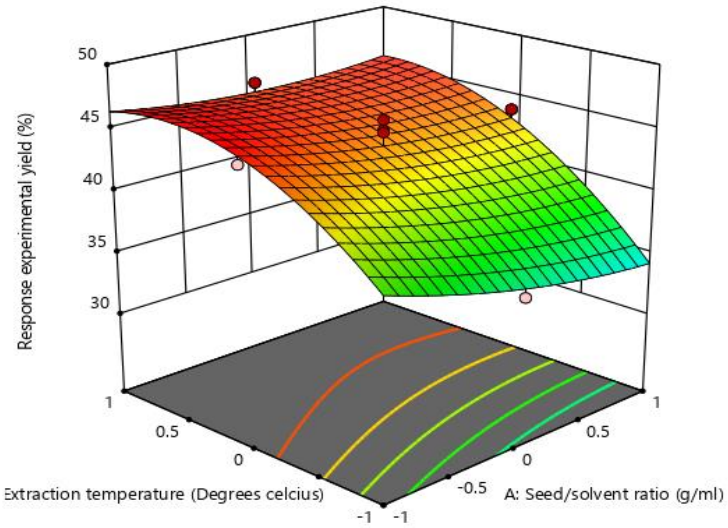


Figure 3. 6. The 3D surface plot showing the effect of extraction temperature and seed/solvent ratio on the oil yield.

The oil yield increases with the increase in both seed/solvent ratio and extraction temperature. The effect of temperature was studied within the range of 60-70^{o}C and the maximum temperature was set closer to the boiling point of hexane. This is because at temperatures above boiling point it was in literature that the oil yield decreases due to the increase in evaporation of the solvent. Afalobi *et al.* (2014) reported that the decrease in oil yield is more significant when hexane is used as the solvent compared to other solvent such as petroleum ether. Based on the 3D surface plot, the oil yield is more optimum at seed/solvent ratio and temperature of about 0.06 g/mL and 65^{o}C. Oil yield of above 45 % can be obtained at this conditions and below these conditions the oil extracted is very small. Bekele *et al.* (2018) obtained maximum oil yield of 56 % at seed/solvent ratio of 0.0667 g/mL using hexane as the solvent.

3.3.4.1.2. Effect of the seed/solvent ratio and extraction time on the oil yield.

The 3D surface plot of the effect of seed/solvent ratio and extraction time on the oil yield was also generated from the model and the result are shown in Figure 3.7.

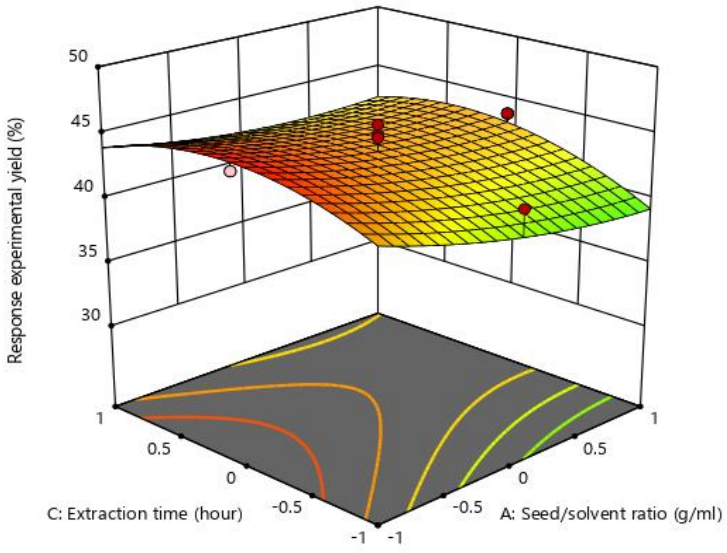


Figure 3. 7. 3D surface plot showing the effect of the seed/solvent ratio and extraction time on the oil yield.

The increase in extraction time favors the extraction rate of oil until the optimum extraction time is reached and start to decrease again above the optimum level. From 2 h to approximately 4 h the oil yield increases and then start to decrease after 4 h. This is because when the oil is heated for a long time, the oil will then start to degrade. Based on the 3D plot, the maximum yield can be obtained between 3-5 h and seed/solvent ratio between 0.04-0.06 g/mL. Bekele

at al. (2018) obtained the maximum oil yield of 57 % at optimum extraction time of 5 h and seed/solvent ratio of 0.067 g/mL during the extraction of castor oil using hexane as the solvent.

3.4.3.1.3. The effect of extraction temperature and extraction time on the oil yield

The 3D surface plot which shows the effect of extraction temperature and extraction time on the oil yield is shown in Figure 3.8. Extraction temperature ad time has a high significance effect on the oil yield.

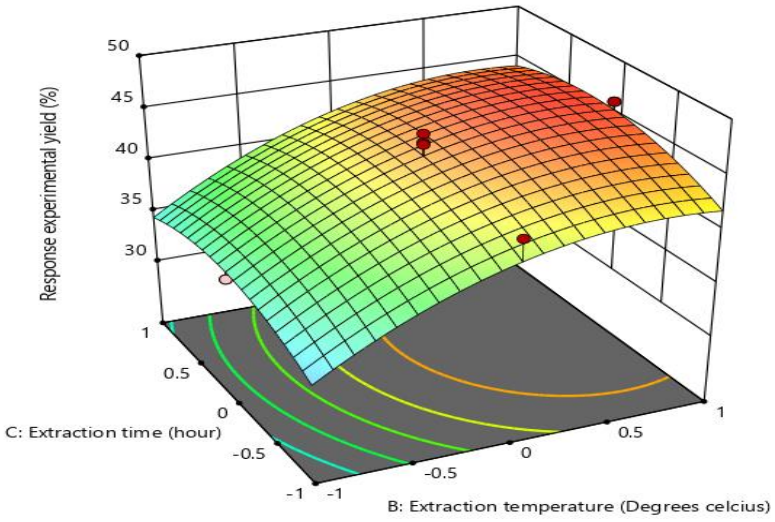


Figure 3. 8. 3D surface plot showing the effect of extraction time and extraction temperature on the oil yield.

The increase in both extraction temperature and time favors the extraction rate of oil until the optimum level is reached. The oil yield increases with the increase in extraction time until the optimum extraction time is reached and above the optimum extraction time the oil yield decreases. The same trend was also observed on the effect of extraction temperature on the oil yield. The oil yield increases with the increase in extraction temperature until the boiling point of the solvent is reached. At high level of both extraction time and extraction temperature results to the decrease on the oil yield. The optimum oil yield can be obtained at temperatures between 65-70^{o} C and the extraction time between 3-5 h. Odewole *et al*. (2017) and Mosquera-Artamonov *et al*. (2017) obtained their maximum oil yield at the optimum temperature of 60 ^{o}C which is lower than the range obtained from the 3D plot.

3.3.5. Optimization of processing parameters for maximum oil yield

The Design expert software was used to optimize the operating conditions to obtain the maximum oil yield. The maximum oil yield of 44.57 % was obtained at the optimum extraction temperature, extraction time, and seed/solvent ratio of 63.28^{o}C, 3.6 h, and 0.03 g/mL,

respectively. The maximum oil yield obtained after optimization is slightly lower than the maximum oil yield of 46.01 % obtained from the actual experiment. The experiment was then repeated by using the optimum conditions obtained from optimization to verify and confirm the agreement of the results obtained from the model. Three runs were taken under same optimized conditions obtained from the model and the average of 45.6 % of oil yield was obtained which is slightly higher than the oil yield obtained from the model. The results obtained from the experiment has produced the optimal conditions for solvent extraction of castor oil from castor seeds.

3.3.6. Characterization of castor oil produced

3.3.6.1. GC-MS and FTIR analysis of oil extracted

The GC-MS analysis chromatograph of the oil extracted is shown in Figure 3.9. The chromatograph assist in determining the main fatty acids present in the oil and types of major fatty acids obtained are shown in Table 3.6.

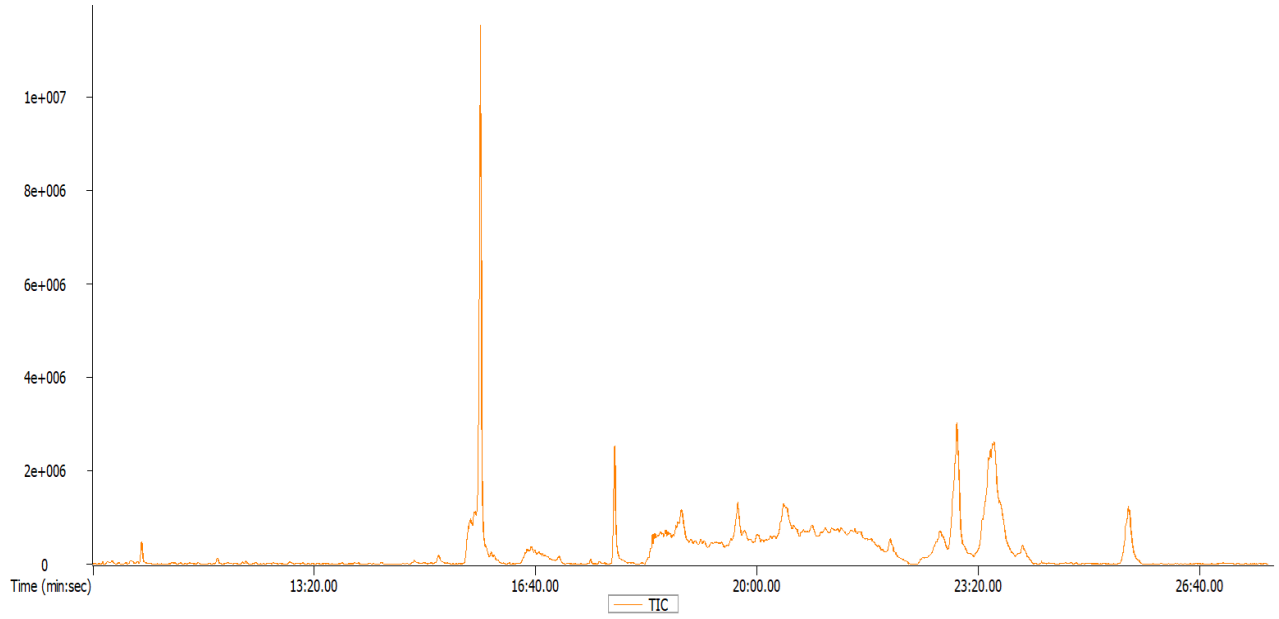


Figure 3. 9. Typical GC-MS total ionic chromatogram (TIC) of Castor oil.

Table 3. 6. Major fatty acids derived from castor oil

Peak #	Name of fatty acid	Molecular formula	MW	Similarity	R.T (min:sec)	S/N	Area (%)
26	Oleic acid	$C_{18}H_{34}O_2$	282	716	23:00.5	1398	13.2
21	Palmitic acid	$C_{19}H_{38}O_2$	270	738	20:24.0	1080.3	2.63
16	Undecylenic acid	$C_{11}H_{20}O_2$	184	851	18:25.8	63.056	0.71
15	Methyl ricinoleate	$C_{19}H_{36}O_3$	312	873	17:51.2	6032	5.15
29	Behenic acid	$C_{23}H_{46}O_2$	354	817	23:34.3	471.7	7.36
9	Tridecylenic acid	$C_{14}H_{28}O_2$	228	820	14:21.2	558.69	0.18
11	13-Hexyloxacyclotridec-10-en-2-one	$C_{18}H_{32}0_2$	280	916	15:50.4	10682	21.21

Note: MW= Molecular Weight, R.T. = Retention time, S/N= Serial Number

Fatty acids and triglycerides are the main components required during the hydrocracking of castor oil to produce biofuel. During hydrocracking, the oxygen atoms from the triglycerides and fatty acids are removed in the form of CO, H_2O, or CO_2 to produce hydrocarbons such as alkanes and alkenes which have carbon range of different types of biofuels.

The main fatty acids obtained from the extracted oil determined from the GC-MS analysis are; Oleic acid, palmitic acid, undercylenic acid, methyl ricinoleate, behenic acid,tridecylenic acid and 13-hexyloxacyclotridec-10-en-2-one. Hexyloxacyclotridec-10-en-2-one was found to be abundant followed by oleic acid. During hydrocracking, the long chain hydrocarbons of the fatty acids are broken down to shorted chains with biofuel carbon range (Al Alwan, Salley and

Ng, 2015).Based on the results obtained from the GC-MS analysis it can be predicted that the castor oil produced can produce biofuel.

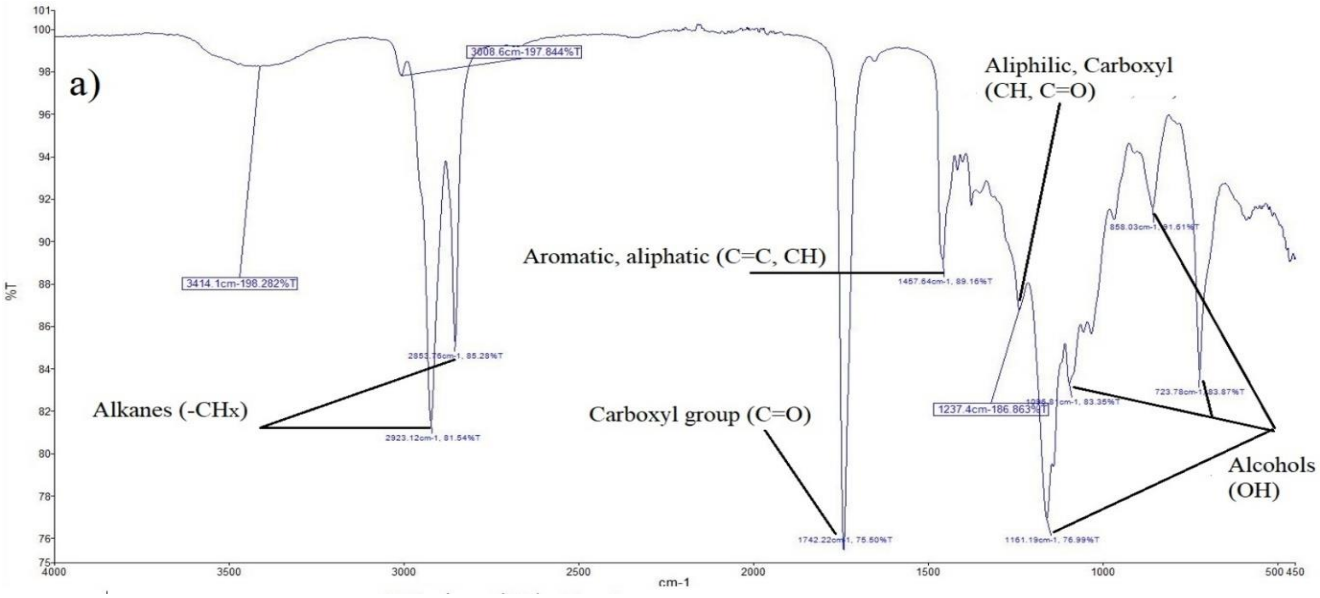


Figure 3. 10. FTIR analysis of castor oil produced

Dominating functional groups in the oil were determined from the FTIR spectra. Heavy alkanes, aromatics, alcohols and carboxylic groups were observed.

3.3.6.2. Physiochemical characteristics

The chemical analysis of the castor oil was performed by following the methods reported (Bagali *et al*., 2010). The following results was obtained.

Table 3. 7. Physiochemical characteristics of castor oil.

Properties	Ranges	Experimental results
Acid value	0.4-4	1.22
Saponification value	175-187	178
Iodine value	82-88	85
Specific gravity 20/25^{o}C	0.957-0.968	0.952
Viscosity at 25^{o}C	6.3-8.8 st	6.6
pH value		6.04

The acid value, saponification value, iodine value, specific gravity, viscosity of the castor oil was compared with ASTM standard specification values. The experimental values of these properties was found to be within the range of ASTM. The pH value of the oil was found to be 6.04.

3.3.7. Conclusion

In this chapter, it was observed that the extraction time, extraction temperature, and seeds/solvent ratio has great influence on the oil yield during solvent extraction. Therefore, it is very important to control these conditions to maximise the oil yield during extraction. The maximum oil yield obtained from castor seeds obtained from Limpopo was found to be 44.57 % at optimal conditions of 63.28^{o}C, 3.6 hours, and 0.03 g/mL of extraction temperature, extraction time and seed/solvent ratio, respectively. Based on the results obtained from the GC-MS analysis of castor oil it was concluded that the castor oil produced can produce biofuel due to the fatty acids present and the physiochemical characteristics of the oil are within the ASTM standard range.

3.4. References

Afolabi T. J., Onifade K. R., Akindipe V.O., and Odetoye T. E., 2014. Optimization of Benth Seed Oil (Parinari polyandra) Using Response Surface Methodology. *British J. Appl. Sci. Tech*., 5, pp.437–445.

Akay, G., 2016. Co-Assembled Supported Catalysts: Synthesis of Nano-Structured Supported Catalysts with Hierarchic Pores through Combined Flow and Radiation Induced Co-Assembled Nano-Reactors. *Catalysts*, 6(6), p.80.

Akpan, U. G., Jimoh, A. & Mohammed, A. D., 2006. Extraction, Characterization and Modification of Castor Seed Oil. *Leonardo Journal of Sciences,* 1(8), pp. 43-52.

Al Alwan B., Salley S. and Ng K. 2015. Biofuels production from hydrothermal decarboxylation of oleic acid and soybean oil over Ni-based transition metal carbides supported on Al-SBA-15. *Applied Catalysis A: General*, 498, pp.32-40.

Bagali S.S., Beena K.V., Anita M.V., and Paramjeet K.B., 2010. Optimisation of Castor Seeds Oil. *Department of Chemical Engineering, Rural Engineering College, Hulkoti, Gadag, Karnataka*, India.

Bekele B.A., Ourgessa A.W., Terefe A.A., and Hailu S.S., 2018. Studies on Ethiopian Castor Seed (Ricinus communis L.): Extraction and Characterization of Seed oil. *Journal of Natural Products and Resources*, 4(2). pp. 188-190.

Danlami, Jibrin & Arsad, Agus & Ahmad Zaini, Muhammad Abbas, 2015. Solvent Extraction of Castor Beans Oil: Experimental Optimization via Response Surface Methodology. 10.1007/978-981-287-505-1_12.

Dasari S.R., and Goud V.V., 2013. Comparative Extraction of Castor seed Oil Using Polar and Non polar Solvents. *International Journal of Current Engineering and Technology*. ISSN 2277 – 4106.

Dawood A., and Li Y., 2013. Modeling and Optimization of New Flocculant Dosage and pH for Flocculation: Removal of Pollutants from Wastewater. *Water*, 5(2), pp.342-355.

Edison M., and Motshumi D., 2012. The Effect of Extraction Conditions on Oil Yield from Waste Lubricating Grease. *Journal of Research in Chemical, Metallurgical and Civil Engg. (IJRCMCE), 1(1).*

Goos P., and Gilmour S., 2017. Testing for Lack of Fit in Blocked, Split-Plot, and Other Multi-Stratum Designs. *Journal of Quality Technology*, 49(4), pp.320-336.

Gupta A., Antil R., and Narwal R., 2004. Utilization of deoiled castor cake for crop production. *Archives of Agronomy and Soil Science*, 50(4-5), pp.389-395.

Hinkelmann K., 2012. *Design and Analysis of Experiments*. Hoboken, N.J.: Wiley-Interscience.

Ibrahim, N. and Zaini, M., 2018. Microwave-assisted solvent extraction of castor oil from castor seeds. *Chinese Journal of Chemical Engineering*, 26(12), pp.2516-2522.

Khuri, A., 2017. A General Overview of Response Surface Methodology. *Biometrics & Biostatistics International Journal*, 5(3).

Mosquera- Artamonov J., Vasco-Leal J., Hernandez-Rios I., Mendez-Gallegos S., Perea-Flores M., Peña-Aguilar J., and Rodriguez-Garcia, M., 2017. Physicochemical characteristics of seeds from wild and cultivated castor bean plants (Ricinus communis L.). *Ingeniería e Investigación*, 38(1), pp.24-30.

Mubofu E., 2016. Castor oil as a potential renewable resource for the production of functional materials. *Sustainable Chemical Processes*, 4(1).

Muzenda E., Kabuba J., Mdletye P., and Belaid M., 2012. Optimization of Process Parameters for Castor oil Production. *Production of the World Congress on Engineering*, 3.

Nde D., and Foncha, A., 2020. Optimization Methods for the Extraction of Vegetable Oils: A Review. *Processes*, 8(2), p.209.

Olaoye J.O, and Busari R.O., 2017. Optimization of Mechaical Expression of Castor Seeds Oil (Ricinus Communis) Using Response Surface Methodology.*Arid Zone Journal of Engineering, Technology and Environment*, 13(6), pp. 878-887.

Odewole M. M., Sunmonu M.O., Oyeniyi S.K., Adesoye O.A., and Ikubanni P.P, 2017. Development of U-Channel Screw Jack for Vegetable Oil Extraction. Nigerian Journal of Technology, 36(3), pp. 979-986.

Omari A., Mgani Q. A., and Mubofu E. B., 2015. Fatty Acid Profile and Physico-Chemical Parameters of Castor Oils in Tanzania. *Green and Sustainable Chemistry,* Volume 5, pp. 154-163.

Oniya O.O., Oyelende J.O., Ogunkuhle O., and Idowu D.O., 2017. Optimiation of Solvent Extraction of Oil from Sandbox Kernals (Hura Creptans L.) by a Response Surface methodology.Energy and Policy Research, 4(1), 36,43.

Patel V., Dumancas G., Viswanath L., Maples R. and Subong B., 2016. Castor Oil: Properties, Uses, and Optimization of Processing Parameters in Commercial Production. *Lipid Insights*, 9, p.LPI.S40233.

Tulashie S., and Salifu S., 2017. Potential production of biodiesel from green microalgae. *Biofuels*, 11(2), pp.201-208.

Ven C. V. D., Gruppen, H., Bont D.B.A.D., and Vorga A.G.J., 2002. Optimization of Angiotensin Converting Enzyme Inhibit by Whey Protein Hydrolysis Using Response Surface Methodology. *J. Int. Dairy*, 12, pp.817–820.

Chapter 4: Catalyst synthesis

This chapter focuses on the synthesis of nickel nanoparticles catalyst supported on carbon dot (Ni/C dots). The aim of this chapter is to find the most suitable and selective catalyst towards the production of biojet and biogasoline fuel during hydrocracking of castor oil.

4.1. Introduction

Carbon dots (C dots) are carbon nanomaterial which attracted numerous researchers for the past decade because of their significant properties such as lack of cytotoxicity, high photostability good biocompatibility, and modifiable functional groups with simple preparation methods (Gupta, 2019).C dots contains oxygen functional groups on the surface which makes them more suitable as supports for nucleation and growth of the pristine nanocrystals. C dots have been widely used in cancer therapy, bioimaging, catalysts, energy, biosensors and sensors, and gene and drug delivery (Gupta, 2019). Metal nanoparticles have also received more attention and have emerged as a new class of materials because of their unique magnetic, electronic, optical, and catalytic properties (Su *et al.,* 2018). More attentions have moved towards non-precious metals particularly nickel nanoparticles for catalysis application. The use of nickel nanoparticles as a catalyst has drawn considerable attention due to their excellent physical, chemical, and electronic properties. These excellent properties include the high performance of nickel catalysts to transform unreactive substrates, chemically less reactive molecules, and large variability of electronic states (Ananikov 2015). Nickel nanoparticles are considered low-cost metal and widely used as catalyst because of their large surface area and additional active sites.

Different studies have been published on use of nickel catalyst supported on carbon materials. Yang *et al*., (2015) studied the use of nickel catalyst supported by carbon quantum dot hybrid as an efficient electrocatalyst for hydrogen evolution under alkaline conditions. Wu and Ritchie (2006) studied the use of Fe-Ni nanoparticles supported by carbon nanotube-co-cyclodextrin polyurethanes for removal of trichloroethylene in water. Zhongbin *et al.,* (2016) studied the use of Ni supported on nitrogen-doped carbon nanotubes as hydrogen oxidation reaction catalyst in alkaline electrolyte.

4.2. Materials and methods

4.2.1. Preparation of C dots

The C dots were prepared through hydrothermal carbonization of chitosan solution. Hydrothermal carbonization is a thermochemical process used to convert organic compounds such as raw biomass or carbohydrates to structured carbons using an autoclave under moderate temperatures (180-250^{o}C) (Laginhas, Nabais and Titirici, 2016). Hydrothermal carbonization is the preferred method because of its low cost production, simplicity, and CO_2 and energy efficiency. Chitosan is an aminopolysaccharide biopolym coming from the deacetylation of chitin, with a complex structure and highly sophisticated functions. It is considered as the green option for synthesizing C dots because of its low toxicity, biocompatibility, and biodegradability (Laginhas, Nabais and Titirici, 2016). Chitosan easily accessible and cheap and widely used in industries and biomedical areas. Hao *et al.*, (2014) produced C dots with surface area greater than 500 $m^2.g^{-1}$ from hydrothermal carbonization of treated waste biomass using chemical and physical activation.



Figure 4. 1. Preparation of C dots.

The C dots were prepared through hydrothermal carbonization of chitosan solution. The C dots were prepared by adding 0.5 g of chitosan into 100 mL of 1 % acetic acid solution. The solution was then mixed using ultrasonicator for 20 minutes. The solution was then placed to the hydrothermal autoclave and heated at 180^{o}C for 12 hours in the oven. After 12 hours, the autoclave was removed from the oven and cooled down to room temperature. The brownish black solution was obtained and this solution was centrifuged at 10 000 rpm for 15 minutes.

The solution was further filtered to remove the remaining unwanted materials. This procedure was repeated until required amount of C dots was reached.

4.2.2. Synthesis of Ni/C dots catalyst

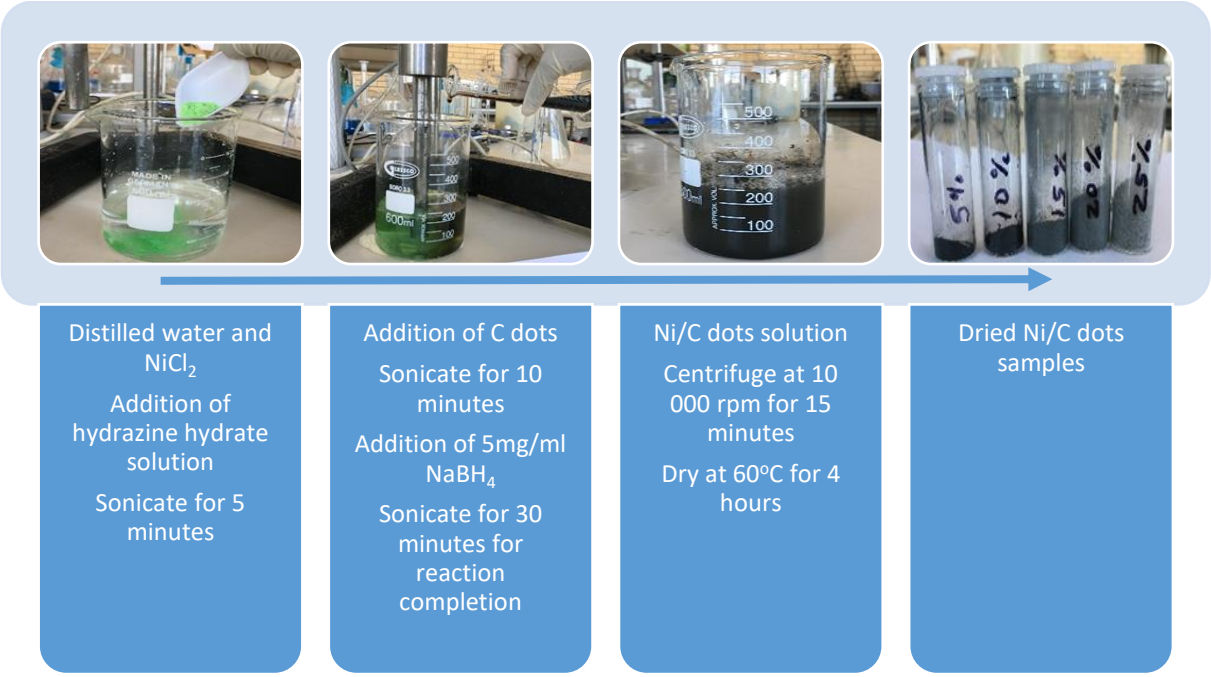


Figure 4. 2. Synthesis of Ni/C dots.

Different samples of Ni/C dots catalyst with five different nickel loadings (5, 10, 15, 20 and 25 wt. %) were prepared to give a 3 g catalyst. Nickel chloride ($NiCl_2 \cdot 6H_2O$) was firstly reduced to nanoparticles using hydrazine hydrate solution. The hydrazine hydrate solution was prepared by preparing 2 moles of hydrazine in a 250 mL conical flask with distilled water. Hydrazine hydrate solution was then added to $NiCl_2$ solution to reduce the particles into nanoparticles and the solution was ultrasonicated for 5 minutes. C dots solution was then added to the nickel chloride and hydrazine hydrate solution and the mixture was ultrasonicated for 10 minutes. After 10 minutes, 5 mg/mL of $NaBH_4$ was added drop wise to initiate the reaction while sonicating. The solution changed from royal purple solution to dark which indicated the formation of nickel nanoparticles. The solution was further sonicated for 30 minutes for complete reaction. The crude product were then isolated from the solution by centrifuging at 10 000 rpm for 15 minute and the products were further washed with absolute alcohol. The products were dried at 60°C for 4 hours and then calcined at 350°C for 4 hours to activate the catalyst.

To investigate the effect nickel loading on the activity of the catalyst, the nickel concentration was varied at 5 wt. %, 10wt. %, 15 wt. %, 20 wt. %, and 25 wt. %. They were then analysed to

determine the catalyst with most favourable properties. The catalyst which shows high thermal stability was then calcined at 450^{o}C, 550^{o}C, 650^{o}C, 750^{o}C, and 850^{o}C to determine the effect of calcination temperature on the activity of the catalyst.

4.3. Catalyst characterisation techniques

Different types of characterisation techniques was performed to study the properties of the catalyst. TGA, BET, SEM, SEM EDS, TEM, XRD, FTIR, and Raman spectrometry were used to characterise the catalyst.

4.3.1. Thermogravimetric analysis (TGA)

TGA was used to study the thermal stability of each catalyst synthesised. About 10 mg of the catalyst sample was inserted to the sample holder and the placed into the instrument and the instrument was adjusted to zero. The samples were then heated at a rate of 20^{o}C.min in the presence of nitrogen gas with the purge rate of 10 mL/min. A SDT Q600 V20.9 instrument was used for the characterisation.

4.3.2. Brunauer-Emmet-Teller (BET)

BET analysis of the catalysts was studied to investigate the effect of nickel loading and calcination temperature on the surface area, pore size, and pore volume of the catalyst. About 500 mg of the catalyst samples were used during the analysis and the unwanted and excess gasses were removed under stream of nitrogen gas for 6 hours at 150^{o}C. Nitrogen gas adsorption and desorption occurred during characterisation. Micromeritics Tristar 3000 surface area and porosity analyzer (V6.05) were used for the analysis.

4.3.3. X-Ray Diffraction (XRD)

XRD was used to identify the crystalline phases present in the catalyst and thereby revealing the chemical composition information. The XRD analysis is performed by directing an x-ray beam at a sample and then measuring the scattered intensity as a function of the outgoing direction. A D2 Phaser Burker X-ray diffract meter was used to analyse the sample which contains cobalt radiation in range of 2θ = 10-90 and the analysis take about 30 minutes per sample with a scanning speed of 1.52 per min.

4.3.4. Fourier Transform Infrared (FTIR) Spectrometry

FTIR analysis was used determine different functional groups present in the catalyst. A Bruker Tensor 27 FT-IR analyser was used to analyse the catalyst. Small amount of the sample was

placed on the instrument and the infrared spectra were generated. The peaks of the spectra were studied to determine the type of functional groups present in the catalyst based on the wave range reported on literature.

4.3.5. Scanning Electron Microscopy (SEM)

SEM was used to study the morphology of the catalyst at different nickel loading and calcination temperatures. Small amount of the samples were placed onto the carbon resins and then placed onto the sample holder. The samples were coated with 2×palladium for clearer images. FEI Quanta 200 ESEM was used to characterise the sample. Energy-Dispersive X-Ray Spectrometry (EDS or EDX) was also used to determine the elemental composition of an area of interest.

4.3.6. Atomic absorption spectroscopy (AAS)

AAS was used to detect the concentration of nickel metal present in the catalyst. This type of analysis method determines the chemical elements by using absorption of optical radiation by free atoms in the gaseous state. Small amount of catalyst sample was dissolved in concentrated nitric acid and the solution was injected into the flame of AAS. The results was obtained in terms of ppm and was then converted to wt. %.

4.4. Results and discussion

4.4.1. C dots characterisation

Figure 4.3 shows the TEM image, FT-IR spectra, and TGA plots for the synthesized C dots. The sphere-like shaped nanoparticles are observed on the TEM image, which agrees with the literature support (Gong *et al.*, 2015) (Li *et al.*, 2012). FT-IR was used to determine the functional groups present in the C dots. The O-H stretch band was observed at 3290 cm-1, this may be caused by the presence of water remained after drying the C dots sample. A low intensity band was observed at 2980 cm^{-1}, which signify C-H stretch. The C=C stretch band was observed at 1620 ccm-1 and the C-O-C stretch band was observed at 1172 cm1-1. The high intensities of C-O-C, O-H, and C=O stretch band indicate that the C dots materials contains high content of oxygen and carbon content. Pal *et al.*, 2018 and Guo *et al.*, 2014, observed similar stretch bands.

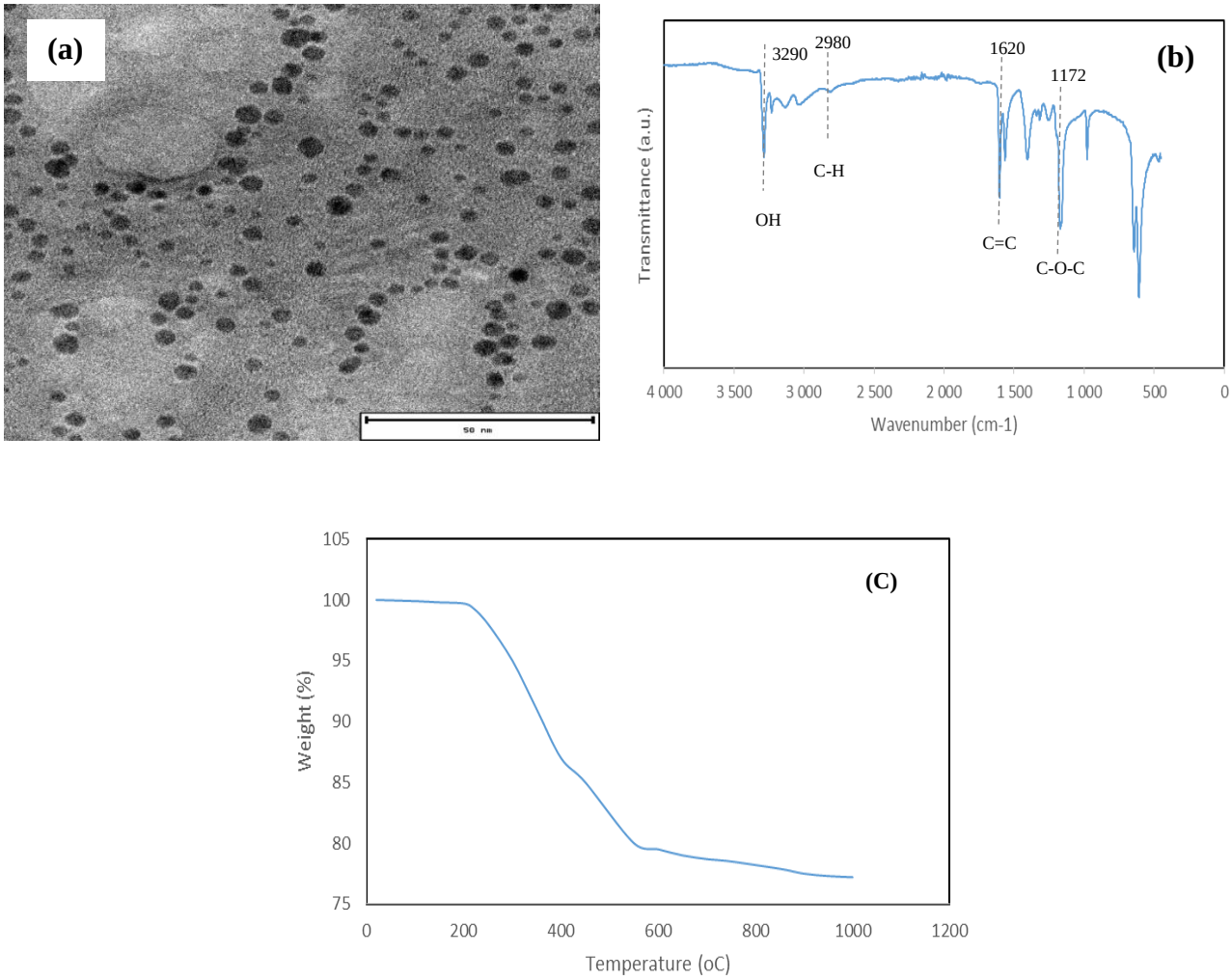


Figure 4. 3. (a) TEM image of synthesized C dots, (b) FT-IR spectrometry of C dots, (c) TGA plot of C dots.

TGA was used to determine the thermal stability of the C dots by measuring the rate of change of weight with respect to temperature in the presence of nitrogen flow. Numerous research reported that carbon with amorphous properties decomposes at temperatures as low as 500^{o}C and graphitic carbon decomposes at temperatures above 700^{o}C to CO and CO_2 (Vidal-abarca *et al.*, 2008) (Kumar *et al.*, 2015). At temperatures above 200^{o}C, the carbon nanostructure in the presence of heteroatoms in the carbon surface start to decompose due to removal of volatile and strongly anchored surface functional groups (Kumar *et al.*, 2015). In this study, a slight weight loss was observed at temperature above 250^{o}C and a drastic weight loss is observed after 400^{o}C.

4.4.2 Actual Ni-loading determination

AAS was used to determine the actual Ni-loading on the catalyst because the amount of nickel loaded into the catalyst during the experiment may differ after the catalyst is synthesised. This may be caused by the loss of materials during catalyst synthesis and human error. Five samples of catalyst were prepared and analysed with Ni-loading varied from 5-25 wt. %. The results obtained from the AAS analysis are presented in Table 4.1.

Table 4. 1. AAS analysis of the catalyst at different loadings.

Sample	Experiment Ni-loading (wt. %)	Actual Ni-loading (wt. %)	Relative error (%)
5% Ni-loading	5	4.51	9.8
10% Ni-loading	10	9.12	8.8
15% Ni-loading	15	14.44	3.7
20% Ni-loading	20	19.61	1.95
25% Ni-loading	25	24.70	1.2

All the actual catalyst loading were found to be lower than the expected loadings and their relative errors are different. At very low loadings the relative error is very significant and decreases as the nickel loading increases. The errors in the Ni-loadings may be caused by the loss of materials during preparation and transfers of materials during catalyst synthesis. The loss of materials at low nickel loading is significant. Therefore, the relative errors should be taken into consideration during catalyst synthesis. Extra amount of nickel should be added based on the relative error to obtain the accurate Ni-loading required.

4.4.3 Effect of Ni-loading on the Ni/C dots catalyst

The Ni/C dots catalyst at 5 %, 10 %, 15 %, 20 %, and 25 % Ni-loadings calcined at 350^{o}C were analysed to determine the effect of Ni-loading on Ni/C dots catalyst.

4.4.3.1 Thermal stability of Ni/C dots catalysts at different Ni-loading

TGA was performed to determine the thermal stability of the catalyst at different Ni-loading. TGA helps in determining the maximum temperature at which the catalyst start to degrade. Figure 4.4 shows the TGA graphs of the Ni/C dots catalyst at different Ni-loadings.

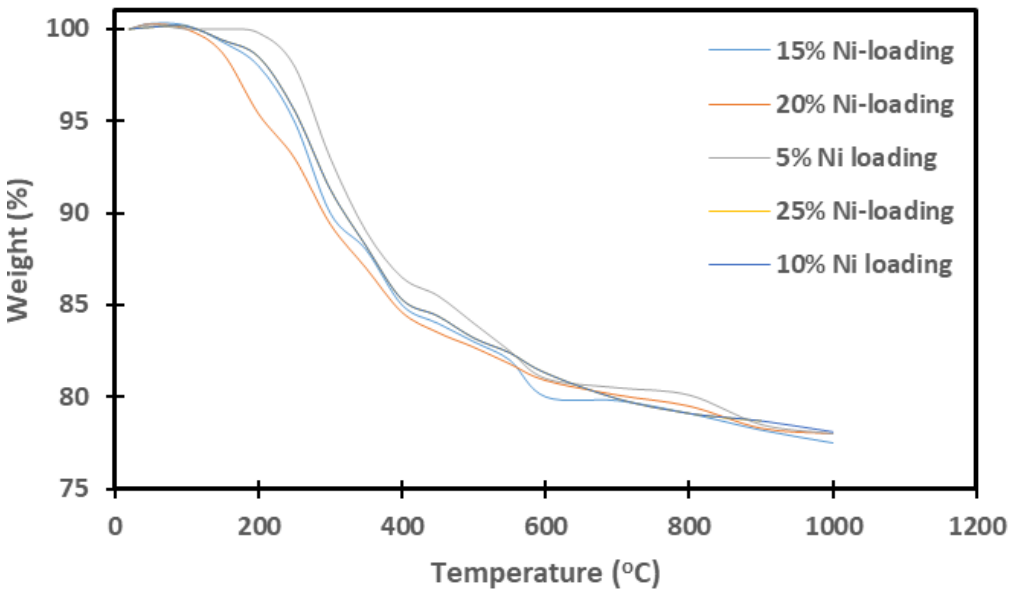


Figure 4. 4. TGA plot of the Ni/C dots catalyst at different Ni-loading.

Based on the TGA plot in Figure 4.4, it was observed that the weight loss of the catalyst decreases as the temperature increases. This means that as the temperature increases, the activeness of the catalyst decreases. Most of the catalysts decomposes very fast at temperatures above 200^{o}C. The decomposition rate increases with the increase in Ni-loading. At 25 % Ni-loading, the catalyst decomposes very fast after 150^{o}C and this catalyst decomposes very fast compared to other catalysts. While at 5 % Ni loading, the catalyst decomposes very slow compared to other catalysts and this catalyst start to decompose after 250^{o}C. Based on this results, it can be concluded that the thermal stability of the catalyst weakens as the Ni-loading increases. Akay (2016) obtained similar results on the effect of loading cobalt into silica (Co/Si). As the concentration of cobalt was increased the decomposition rate of the catalyst increased (Akay, 2016). It can be concluded that the Ni/C dots catalyst in this study should be calcined at Ni-loading of 5 wt. % or less to investigate the effect of calcination temperature.

4.4.3.2. Effect of Ni-loading on the pore size, surface area, and pore volume on the catalyst

The pore size, surface area, pore volume of the catalyst also affect the activity of the catalyst (Lu *et al*., 2015). Studies showed that the pore volume and surface area of the catalyst is affected by the amount of metal loading on support. Dewajan *et al.* (2016), investigated the effect of Ni-loading in Ni-ZNi/ZSM-5 catalysts by varying the Ni-loading from 2-7 wt. % using impregnation method and they observed that surface area and the pore volume decreases with the increase in Ni-loading. Lu *et al*. (2015) investigated the effect of cobalt loading from 10-30 wt. % supported by SBA-15 (Co/SBA-15) and they also observed that the surface area and

the pore volume decreases with the increase in cobalt loading. Regali *et al.* (2014) investigated the effect of palladium (Pd) loading from 0.18-1.2 wt. % supported by silica-alumina and they also observed that the surface area and the pore volume decreases with the increases in cobalt loading. These studies highlights the importance of metal loading on supports. Table 4.2 shows the BET results obtained for the 5 catalysts prepared with different metal loading.

Table 4. 2. The pore size, surface area, pore volume of the Ni/C dots catalyst at different Ni-loadings.

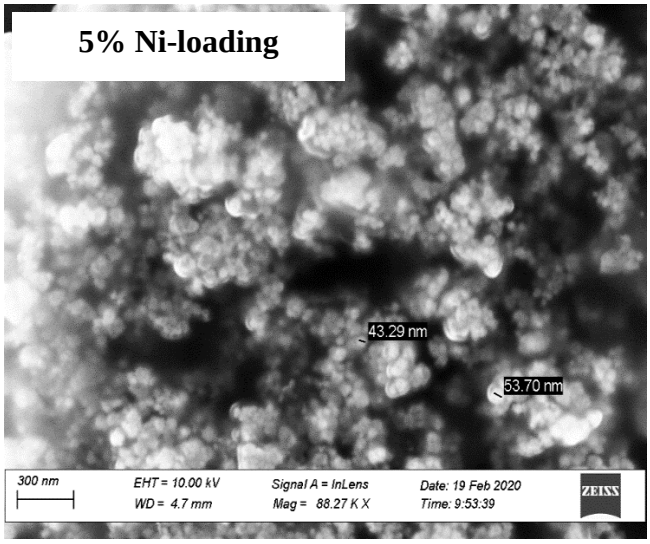
Sample	BET Surface area (m^2/g)	Pore volume (cm^3/g)	Pore size (nm)
5% Ni-loading	71.6940	0.3354	3.3274
10% Ni-loading	59.4814	0.2258	3.6919
15% Ni-loading	63.0306	0.1477	3.5898
20% Ni-loading	53.6665	0.1255	8.5783
25% Ni-loading	50.5456	0.1033	8.7043

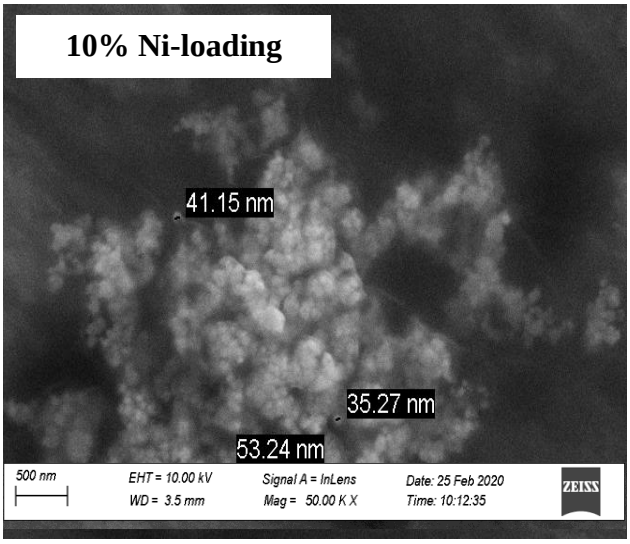
As expected, it was observed that an increase in Ni-loading resulted in decrease in BET surface area of the catalyst. As more nickel is loaded onto the C dots, the catalyst pores are being filled up resulting in the decrease in surface area. Majidian *et al.* (2014) studied the effect of nickel loading on the surface area of the catalyst supported on mesoporous nanostructured γ-Al_2O_3. They observed a decrease in the surface area of the catalyst from 182 to 160 m^2g^{-1} when the nickel loading is increased from 5 to 15 wt. %. Regali *et al*. (2014) studied the effect of loading palladium from 0 to 1.2 wt. % on amorphous silica-alumina in the hydrocracking of n-hexadecane. The similar trend was observed, the BET surface area increased with the increase in palladium loading (Regali *et al.*, 2014).The pore volume was observed to be decreasing with the increase in Ni-loading. The pore volume increased from 0.3354 cm^3/g to 0.1033 cm^3/g with increase of Ni-loading from 5 % to 2 %. Ragali *et al.*, 2014 observed the same trend, the pore volume decreased with the increase in palladium loading. The pore size of the catalyst increased with the increase in Ni-loading and this is caused by the increase in collection of nickel particles resulting to the formation of nickel crystals (Ragali *et al.*, 2014). The pore size of the catalyst affect the size of the molecules that can be diffused onto the solids, the total surface area available for adsorption, and also have an effect on the porosity of the catalyst (Dewajani *et al.*, 2016). Based on the results, the catalyst has the average pore size in the mesoporous region. Our data, is consistent to what is reported in literature.

4.4.3.3. Effect of Ni-loading on the morphology of the catalyst

Scanning electron microscope (SEM) and transmission electron microscope (TEM) were used to determine the morphology, topography, and the crystallinity of the Ni/C dots catalyst. The SEM images of the Ni/ C dots catalyst at different Ni-loadings are shown in Figure 4.5. The particles are spherical, the particle sizes are non-uniform, and they become more non-uniform as the Ni-loading is increased. More aggregated particles are being formed as the Ni-loading is increased and this may negatively affect the activity of the catalyst during the hydrocracking reaction because it was difficult to access the active site of the catalyst. The average size of the particles was also roughly determined by measuring the diameter of the particles in each Ni-loading as shown in Figure 4.5. The increase in Ni-loading resulted to the increase in the diameter of the particles which suggests the agglomeration of Ni particles into big particles. There is also uneven distribution of Ni and C dots over the catalyst and this means that the mixing of the catalyst was not thoroughly done.

The TEM images of the Ni/C dots catalyst at different Ni-loadings are shown in Figure 4.6. The spherical shape of the particles are also observed in the TEM images. The greyish layer around the dark particles is C dots and the dark particles are the Ni particles. Similar TEM images of Ni/C dots catalyst was observed by Guo *et al.,* 2014 and similar synthesis method was used. The dark particles are increasing as the Ni-loadings is increasing which shows the increase in Ni-particles. The particles becomes more aggregated as the Ni-loading is increased as observed in the SEM images.





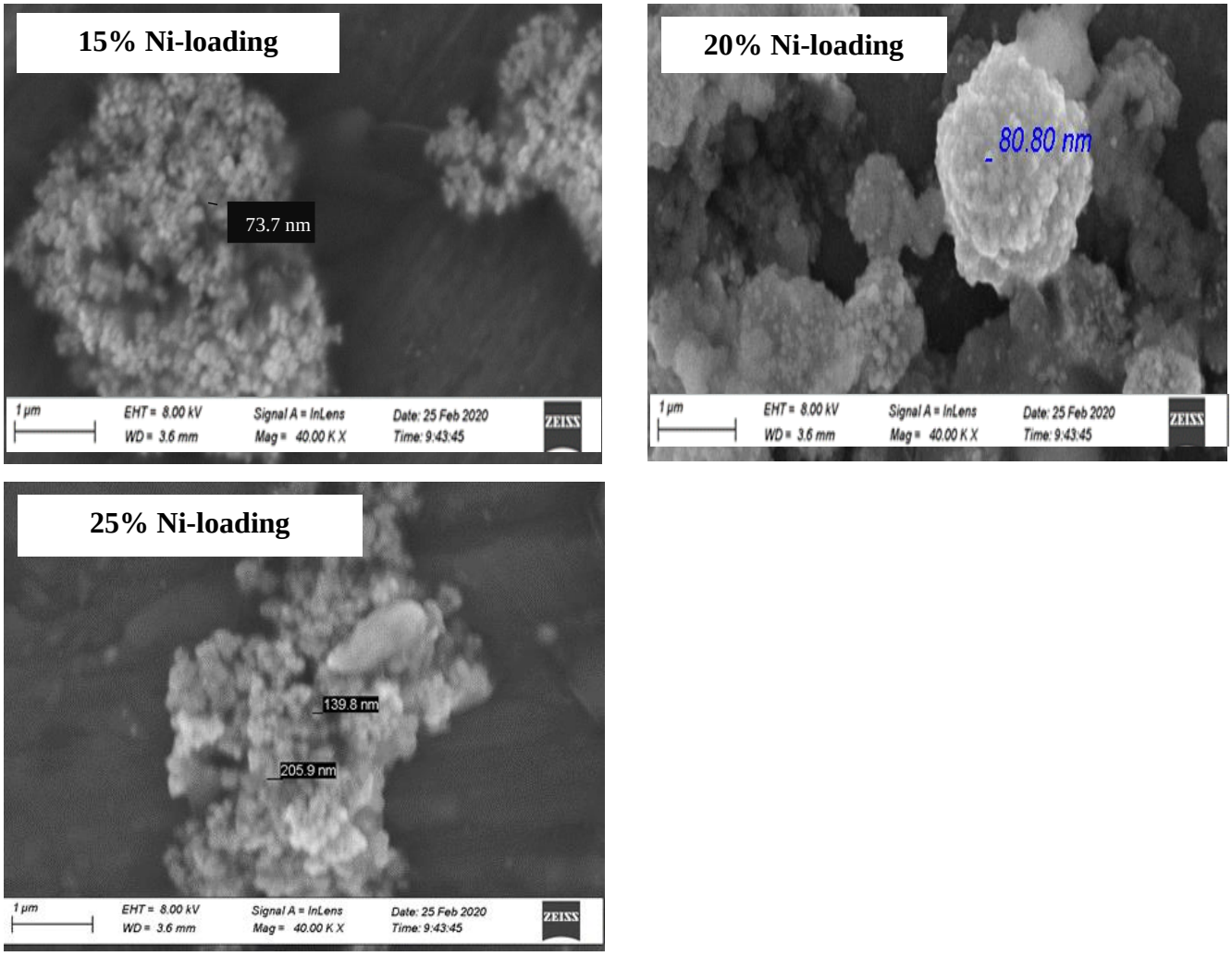
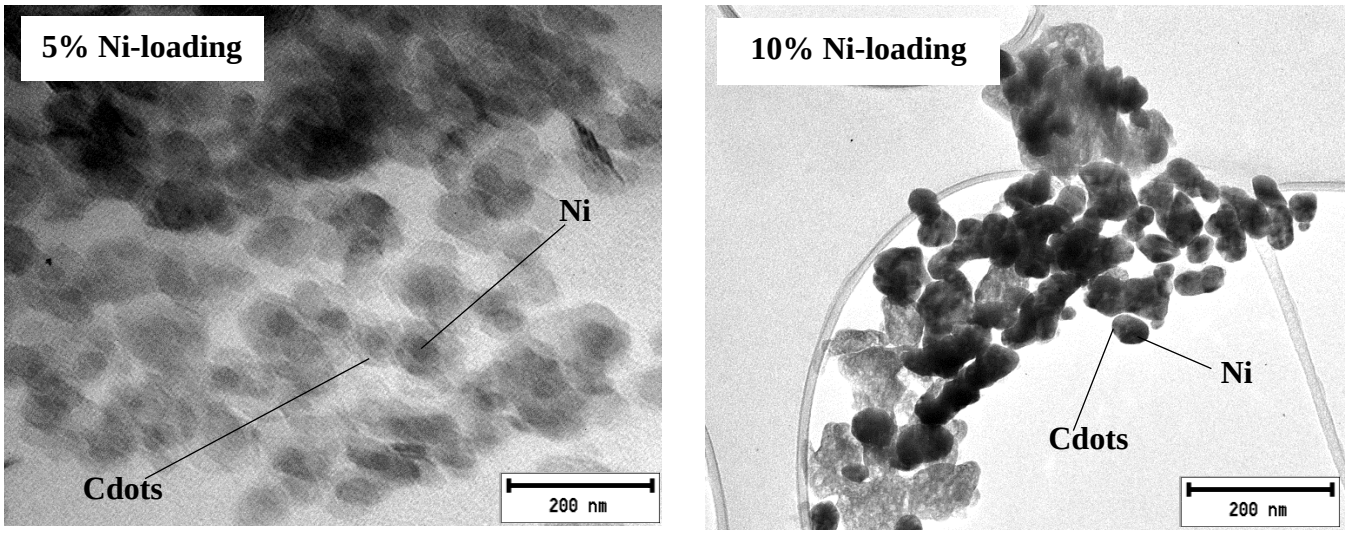


Figure 4. 5. SEM images for Ni/C dots catalyst at different Ni-loading.



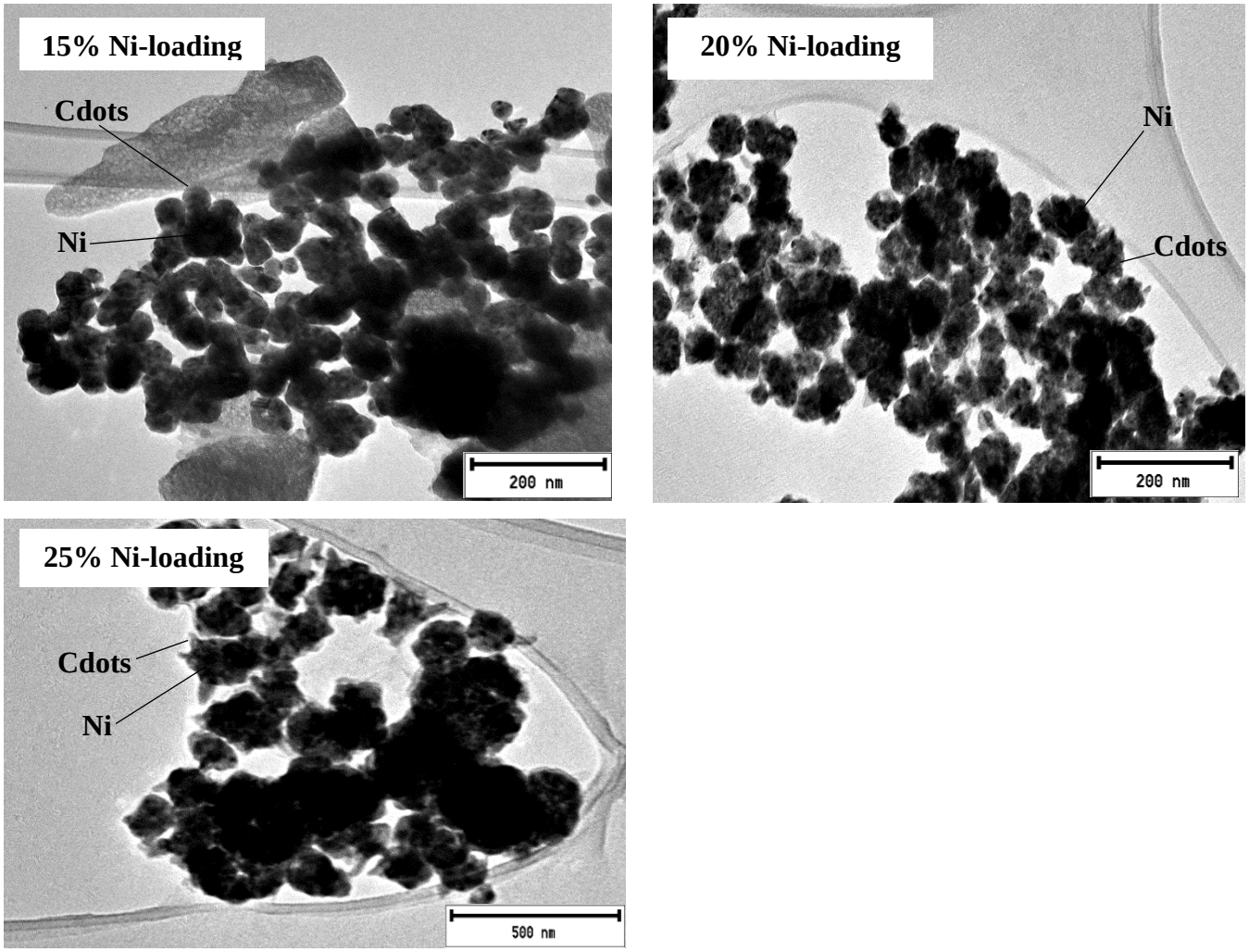


Figure 4. 6. TEM images for Ni/C dots catalyst at different nickel loading

4.4.3.4. FT-IR spectra of the catalyst at different Ni-loading

The FTIR spectra of the Ni/C dots catalyst at different Ni-loadings is shown in Figure 4.7. The spectra of each catalyst was obtained in the frequency range of 4000-500 cm-1. In this frequency range, the variation of the absorption profiles can be observed.

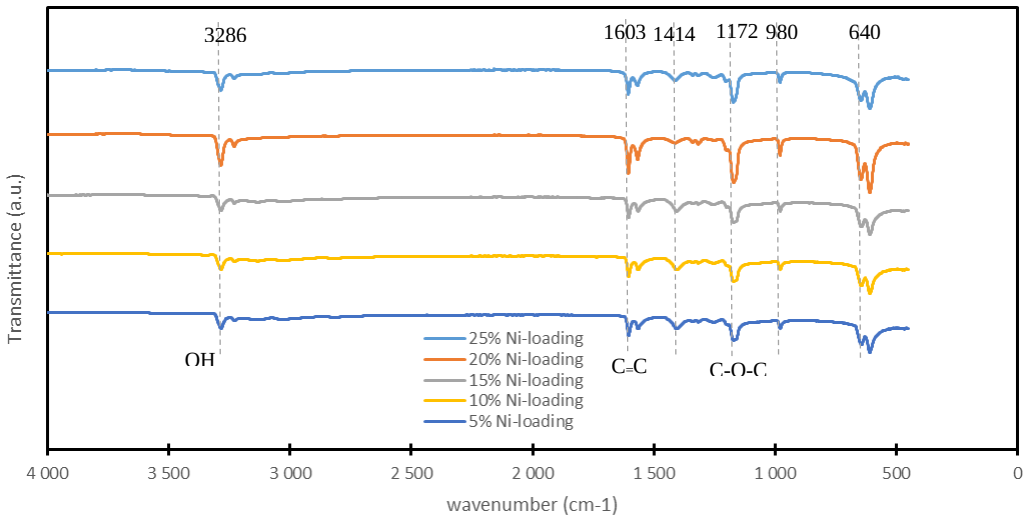


Figure 4. 7. FT-IR Spectra for Ni/C dots catalyst at different catalyst loading

The FTIR spectra of all the Ni/C dots catalyst exhibited the same trend on the characteristics of the stretching vibrations absorption band. The band at 3286 cm-1, 1603 cm-1,, and 1172 cm-1 are the characteristics of the stretching of –OH, C=C, and C-O-C groups on the surface of the catalyst. These characteristics was also observed by Guo *et al.* (2014) on Ni/C dots catalyst. The results showed the bands of O-H at 3434 cm-1, C=O at 1761 cm-1 and 1565 cm-1. There is no significance shift on the vibrations absorption bands with the change in Ni-loadings, which means that the change in Ni-loading does not affect the types of bonds in the catalyst. The peaks became more sharpener with the increase in Ni-loading. The same trend was observed by Parvas *et al*. (2019) on Ni/CeO_2–ZrO_2 nano-catalysts at different Ni loadings (0 %-20 %). At 0 %, 5 %,10 %,15 %, and 20 % there was no significance shift on the absorption bands but only the peaks became sharpener with the increase in Ni-loading and that was caused by more crystalline structure of NiO at high Ni-loading (Parvas *et al.*, 2019).

4.4.3.5. XRD analysis of the catalyst at different catalyst loading

The XRD analysis of Ni/C dots catalyst was done to determine the crystal phases in the structure of the catalysts at different Ni-loading. The XRD spectra of the Ni/C dots catalyst at different Ni-loading is shown in Figure 4.8.

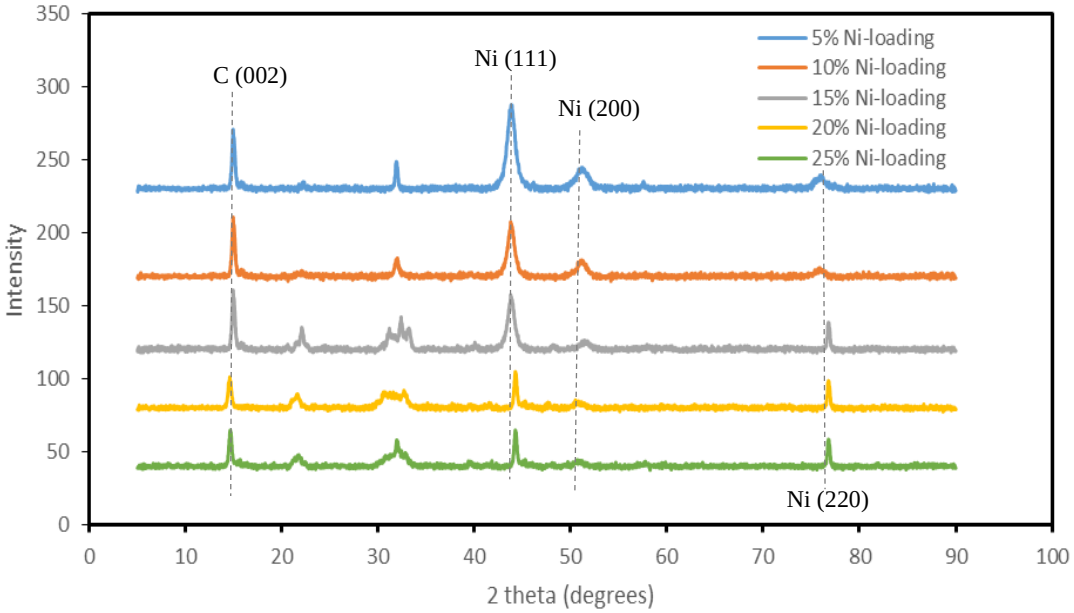


Figure 4. 8. XRD spectra of Ni/C dots at different Ni-loading

The XRD Spectra shows the bulk structure of Ni/C dots. The first peak at about 2θ value of 15^{o} labelled C (002) shows the present of carbon material and peak decreases with the increase in Ni-loading. This is because, an increase in Ni-loading result to a decrease in surface area of the catalyst caused by the blockage of the catalyst pores. The other three peaks named Ni (111), Ni (200), and Ni (220) at 2θ values of about 44.3^{o}, 52^{o}, and 77.5^{o} respectively, are the characteristics of face centered crystalline Ni (JPDS, Card No. 05-0681). Very small NiO peaks were also observed and this is because nickel particles are air-sensitive, they can react with oxygen. Similar XRD trend was observed by Lu *et al*. (2017) on the microwave-activated Ni-carbon catalyst.

4.4.4. Effect of calcination temperatures on the Ni/C dots

5 % Ni-loading catalyst was found to be the most desirable catalyst because it is stable on high temperatures and has large BET surface are compared to the other catalysts at different Ni-loadings. It was then calcined at 350^{o}C, 450^{o}C, 550^{o}C, 650^{o}C, and 750^{o}C to determine the effect of calcination temperatures on the characteristics and activity of the catalyst. TGA, BET, TEM, FTIR, and XRD were performed to determine the characteristics of the catalyst.

4.4.4.1. Thermal stability of the catalyst at different calcination temperatures

TGA of Ni/C dots at different calcination temperatures was performed to determine the thermal stability of the catalyst after calcination. Figure 4.9 shows the TGA graphs of the Ni/C dots catalyst at different calcination temperatures.

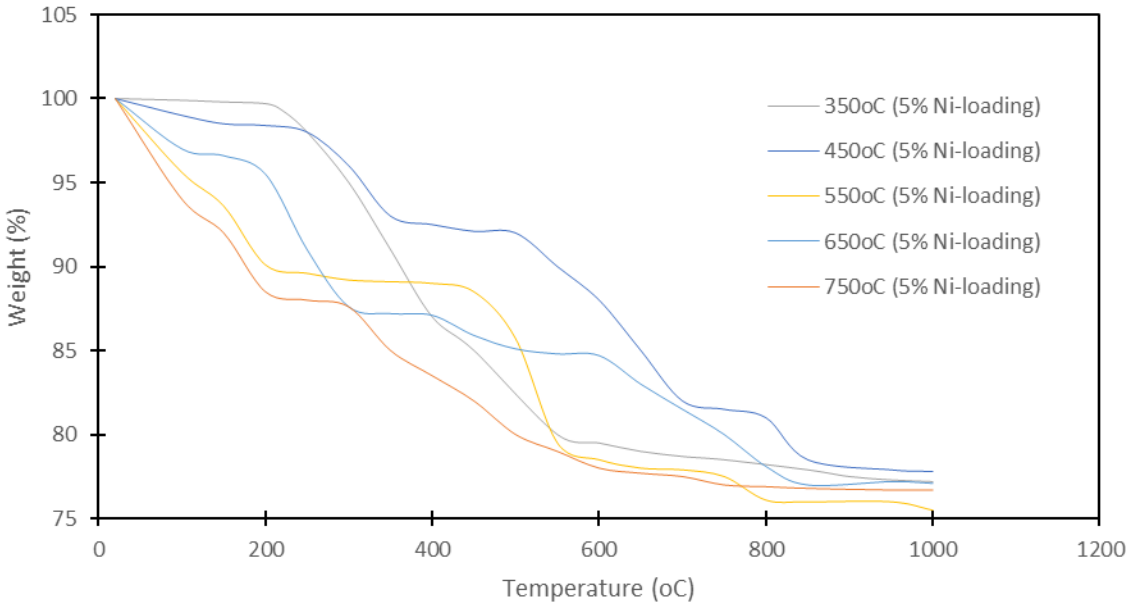


Figure 4. 9. TGA plot of Ni/C dots catalyst at different calcination temperatures

The thermal stability of the catalyst shows a different trend at calcination temperatures. The thermal stability of the catalyst decreases with the increase in calcination temperature. At 750^{o}C, the catalyst decomposes very fast compared to other catalyst calcined at 350-650^{o}C. This indicates that the catalyst calcined at higher temperatures are unstable. The catalyst calcined at 350^{o}C and 450^{o}C are more thermally stable compared to other catalyst. However, the catalyst calcined at 350^{o}C decomposes very fast after 210^{o}C. The catalyst calcined at 450^{o}C decomposes slowly after 300^{o}C and start to decrease very fast 550^{o}C. Therefore, the catalyst calcined at 450^{o}C was considered to be more thermally stable compared to the other catalyst.

4.4.4.2. Effect of calcination temperatures on the pore size, surface area, and pore volume of the catalyst

BET analysis was performed to determine the effect of calcination temperature on the pore size, surface area, and pore volume of the catalyst. Different papers have been reported on the effect of calcination temperature on the surface area, pore size, and pore volume of the catalyst. Xiao *et al.* (2018) reported the effect of calcination temperature on the mesoporous $ZnCo_2O_4$ rods catalyst synthesized by oxalate co-precipitation method calcined from 250-400^{o}C. The BET surface area decreased from 102.335-43.247 m^2/g with the increase in calcination temperature and both pore volume and pore size increased from 0.256-0.261 cm^3/g and 3.410-12.379 nm with increase in calcination temperature, respectively (Xia *et al*., 2018). Akbarzadeh *et al.* (2018) studied the effect of calcination temperature on Co/CNT (carbon nanotubes)

catalyst by calcined from 300ºC to 450ºC. They observed that the BET surface area decreases with the increase in calcination temperature from 208.8-211.3 m^2/g and the pore volume increased from 0.40-0.71 cm^3/g (Akbarzadeh *et al.*, 2018).

The results obtained from BET characterisation of the Ni/C dots catalyst at different calcination temperature are shown in Table 4.3.

Table 4. 3. The pore size, surface area, pore volume of the Ni/C dots catalyst at different calcination temperatures.

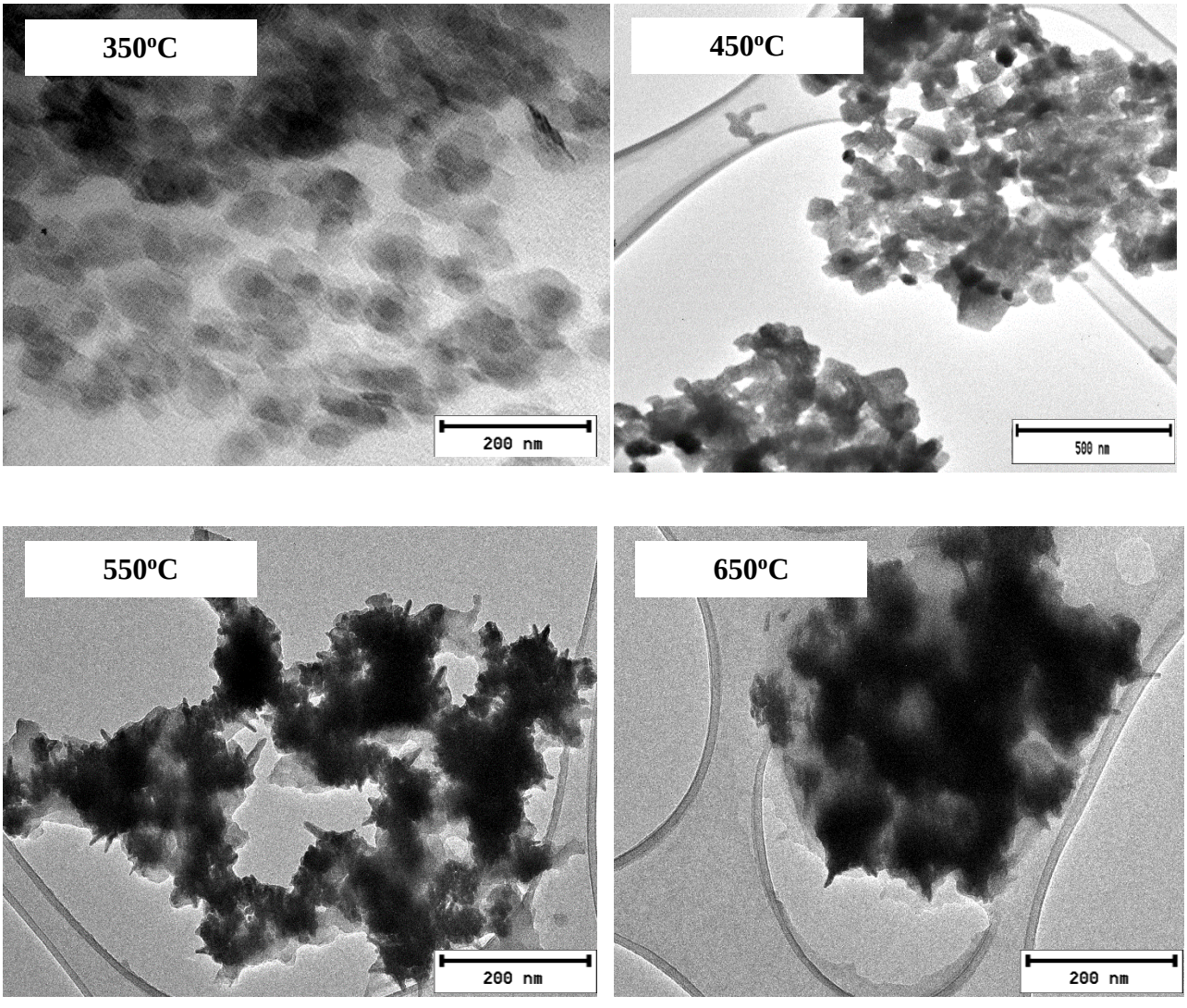
Sample	**BET Surface area (m^2/g)**	**Pore volume (cm^3/g)**	**Pore size (nm)**
350ºC (5% Ni-loading)	71.6940	0.3354	3.3274
450ºC (5% Ni-loading)	67.5768	0.3058	6.7911
550ºC (5% Ni-loading)	69.0323	0.2271	10.0898
650ºC (5% Ni-loading)	58.0533	0.1515	9.8788
750ºC (5% Ni-loading)	61.5215	0.1013	12.8941

The BET surface area of the Ni/C dots catalyst decreased with the increase in calcination temperature. The BET surface area of Ni/C dots calcined at 350ºC, 450ºC, 55ºC, 650ºC, and 750ºC are determined to be 71.6940, 67.5768, 69.0323, 58.0533, and 61.5214 m^2/g, respectively. The results obtained shows that the calcination temperature has a significant effect on the surface area of the catalyst. The pore volume of the catalyst increases with the increase in calcination temperature. The pore volume decreased from 0.3354 cm^3/g to 0.101 $3cm^3/g$. The pore size of the catalyst increased from 3.3274 nm to 12.8941nm with the increase in calcination temperature. Inmanee *et al*. (2017) suggested that the increase in calcination temperature causes the catalyst to be more aggregated resulting in losing the surface area, reducing the pore volume, and increasing the pore size of the catalyst.

4.4.4.3. Effect of calcination temperatures on the morphology of the catalyst

TEM was used to investigate the effect of calcination temperatures on the morphology, topography, and the crystallinity of Ni/C dots catalyst. The TEM images of Ni/C dots catalyst calcined from 350-70ºC.

The TEM images of Ni/C dots catalyst calcined from 350- 450ºC are shown in Figure 4.9. The increase in calcination temperature resulted to the increase in agglomeration of the catalyst. As the calcination temperature is increased, the spherical structure of Ni/C dots catalyst is being damaged. C dots start to disappear at higher temperatures and this is because C dots at higher temperatures is very unstable. Dong *et al.* (2020) observed the similar effect of calcination on the morphology of ZIF-67-Derived FeCo bimetallic catalysts. As they increase calcination temperature, the original structure of ZIF-67 was damaged and the particle surface became rough and blurry (Dong *et al.*, 2020).



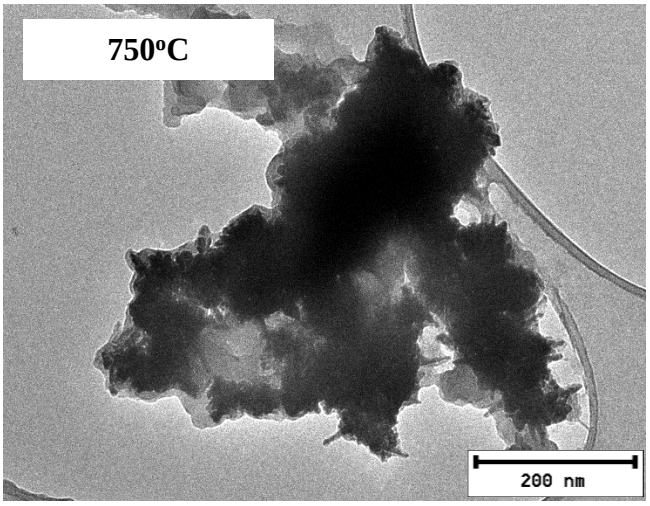


Figure 4. 10. TEM images of Ni/C dots catalyst at different calcination temperature.

4.4.4.4. FT-IR Spectra analysis of the catalyst at calcination temperatures

The FTIR spectra of Ni/C dots catalyst at different calcination temperature is shown in Figure 4.11.

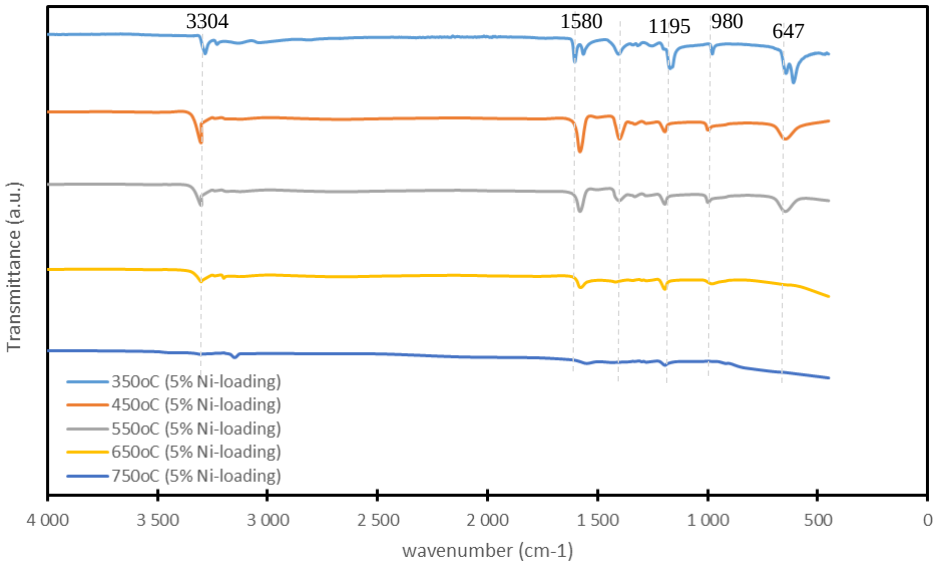


Figure 4. 11. FTIR spectra of Ni/C dots catalyst at different catalyst loading.

The FTIR spectra of all the Ni/C dots catalyst exhibited the same trend on the characteristics of the stretching vibrations absorption band. The band at 3304 cm-1, 1580 cm-1,, and 1195 cm-1 are the characteristics of the stretching of –OH, C=C, and C-O-C groups on the surface of the catalyst. The band FTIR spectra becomes flat with the increase in calcination temperature and that means that the catalyst loses the absorption bands with the increase in calcination temperature. The C-O-C and C=C band disappears with the increase with calcination temperatures this is because at higher temperatures the presence of heteroatoms in the carbon

surface start to decompose due to removal of volatile and strongly anchored surface functional groups (Kumar *et al.*, 2015).

4.4.4.5. XRD analysis of the catalyst at different calcination temperatures

The XRD spectra of Ni/C dots catalyst at different calcination temperatures is shown in Figure 4.12.

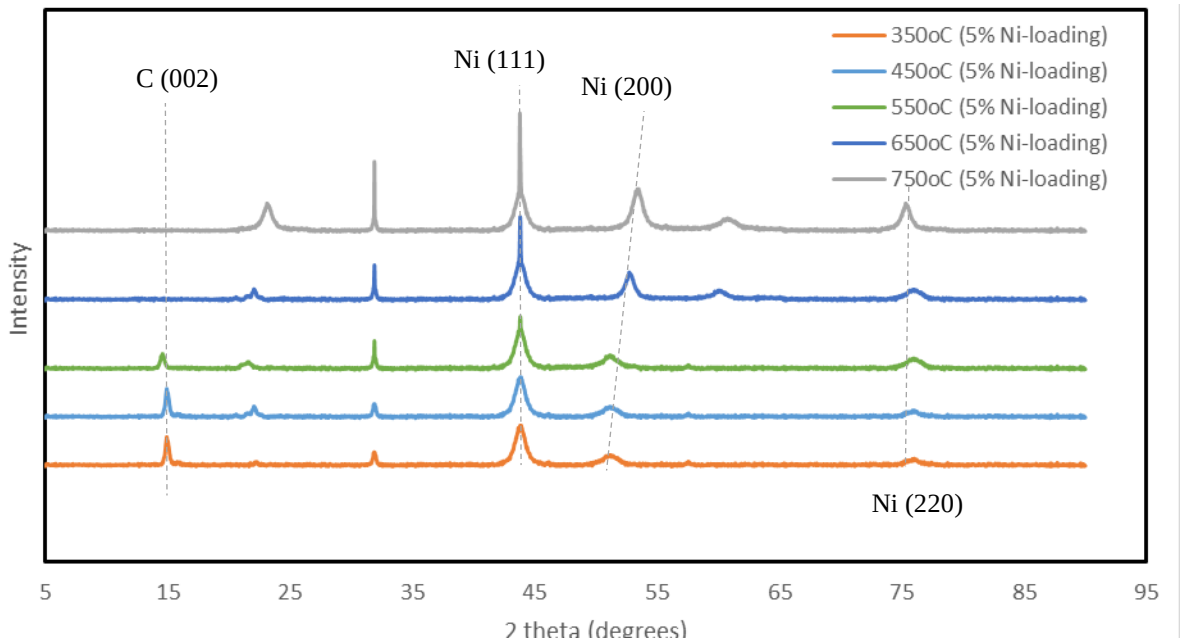


Figure 4. 12. XRD spectra of Ni/C dots catalyst at different calcination temperatures

The presence of carbon material at the first peak of about 2θ value of 15º named C (002) was also observed .After 550ºC, the carbon materials start to disappear and this may be caused by decomposition of carbon dots at higher temperatures. The other three peaks named Ni (111), Ni (200), and Ni (220) are also observed at 2θ values of about 44.3º, 52º, and 77.5º respectively, are the characteristics of face centered crystalline Ni (JPDS, Card No. 05-0681). These peaks increases with the increase in calcination temperature. NiO peaks were also observed and they increases with the increase in calcination temperatures.

4.5. Conclusion

The catalysts were successfully produced by impregnating nickel particles into C dots. The effect of Ni-loading and calcination temperatures on the characteristics of the catalysts were studied. Ni-loading was varied within the range of 5-25 wt. % to study the effect of Ni-loading on the characteristics of the catalysts. The thermal stability of the catalyst decreased with increase in Ni-loading and 5 wt. % Ni-loading showed the highest thermal stability. The BET

surface area decreased with increase in Ni-loading and 5 wt. % Ni-loading showed highest surface area of 71.6940 m^2/g. SEM and TEM were performed to determine the morphology, topography, and the crystallinity of the catalyst. All the catalysts were observed to be spherical and became more aggregated as Ni-loading is increased. The diameter of the catalysts increased with the increase in Ni-loading. It was also noticed that there was uneven distribution of Ni and C dots over the catalyst and this means that the mixing of the catalyst was not thoroughly done. FT-IR spectrometry was performed to determine different functional groups present in the catalysts. All the catalyst exhibited the same trend on the characteristics of the stretching vibrations absorption band and the peaks became more sharpener with the increase in Ni-loading. The band at 3286 cm-1, 1603 cm-1,, and 1172 cm-1 are the characteristics of the stretching of –OH, C=C, and C-O-C groups on the surface of the catalyst. The XRD peaks increased with the increase in Ni-loading and this means that more nickel particles were detected as Ni-loading is increased.

5 wt. % Ni-loading catalyst was calcined within the range of 350-750^{o}C to study the effect of calcination temperatures on the characteristics of the catalysts. The thermal stability of the catalyst decreased with the increase in calcination temperature and the catalyst calcined at 350^{o}C showed highest thermal stability. The BET surface area decreased with the increase in calcination temperature and the catalyst calcined at 350^{o}C showed the highest BET surface area. The increase in calcination temperature caused the catalyst to lose the spherical shape and the catalyst became more agglomerated. The FTIR spectra of all the Ni/C dots catalyst exhibited the same trend on the characteristics of the stretching vibrations absorption band however, the peaks became less sharpener with the increase in Ni-loading. The XRD spectra showed the increase in number of peaks and the peaks became more sharpener with the increase in calcination temperature.

5 wt. % catalyst calcined at 350^{o}C showed favourable characteristics compared to the other catalyst. It is highly thermally stable and has the highest BET surface area.

4.5. Refferences

Akbarzadeh, O., Mohd Zabidi, N., Abdul Wahab, Y., Hamizi, N., Chowdhury, Z., Aljunid Merican, Z., Ab Rahman, M., Akhter, S., Shalauddin, M. and Johan, M., 2018. Effects of Cobalt Loading, Particle Size, and Calcination Condition on Co/CNT Catalyst Performance in Fischer–Tropsch Reactions. *Symmetry*, 11(1), p.7-32.

Ananikov, V., 2015. Nickel: The "Spirited Horse" of Transition Metal Catalysis. *ACS Catalysis*, 5(3), pp.1964-1971.

Dewajani H., Rochmadi, Purwono S., and Budiman A., 2016. Effect of Modification ZSM-5 Catalyst in Upgrading Quality of Organic Liquid Product Derived from Catalytic Cracking of Indonesian Nyamplung Oil (Calophyllum inophyllum). *Advances of Science and Technology for Society*, 1755(1), pp.10-63.

Dong, Z., Zhao, J., Tian, Y., Zhang, B. and Wu, Y., 2020. Preparation and Performances of ZIF-67-Derived FeCo Bimetallic Catalysts for CO2 Hydrogenation to Light Olefins. *Catalysts*, 10(4), p.455-607.

Gong, J., Lu, X., and An, X., 2015 Carbon dots as fluorescent off–on nanosensors for ascorbic acid detection. RSC Adv. 5, pp.8533–8536.

Gupta, A., 2019. *Application Of Carbon Nano Dots*. Ashland: Arcler Press.

Guo, Y., Wang, D., Liu, X., Wang, X., Liu, W. and Qin, W., 2014. Synthesis and characterization of the nickel@carbon dots hybrid material and its application in the reduction of Cr(vi). *New J. Chem.*, 38(12), pp.5861-5867.

Inmanee, T., Pinthong, P. and Jongsomjit, B., 2017. Effect of Calcination Temperatures and Mo Modification on Nanocrystalline (γ-χ)-Al2O3 Catalysts for Catalytic Ethanol Dehydration. *Journal of Nanomaterials*, 6(1), pp.1-9.

Kumar, K. S., Pittala, S., Sanyadanam, S. and Paik, P., 2015. A new single/few-layered graphene oxide with a high dielectric constant of 10^6: contribution of defects and functional groups. *RSC Adv. 5,* 14768–14779.

Laginhas, C., Nabais, J. and Titirici, M., 2016. Activated carbons with high nitrogen content by a combination of hydrothermal carbonization with activation. *Microporous and Mesoporous Materials*, 226, pp.125-132.

Li, H., Kang, Z., Liu, Y. and Lee, S. T., 2012. Carbon nanodots: synthesis, properties and applications. J. Mater. *Chem. 22,* 24230.

Pal, A. Ahmad, K., Pan, U., Chattopadhyay, A. and Paul, A., 2018. Synthesis of single-particle level white-light-emitting carbon dots via a one-step microwave method. *Journal of Materials Chemistry C,* 6(25), pp.6691-6697.

Parvas, M., Haghighi, M. and Allahyari, S., 2019. Catalytic wet air oxidation of phenol over ultrasound-assisted synthesized Ni/CeO2–ZrO2 nanocatalyst used in wastewater treatment. *Arabian Journal of Chemistry*, 12(7), pp.1298-1307.

Regali, F., Liotta, L., Venezia, A., Montes, V., Boutonnet, M. and Järås, S., 2014. Effect of metal loading on activity, selectivity and deactivation behavior of Pd/silica–alumina catalysts in the hydroconversion of n-hexadecane. *Catalysis Today*, 223, pp.87-96.

Su, F., Qiu, X., Liang, F., Tanaka, M., Qu, T., Yao, Y., Ma, W., Yang, B., Dai, Y., Hayashi, K. and Watanabe, T., 2018. Preparation of Nickel Nanoparticles by Direct Current Arc Discharge Method and Their Catalytic Application in Hybrid Na-Air Battery. *Nanomaterials*, 8(9), p.684-702.

Vidal-Abarca, C., Lavela, P. and Tirado, J. L., 2008. Cobalt Oxide Nanoparticles Prepared from Reverse Micelles as High-Capacity Electrode Materials for Li-Ion Cells. *Electrochem. Solid-State Lett. 11,* A198–A201.

Wu, L. and Ritchie, S., 2006. Removal of trichloroethylene from water by cellulose acetate supported bimetallic Ni/Fe nanoparticles. *Chemosphere*, 63(2), pp.285-292.

Yang, Y., Liu, J., Guo, S., Liu, Y. and Kang, Z., 2015. A nickel nanoparticle/carbon quantum dot hybrid as an efficient electrocatalyst for hydrogen evolution under alkaline conditions. *Journal of Materials Chemistry A*, 3(36), pp.18598-18604.

Zhuang, Z., Giles, S., Zheng, J., Jenness, G., Caratzoulas, S., Vlachos, D. and Yan, Y., 2016. Nickel supported on nitrogen-doped carbon nanotubes as hydrogen oxidation reaction catalyst in alkaline electrolyte. *Nature Communications*, 7(1), p.101-123.

Chapter 5: Hydrocracking process

This chapter focuses on the hydrocracking of castor oil using Ni/C dots catalyst. The effect of hydrocracking temperature, catalyst amount, and hydrocracking time was studied to determine the optimum operating conditions of the hydrocracking process.

5.1. Introduction

Different technologies are available for bio-fuel production from plants oils including catalytic hydrocracking, thermal cracking, and transesterification (Bezergianni and Kalogianni, 2009). These technologies are more discussed in the literature review section. Catalytic hydrocracking was found to be the better technology to produce bio-fuel from castor oil because of more desirable fuel properties and it also enhance engine fuel economy (Dizge et *al.,* 2009). The industrial application of producing bio-fuel from non-edible plant oils would be successful whenever the suitable technology is used properly through optimisation of operating conditions to produce maximum bio-fuel and when then feedstock sufficient to guarantee a steady and continuous production process (Zaher *et al.* 2015).

The production of biogasoline and biojet from hydrocracking of plant oils have been successfully done by researchers. Mampuru *et al.* (2019) produced 59.50 wt. % biogasoline from waste cooking oil at reaction temperature of 250^{o}C, reaction time of 1 h, and with 5 wt. % Ni-loading calcined at 300^{o}C. Habibie *et al.* (2018) produced 36.43 wt. % and 23.08 wt. % of biojet and biogasoline, respectively from hydrocracking of vegetable oil using NiMo/Zeolite catalyst at reaction temperature of 375^{o}C, reaction time of 1.5 h. This chapter aim to maximise the production of biogasoline and biojet from castor oil using Ni/C dots catalyst through hydrocracking. For this study, the biogasoline carbon range was classified to be within C_5-C_{10}, biojet fuel to be within C_9-C_{16}, and biodiesel to be within C_{15}-C_{20}.

5.2. Materials and methods

The method and setup for hydrocracking of castor oil in this study was developed based on the previous work done by researchers. The hydrocracking setup was constructed within the safety measures to mainly protect the environment from hydrogen gas exposure and high temperature. The hydrocracking reaction was performed inside liquid phase batch reactor set-up at constant hydrogen pressure flow of 0.5 kPa

The samples were prepared by adding fixed volume of 100 mL of castor oil into a beaker and the required amount of catalyst was measured and transferred into the beaker. The mixture was then ultra-sonicated for 20 minutes to disperse the solids of the catalyst throughout the oil. The mixture was then transferred to 500 mL three neck round bottom flask (reactor) and was then placed into the heating mantle and connected to a condenser and gas inlet pipe. The hydrocracking set-up is shown in Figure 5.1.

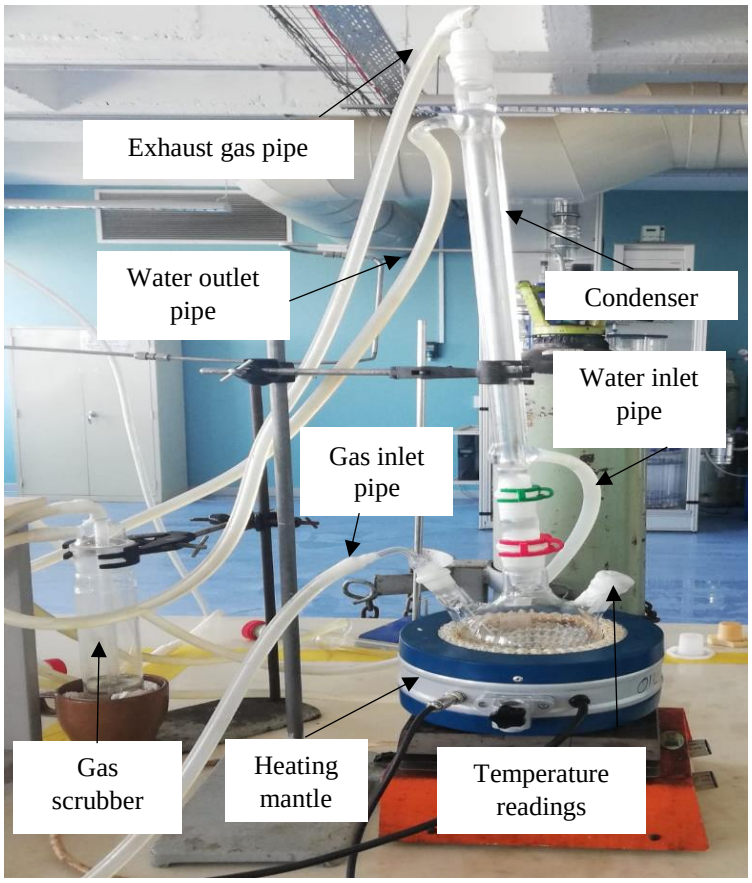


Figure 5. 1. Hydrocracking experimental setup

Before each run, the system was purged with nitrogen gas at 0.5 kPa for 20 minutes to remove unwanted materials. The reaction temperature was varied within the range of 150-350^{o}C, reaction time of 0.5-2.5 h, and catalyst: oil ratio of 0.001-0.005 g/mL.

5.3. Results and discussion

The effect of Ni-loading, calcination temperature, reaction temperature, reaction time, and catalyst ratio on the production of biojet and biogasoline was studied. The system was then optimised using response surface methodology (RSM) to determine the optimal operating conditions that maximises production. The hydrocracked product was characterised using GC-MS analysis.

5.3.1. Effect of Ni-loading and calcination temperature on the production yield

The effect of Ni-loading and calcination temperature on the production of biojet and biogasoline was studied by varying Ni-loading and calcination temperature within the range of 5-25 % and 350-750^{o}C, respectively. Reaction temperature, reaction time, hydrogen pressure, and catalyst/oil ratio was kept constant at 250^{o}C, 1.5 h, 0.5 kPa, and 0.003 g/mL, respectively.

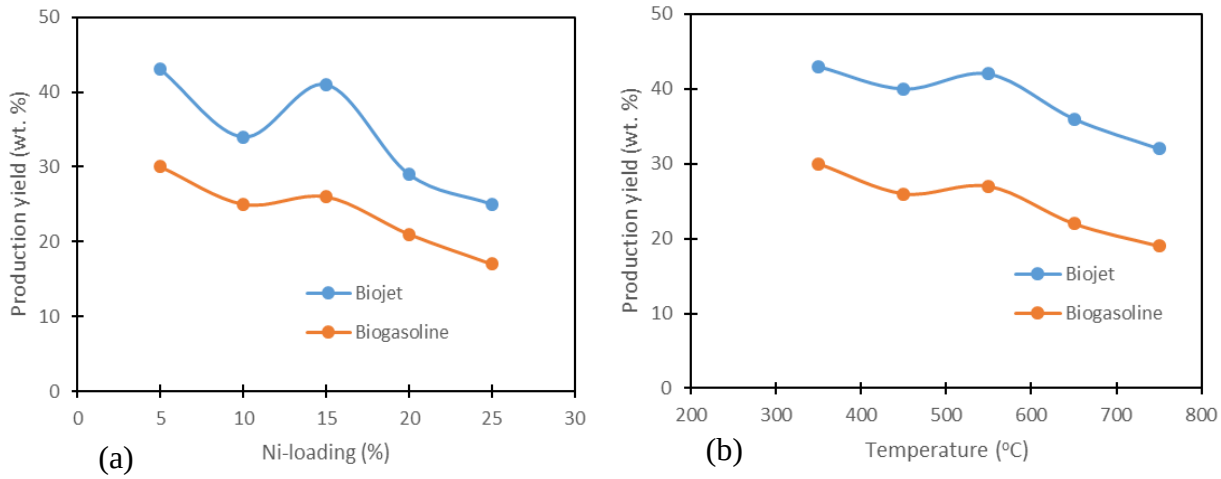


Figure 5. 2. (a) Effect of Ni-loading on the production of bi-jet and biogasoline, and (b) Effect of calcination temperature on the production of biojet and biogasoline.

The production yield of biogasoline and biojet decreased from 5-10 % Ni-loading at constant calcination temperature of 350^{o}C, increased from 10-15 % and decreased drastically after 15 % Ni-loading. This trend is supported by the BET surface area results reported in section 4.4.2.2. The BET surface area decreased from 71.69-59.48 m^2/g at 5-10 %, increased to 63.03 m^2/g at 15 %, and then decreased after 15 % Ni loading. This means that the increased in surface area of the catalyst has positive effect on the production of biojet and biogasoline and similar effect was observed by Dewajani,*et al.* (2016) . It was also observed on the SEM images that the increase in Ni-loading result to the increase in agglomeration of Ni-particles, which negatively affect the activity of the catalyst and similar effect was also observed by Dewajani *et al.* (2016). The highest production of 43 wt. % and 30 wt. % of biojet and biogasoline, respectively was observed at 5 % Ni-loading. Chen *et al.* (2005) observed that lower Ni-loading resisted coking compared to higher Ni-loading during catalytic partial oxidation of methane to syngas.

5 % Ni-loading catalysts was calcined from 350-750^{o}C to study the effect of calcination temperature on the production yield of biojet and biogasoline. The trend was agrees with the BET surface area results reported in section 4.4.3.2. It was also observed on the TEM images

that the increase in calcination temperature caused the catalyst to lose its spherical structure and the catalyst became more agglomerated which negatively affect the production yield and similar effect was observed by Dong *et al.* (2020). The highest production of biogasoline and biojet was observed at calcination temperature of 350°C and this catalyst was observed to be thermally stable and has highest BET surface area compared to the other catalysts.

5.3.2. Effect of reaction temperature, reaction time, and catalyst/oil ratio on the production yield

The effect of reaction temperature, reaction time, catalyst/oil ratio was studied using the catalyst that showed favourable characteristics and highest production of biojet and biogasoline, which is 5 % Ni loading catalyst calcined at 350°C.

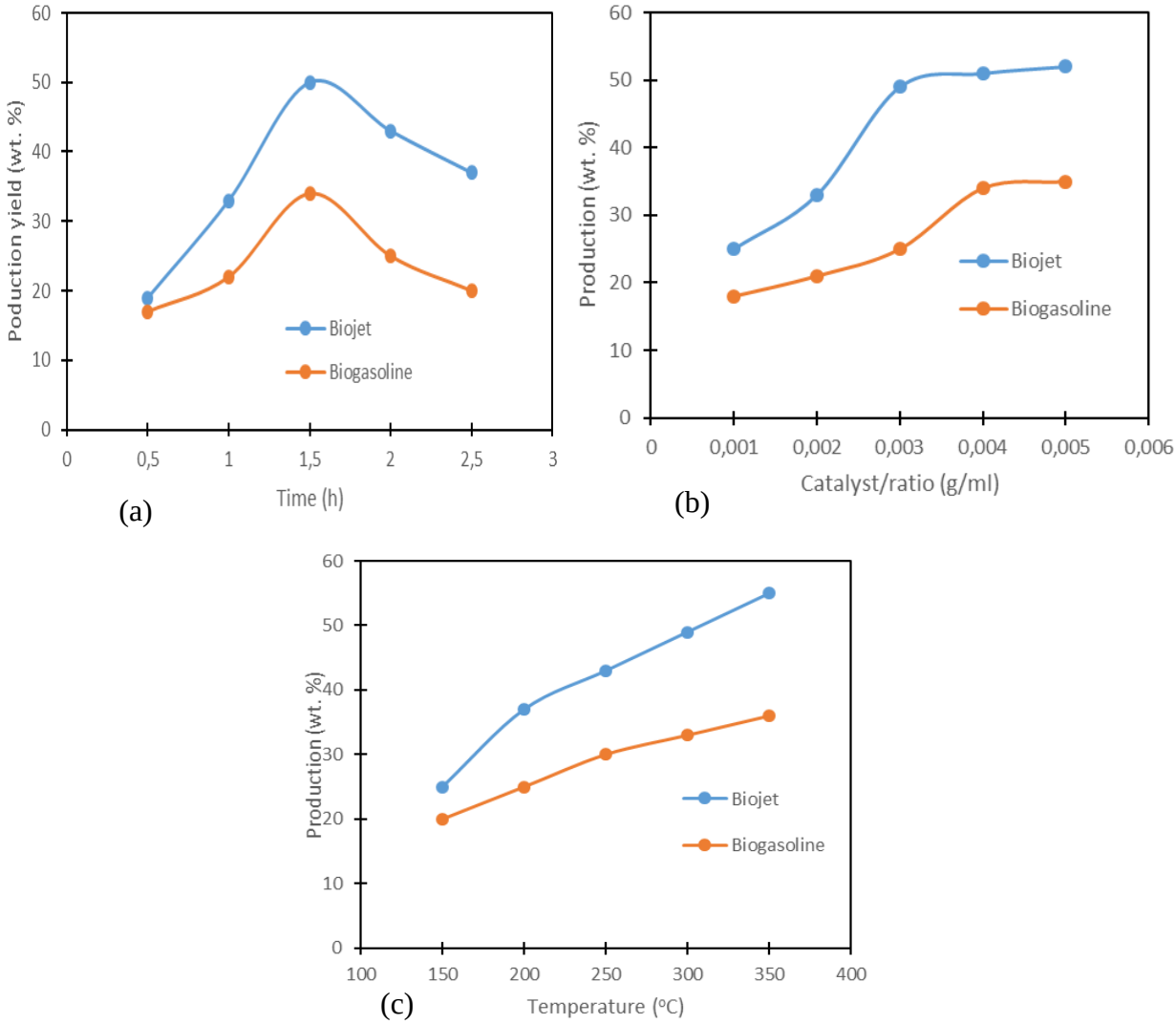


Figure 5. 3. (a) Effect of time on the production yield, (b) effect of catalyst/ratio on the production yield, and (d) effect of temperature on the production yield.

The effect of reaction time on the production yield was studied by varying the time within 0.5-2.5 h while reaction temperature and catalyst/oil ratio was kept constant at 250^{o}C and 0.003 g/mL, respectively. It was observed that the production yield increases from 0.5 to 1.5 h and then start to decrease after 1.5 h. The production yield increases with the increase in reaction time because more time is allowed for heavy hydrocarbons to break into light hydrocarbons until optimal reaction time is reached. The decrease of production yield after 1.5 h may be cause by the evaporation of light fraction hydrocarbons to become gas phase due to longer reaction time. Morgan *et al.* (2012) suggested that the decrease of biojet and biogasoline over longer reaction time is caused by more coking and cracking of unsaturated triglycerides in thee feedstock. Similar trend was observed Yotsomnuk and Skolpap (2018) during hydrocracking of waste virgin coconut oil using HZSM-5 zeolite catalyst to produce biofuel. After 1 h the production of biojet decreased and biogasoline production increased very slowly operating at reaction temperature of 400^{o}C and hydrogen pressure of 40 bar. 50 wt. % and 34 wt. % was obtained as maximum biojet and biogasoline yield, respectively at 1.5 h (Yotsomnuk and Skolpap, 2018).

The effect of catalyst/oil ratio on the production yield was studied by varying catalyst/oil ratio within the range of 0.001-0.005 g/mL while reaction time and reaction temperature was kept constant at 1.5 h and 250^{o}C, respectively. The production yield increased with the increase in catalyst/oil ratio for both biogasoline and biojet until the optimal catalyst/oil ratio of 0.04 g/mL is reached. The higher ratio of catalyst to the feed resulted to the increase in production yield because of the increase in surface area of the catalyst during hydrocracking. Similar trend was observed by Dewi *et al.* (2014) during hydrocracking of waste lubrication oil into biofuel. They observed that the production of gasoline and kerosene increased with the increase in catalyst/oil ratio (Dewi *et al*. 2014). Fanani (2010) stated that the increase on the amount of catalyst used causes the surface area of the catalyst to increase. The increase in surface area increases the active sites of the catalyst resulting to increase in cracking rate of the oil (Fanani, 2010).

The effect of reaction temperature on the production yield of biogasoline and biojet was studied by varying the reaction temperature within the range of 150-350^{o}C while reaction time and catalyst/oil ratio was kept constant at 1.5 h and 0.003 g/mL, respectively. It was observed that the production yield increases with the increase in reaction temperature. Similar trend was observed Yotsomnuk and Skolpap (2018) during hydrocracking of waste virgin coconut oil using HZSM-5 zeolite catalyst at temperature within 350-400^{o}C. The increase in temperature favoured the production of gasoline and kerosene.

Table 5. 1. Comparison of biojet and biogasoline production yield from different researchers.

Oil source	Nickel based catalyst	Operating conditions	Production yield	Reference
Waste cooking oil	NiMo/SBUY-MCM-41	T=380^{o}C P= 3MPa H_2/Oil=500mL/mL	54 wt. % biojet 28 wt. % biogasoline	(Zhang *et al*., 2019)
Waste cooking oil	Ni-Mo/alumina	T=250^{o}C Time= 1 h Catalyst/oil= 1/75	59.5 wt. % biogasoline	(Mampuru *et al.*, 2019)
Vegetable oil	NiMo/Zeolite	T= 375^{o}C Time= 1.5 h P=atmospheric	36.43 wt. % biojet 23.1 wt. % biogasoline	(Habibie *et al*., 2018)
Castor oil	Ni/C dots	T= 350^{o}C Time= 1.5 h Catalyst/oil=0.03 g/mL (3g/100mL)	55 wt.% biojet 36 wt.% biogasoline	This study

Table 5.1 shows the biojet and biogasoline production yield obtained by different researchers at different operating conditions. In this study, 55 wt. % biojet was produced which is higher compared to the biojet yield obtained by other researchers. Mampuru *et al.* (2019) produced biogasoline with 4 % more than this study without promoting biojet fuel. Zhang *et al*. (2019) produced a comparable amount of biofuels with the current study, but this study reduce the energy consumption by an equivalent of 30^{0}C less increasing the biogasoline by 8 wt. %. The results showed that nickel supported on C dots is a potential catalytic material for the production of biojet and biogasoline fuels. Future investigation should be done decrease the energy used in this process.

5.3.3. Reaction kinetics

Most studies reported on the hydrocracking of plant oil have dealt with the physical and chemical properties of the hydrocracked products, production yield distribution, and development of new hydrocracking process. Kinetics studies of hydrocracking process have received much less attention. Qader *et al.*, (1969) studied the kinetics of hydrocracking reaction

of gas oil in the temperature range of 300-400^{o}C over as sulfided nickel-tungsten catalyst supported on silica-alumina and they reported that the reaction followed first order kinetics with activation energy of 21.1 kcal/mol. Sikonia (1985) obtained activation energy ranging from 40-65 kcal/mol for hydrocracking reaction of vacuum gas oils from different crude oils. This study investigates the reaction order and activation energy of hydrocracking reaction of castor oil using Ni/C dots catalyst.

The reaction order gives the relationship between the concentrations of the reactants and the rate of reaction. The rate law for a reaction is known to be of the form:

$$r = k[A]^n \quad (5.1)$$

Where r is the reaction rate, k is the rate constant, and n is the reaction order. The order of the reaction in this study was determined graphically for the production of biojet and biogasoline. Table 5.2 shows the R^2 values of different reaction orders for biojet production.

Table 5. 2. Biojet reaction orders

	Zero Order	**Half Order**	**First Order**	**First half Order**	**Second Order**	**Third order**	**Third half**	**Forth order**	**Forth half**
Time (h)	Conc (Wt. %)	$Conc^{0.5}$	ln(Conc)	$Conc^{-1.5}$	$Conc^{-1}$	$Conc^{-2}$	$Conc^{-2.5}$	$Conc^{-3}$	$Conc^{-3.5}$
0.5	19	4,3589	2,9444	0,0121	0,0526	0,002770	0,000636	0,000146	0,000033
1	33	5,7446	3,4965	0,0053	0,0303	0,000918	0,000160	0,000028	0,000005
1,5	50	7,0711	3,9120	0,0028	0,0200	0,000400	0,000057	0,000008	0,000001
2	43	6,5574	3,7612	0,0035	0,0233	0,000541	0,000082	0,000013	0,000002
2,5	37	6,0828	3,6109	0,0044	0,0270	0,000730	0,000120	0,000020	0,000003
R^2	**0,3895**	**0,4305**	**0,4651**	**0,5225**	**0,5107**	**0,5286**	**0,5306**	**0,5299**	**0,5276**

- The trial run from zero order to forth and half order was carried out to determine the reaction order for biojet production
- The 5th order reaction was not performed because it's highly unlikely that five atoms or molecules would collapse at one point of time. This is not possible theoretically but research is also going on to figure it out.
- The R^2 values for all the reaction orders are below 90 % which means that reaction order for biojet production does not fall within this range.
- Further investigation should be carried out to model the reaction order for biojet production

The reaction orders for the production of biogasoline was also investigated and the R^2 values at different reaction orders are shown in Table 5.3.

Table 5. 3 Biogasoline reaction orders

	Zero Order	**Half Order**	**First Order**	**First half Order**	**Second Order**	**Third order**	**Third half**	**Forth order**	**Forth half**
Time (h)	Conc (Wt. %)	$Conc^{0.5}$	ln(Conc)	$Conc^{-1.5}$	$Conc^{-1}$	$Conc^{-2}$	$Conc^{-2.5}$	$Conc^{-3}$	$Conc^{-3.5}$
0.5	17	4,1231	2,8332	0,0143	0,0588	0,0035	0,000839	0,000204	0,000049
1	22	4,6904	3,0910	0,0097	0,0455	0,0021	0,000440	0,000094	0,000020
1,5	34	5,8310	3,5264	0,0050	0,0294	0,0009	0,000148	0,000025	0,000004
2	25	5,0000	3,2189	0,0080	0,0400	0,0016	0,000320	0,000064	0,000013
2,5	20	4,4721	2,9957	0,0112	0,0500	0,0025	0,000559	0,000125	0,000028
R^2	**0,0479**	**0,0605**	**0,0752**	**0,1299**	**0,1103**	**0,1504**	**0,1713**	**0,1920**	**0,2133**

- The trial run from zero order to forth and half order was carried out to determine the reaction order for biogasoline production
- The R^2 values for all the reaction orders are below 90 % which means that reaction order for biogasoline production does not fall within this range.
- Further investigation should be carried out to model the reaction order for biogasoline production

The reaction order was then investigated from 0-1.5 h and from 1.5-2.5 h, the reverse process yield of biofuel reduced was assumed. Second order rate plots best fitted for both biojet and biogasoline production.

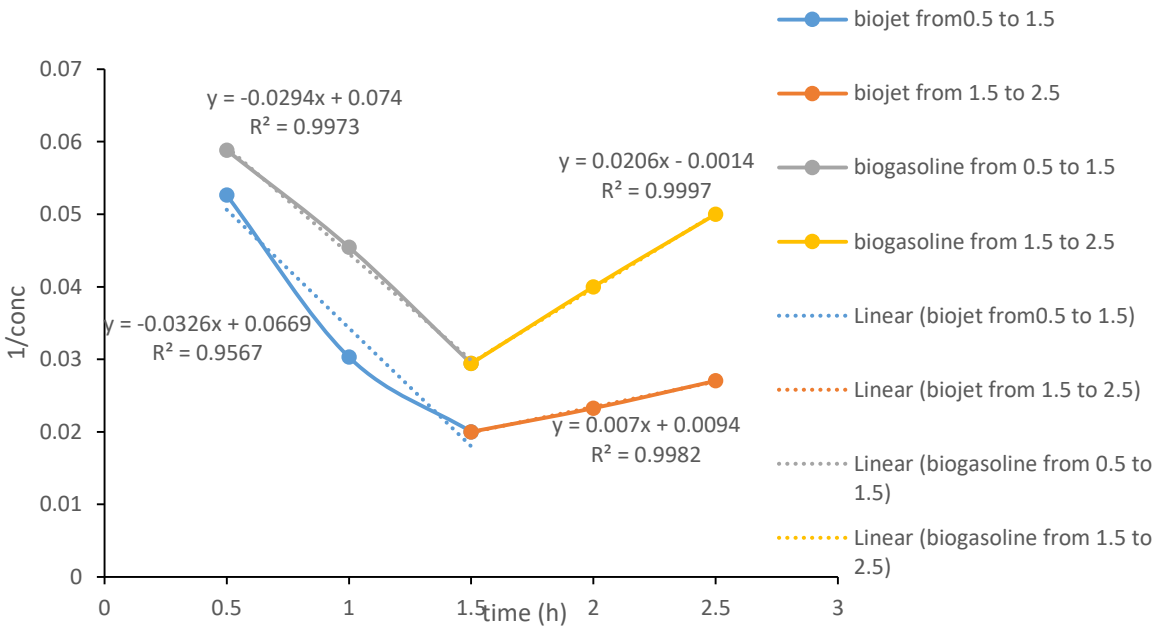


Figure 5. 4. Second order plots for the hydrocracking of castor oil.

The rate constant (k) can be obtained from the slope of the plots. The rate constants for biojet production from 0.5-1.5 h and 1.5-2.5 h is 0.0326 and 0.007, respectively. The rate constants for biogasoline production from 0.5-1.5 h and 1.5-2.5 h is 0.0294 and 0.0206, respectively.

To determine the activation energy of the reaction, Arrhenius equation must be used.

$$lnk \sim \ln\frac{1}{t} = -\left(\frac{E_a}{R}\right)\left(\frac{1}{T}\right) + lnA \qquad (5.2)$$

Where k is the rate constant, T is the temperature, R is the ideal gas constant (8.314 J/ mole-K), A is the constant called the frequency factor which is related to the fraction of collisions between reactants, and E_a is the activation energy.The activation energy can be obtained from the slope of the graph 1/T vs. ln(1/t).

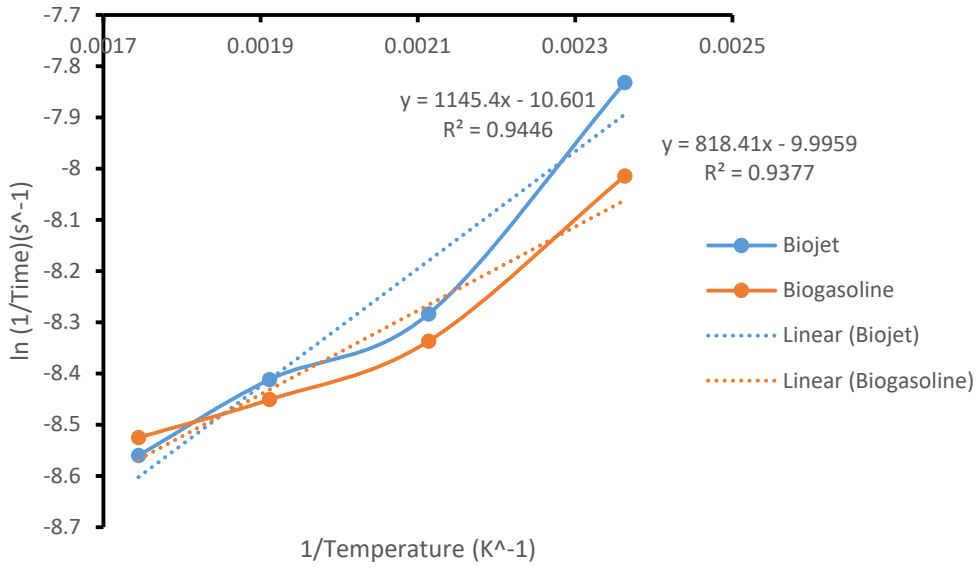


Figure 5. 5. 1/Temperature versus ln(1/time) graph plots.

$$E_a = -(slope)(R) \tag{5.3}$$

$$E_a\,(Biojet) = -(1145.4)(8.314)\left(\frac{1}{1000}\right) = -9.52\ kJ/mol$$

$$E_a(Biogasoline) = -(818.41)(8.314)\left(\frac{1}{1000}\right) = -6.80\ kJ/mol$$

The activation energy of bio-jet and bio-gasoline production were found to be -9.52 kJ/mol and -6.80 kJ/mol, respectively. The activation energies for both biojet and biogasoline production were found to be negative. This means that the increase in temperature resulted to the decrease in rate of reaction. These results were not expected since the increase temperature favours the hydrocracking reaction (Habibie *et al*., 2018).

5.3.4. Response surface methodology

RSM from Design Expert version 11.0.4 software was used to determine the optimum process conditions for the hydrocracking of castor oil. Center composite design from RSM was used for optimisation, which consist of 2^k factorial points (Ven *et al*., 2002). Reaction temperature, reaction time, and catalyst/oil ratio are the independent variables while biojet and biogasoline production are the dependent variables. From the dependent and independent variable, the software to examine the optimum conditions generated 20 experimental runs. The independent

variables have three levels: high level (+1), center level (0), and low level (-1) as indicated in Table 5.4.

Table 5. 4. Summary of experimental design

			Level		
Factor	**Name**	**Unit**	**-1**	**0**	**1**
A	Reaction temperature	^{o}C	150	250	350
B	Reaction time	h	0.5	1.5	2.5
C	Catalyst/oil ratio	g/ml	0.001	0.003	0.005

The production yield of biojet and biogasoline obtained from hydrocracking castor oil using Ni/C dots catalyst is presented in Table 5.5. Design expert generated the experimental runs of 20 runs and the production yield was obtained from GC-MS analysis. The production yield of biojet and biogasoline in each run is different and this indicates that these operating conditions affects the production yield.

Table 5. 5. Experimental design layout.

Runs	**A: Reaction temperature (^{o}C)**	**B: Reaction time (h)**	**C: Catalyst/oil ratio (g/ml)**	**Biojet production (wt. %)**	**Biogasoline production (wt. %)**
1	250	1.5	0.001	25	18
2	350	0.5	0.001	20	13
3	350	0.5	0.005	23	16
4	350	2.5	0.001	23	15
5	350	1.5	0.003	55	36
6	150	0.5	0.005	12	6
7	250	1.5	0.003	50	34
8	250	1.5	0.003	49	33
9	250	1.5	0.003	49	34
10	250	2.5	0.003	37	20
11	150	1.5	0.003	35	20
12	250	1.5	0.003	51	32
13	250	1.5	0.003	50	33
14	250	0.5	0.003	19	19
15	150	2.5	0.001	18	10
16	150	2.5	0.005	33	19
17	250	1.5	0.005	56	35
18	350	2.5	0.005	41	28

19	150	0.5	0.001	15	9
20	250	1.5	0.003	48	32

The maximum production yield of biojet was obtained to be 56 wt. % at reaction temperature of 250^{o}C, reaction time of 1.5 h, and catalyst/oil ratio of 0.005 g/ml and the maximum production yield of biogasoline was obtained to be 36 wt. % at 350^{o}C, 1.5 h, and 0.003 g/mL.

5.3.4.1. ANOVA analysis

The ANOVA analysis table of biojet and biogasoline production table is shown in Appendix C Table C.1 and Table C.2. The model for both biojet and biogasoline production was found to be significant and can be used to optimise reaction time, reaction temperature, and catalyst/oil ratio.

The actual production yield values of biojet and biogasoline obtained from the experiment are 93 % and 94 % closer to the predicted production yield from the model. According to Goos and Gilmour (2013), the predicated values should be more than 90 % closer to the actual values before the model can be used for optimization. Therefore, the model can be used for optimization.

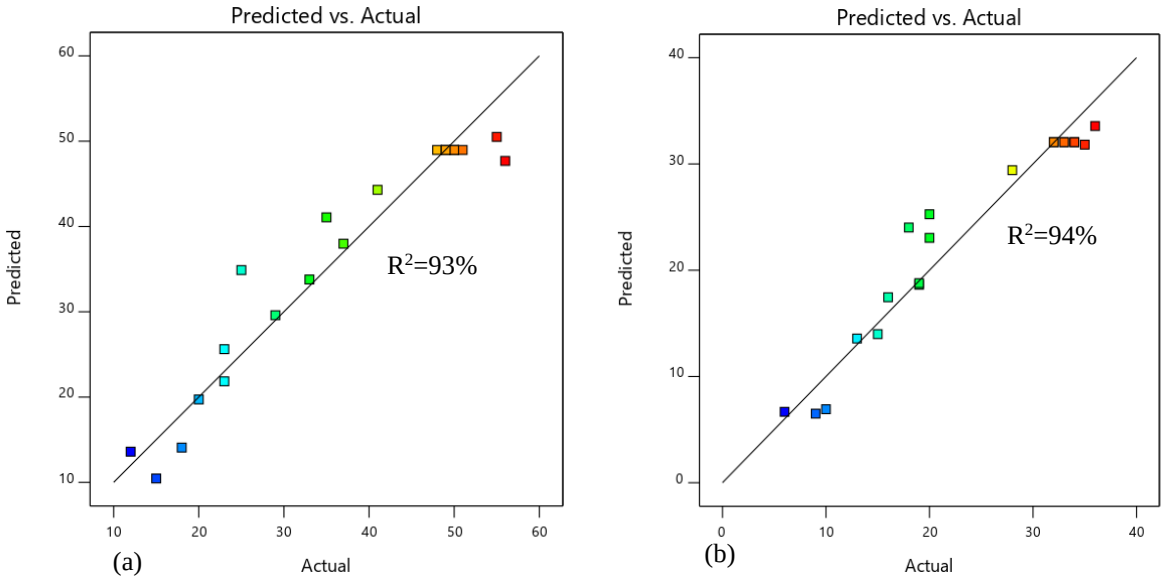


Figure 5. 6. (a) Actual production yield versus predicted production yield of biojet and (b) Actual production yield versus predicted production yield of biogasoline.

The final following equations in terms of coded factors for biojet and biogasoline production can be used to make predictions about production yield of biojet and biogasoline for given levels of each factor. The coded equation is useful for identifying the relative impact of the factors by comparing the factor coefficients.

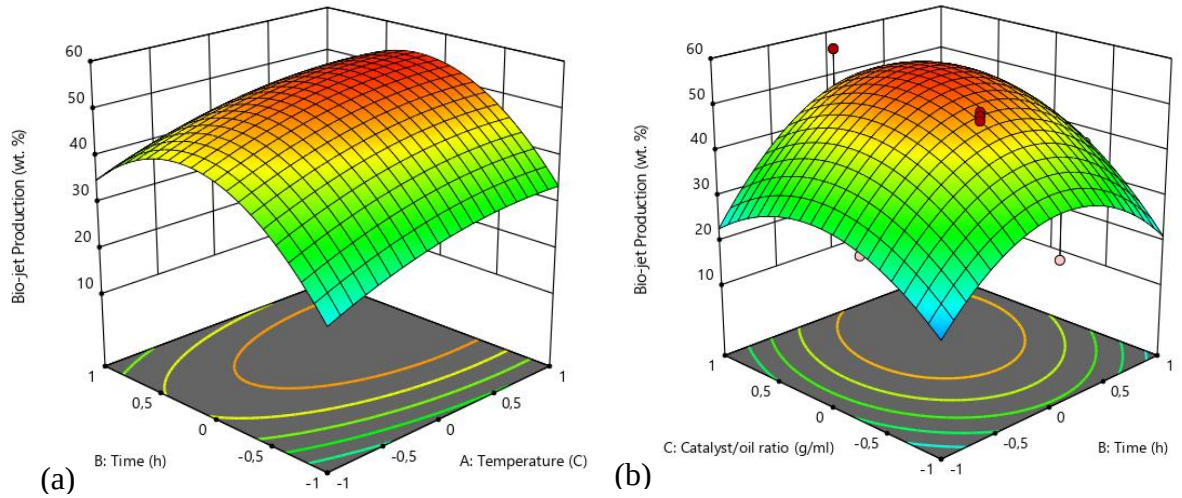
Biojet production yield = 52.33 + 4.95A + 5.58B + 6.40C – 0.3750AB + 0.6848AC + 4.14BC - 3.18A^2 – 15.18B^2 -11.04C^2 (5.4)

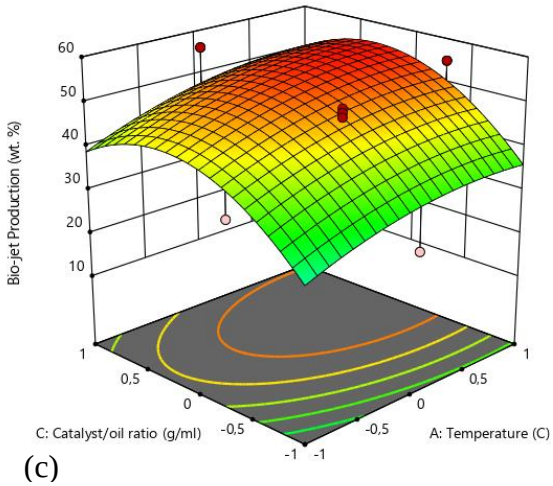
Biogasoline production yield= 34.03 + 4.46A + 3.09B + 3.90C + 0AB+ 0.93AC + 2.89BC – 2.64A^2 -11.14B^2 – 6.12C^2 (5.5)

Where A, B, and C are the coded forms of reaction temperature, reaction time, and catalyst/oil ratio respectively. AB, AC, and BC are the interaction terms, and A^2, B^2, and C^2 are the squared terms of the independent variables. Positive coefficient in the equation has positive effect on the production yield, whereas negative coefficient has negative effect on the production yield.

5.3.4.2. 3D response surface plots for biojet and biogasoline production

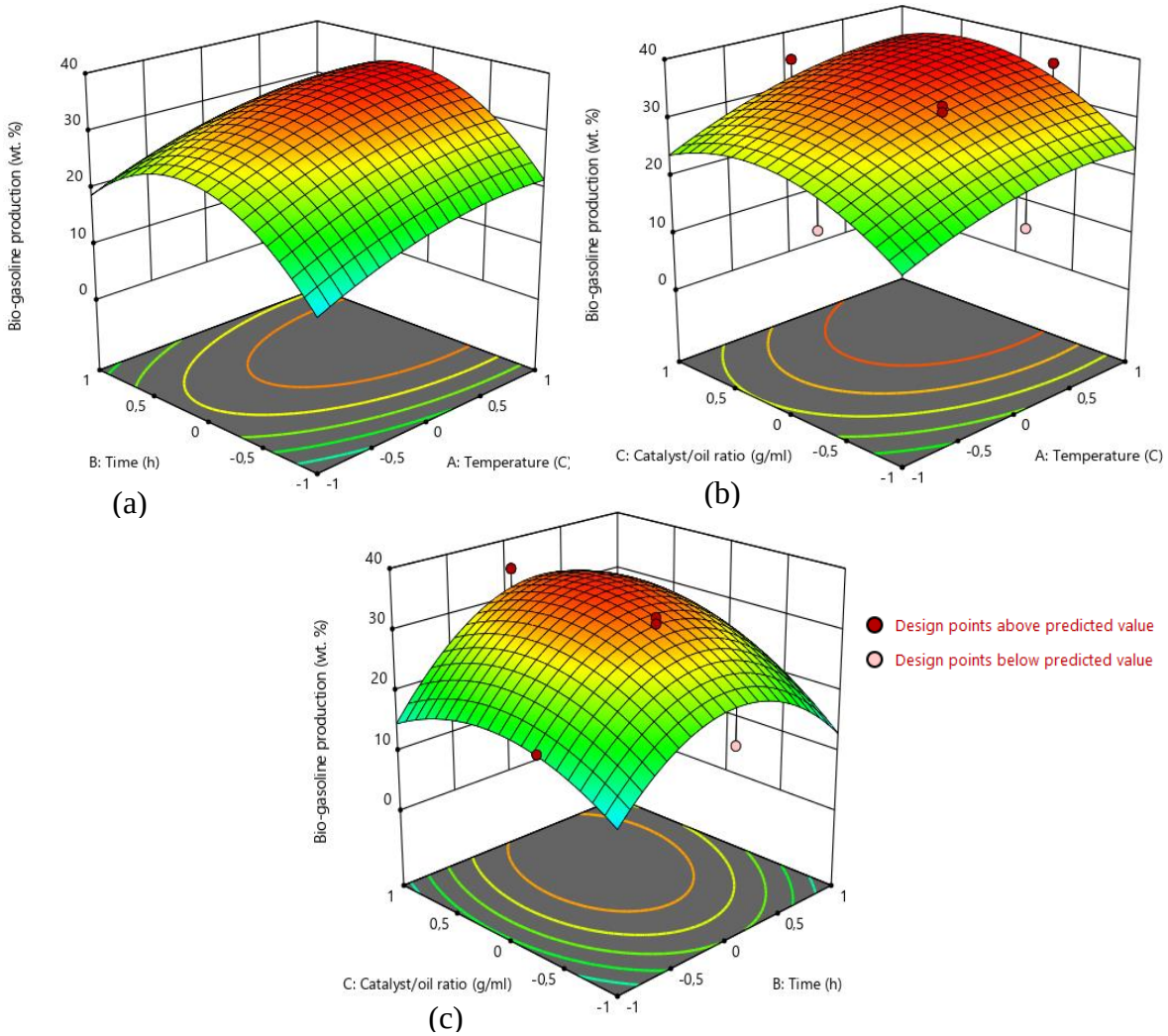
3D response surface plots are the important tools to study the correlation and interaction of two different independent variable on the production yield while keeping the other independent variables at a constant value of arbitrary zero. The 3D response surface plot for biojet and biogasoline production are shown in Figure 5.7 and Figure 5.8 respectively.





(c)

Figure 5. 7. 3D surface plot for (a) effect of reaction time and temperature on the biojet production yield, (b) effect of catalyst/oil ratio and reaction time on the biojet production yield, and (c) effect of catalyst/oil ratio and reaction temperature on the biojet production yield.



(a) (b)

(c)

Figure 5. 8. 3D surface plot for (d) Effect of reaction time and temperature on the biogasoline production yield, (e) effect of catalyst/oil ratio and reaction temperature on the biogasoline

production yield, and (f) effect of catalyst/oil ratio and reaction time on the biogasoline production yield.

Figure 5.7 (a) and Figure 5.8 (a) shows the response surface for the biojet and biogasoline production yield respectively as function of reaction temperature and reaction time. The increase in reaction time from 0.5-1.5 h increased the production yield for both biojet and biogasoline. However, increasing the reaction time beyond 1.5 h did not favour the production of biojet and biogasoline. The production yield decreased as time prolonged after 1.5 h. This finding is also similar to the results obtained by Tan *et al.* (2017) during hydrocracking of waste cooking oil. Pandit *et al*. (2017) also reported similar results during production of biofuel from eggshell waste. The increase in temperature from 150-350^{o}C increased the production yield of both biojet and biogasoline. The maximum biojet production was obtained at 250^{o}C and 1.5 h and the maximum biogasoline production was obtained at 350^{o}C and 1.5 h.

Figure 5.7 (b) and Figure 5.8 (b) shows the response surface for the biojet and biogasoline production yield respectively as function of reaction temperature and catalyst/oil ratio. The increase in temperature favoured the production of biojet and biogasoline. The hydrocracking reaction is endothermic, thus high temperatures increases the rate of reaction. However, Wang *et al.* (2019) reported that high temperature operation must be carefully controlled to avoid over cracking and dehydrogenation. Similar results was observed Yotsomnuk and Skolpap (2018) during hydrocracking of waste virgin coconut oil using HZSM-5 zeolite catalyst at temperature within 350-400^{o}C. The increase in catalyst/oil ratio from 0.001-0.005 g/mL favoured the production of biojet and biogasoline.

Figure 5.7 (c) and Figure 5.8 (c) shows the response surface for the biojet and biogasoline production yield respectively as function of reaction time and catalyst/oil ratio. The increase in catalyst/oil ratio favoured the production of biojet and biogasoline. The maximum biojet production yield was obtained at 0.005 g/mL and 1.5 h and the maximum biogasoline production yield was obtained at 0.003 g/mL and 1.5 h. As the amount of the catalyst is increased, the rate of hydrocracking reaction is increased and thus, increasing the production yield. Dewi *et al*. (2014) observed similar trend during hydrocracking of waste lubrication oil into biofuel. The increase in reaction time resulted to the increase in production yield until the optimal level of 1.5 h is reached (Dewi *et al*. 2014).

5.3.4.3. Optimization the hydrocracking process

Optimization of the hydrocracking process was done by employing RSM numerical optimization method. The optimal reaction conditions were calculated within the range of the independent factors by considering the standard error occurred in the model. Figure 5.8 shows the optimization process, which includes the lower and upper limits range of all the parameters. Equation 5.4 and 5.5 was used to generate several optimum-operating conditions by using numerical RSM optimization approach. To produce an effective method to obtain the optimum reaction conditions, the desirability function was applied.

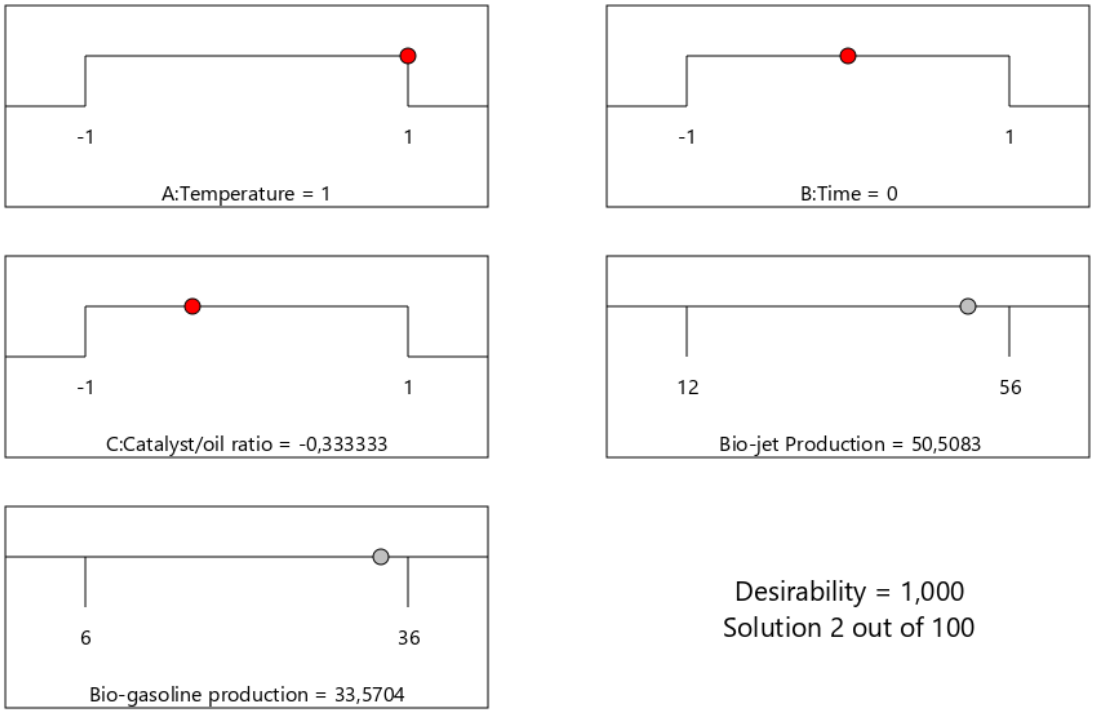


Figure 5. 9. The optimal reaction condition for biojet and biogasoline production.

The desirability function values lies between 0 and 1. The value of 0 is assigned when the factors gives undesirable response, and the value of 1 correlate with the optimal performance of the studies factors (Amdoun et al., 2018). The optimal reaction temperature, reaction time, and catalyst/oil ratio were found to be 350^{o}C (level 1), 1.5 h (level 0), and 0.002 g/mL (level -0.33333). These optimal reaction conditions will produce the maximum production of 50.51 wt. % and 33.57 wt. % of biojet and biogasoline respectively. To validate this results, hydrocracking process was done three time using these optimal conditions and the average production yield was recorded. 46.01 wt. % and 31.21 wt. % of biojet and biogasoline production yield was obtained. These values are lesser that the predicted values because of the standard error in the model.

5.3.4. Product characterisation

Hydrocracked products were analysed using GC-MS to determine the present compounds and their quantity. Figure 5.10 shows the chromatograph of the hydrocracked products obtained from this study.

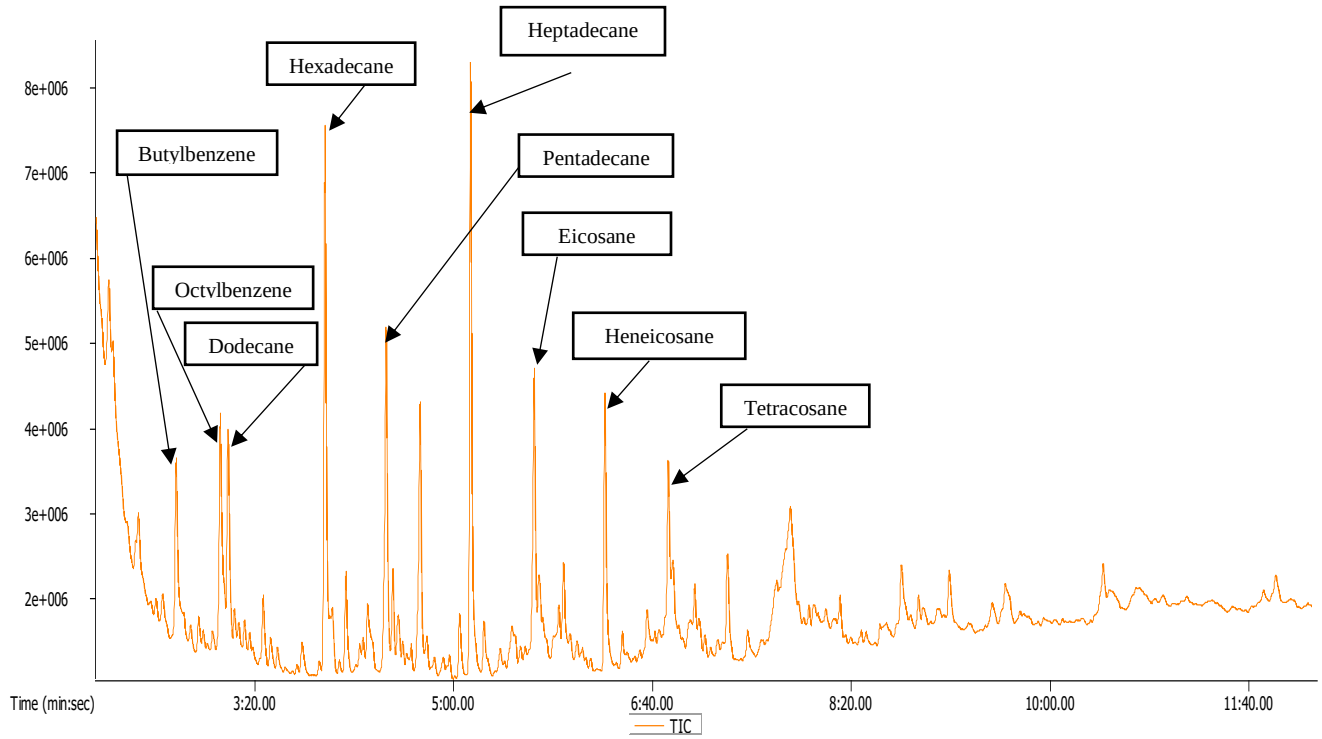


Figure 5. 10. Total Ion Chromatograph (TIC) for hydrocracked product.

The hydrocracked products were found to be containing compounds with biogasoline, biojet, and biodiesel carbon range. Compounds with biogasoline carbon range such as butylbenzene and naphthalene were found at early retention time with low area %. Biojet compounds such as octylbenzene, dodecane, pentadecane, and hexadecane were also found with area% greater than biogasoline compounds. Biodiesel compounds such as heptadecane, eicosane, and heneicosane were found. Number of oxygenated compounds were found and García-Dávila *et al*. (2014) reported that the oxygenated compounds are produced as the results of the first step hydroconversion reaction. The carboxylic acids such as oleic acid and roughanic acid were found which indicates that the compounds were not completely converted to hydrocarbon compounds.

5.4. References

Amdoun, R., Khelifi, L., Khelifi-Slaoui, M., Amroune, S., Asch, M., Assaf-ducrocq, C. and Gontier, E., 2018. The Desirability Optimization Methodology; a Tool to Predict Two Antagonist Responses in Biotechnological Systems: Case of Biomass Growth and Hyoscyamine Content in Elicited Datura starmonium Hairy Roots. *Iranian Journal of Biotechnology*, 16(1), pp.11-19.

Bezergianni S., and A. Kalogianni, 2009. Hydrocracking of Used Cooking Oil for Biofuels Production. *Bioresource Technol*., 100: 3927.

Chen, L., Lu, Y., Hong, Q., Lin, J., & Dautzenberg, F., 2005. Catalytic partial oxidation of methane to syngas over Ca-decorated-AloCb-supported Ni and Ni-B catalysts. *Applied Catalysis A: General, 292*, 295-304.

Dewajani, H., Rochmadi, R., Purwono, S. and Budiman, A., 2016. Effect of modification ZSM-5 catalyst in upgrading quality of organic liquid product derived from catalytic cracking of Indonesian nyamplung oil (Calophyllum inophyllum). *AIP Conference Proceedings*, 1755(1).

Dewi T.K., Fanani Z., Saleh A., Pardamena C., and Herla, 2014. Conversion of Waste Oil into Fuel Oil: Effect of Catalyst Ratio. *Energy and Environmental Science & Technology.*

Dizge N., C. Aydiner, D. Y. Imer, M. Bayramoglu, A. Tanriseven, and B. Keskinler, 2009. Biodiesel production from sunflower, soybean, and waste cooking oils by transesterification using lipase immobilized onto a novel microporous polymer. Bioresour. Technol., 100: 1983-1996.

Dong, Z., Zhao, J., Tian, Y., Zhang, B. and Wu, Y., 2020. Preparation and Performances of ZIF-67-Derived FeCo Bimetallic Catalysts for CO2 Hydrogenation to Light Olefins. *Catalysts*, 10(4), p.455-601.

Fanani, Z. (2010). Hidrocracking Tir Batubara Menggunakan Katalis Ni-Mo-S/ZAA untuk Menghasilkan Fraksi Bensin dan Fraksi Kerosin. *Jurnal Penelitian Sains*. 10(33), pp.1000-1056.

Habibie, T., Susanto, B. and Carli, M., 2018. Effect of NiMo/Zeolite Catalyst Preparation Method for Bio Jet Fuel Synthesis. *E3S Web of Conferences*, 67, p.02-24.

Mampuru, M., Nkazi, D. and Mukaya, H., 2019. Hydrocracking of waste cooking oil into biogasoline in the presence of a bi-functional Ni-Mo/alumina catalyst. *Energy Sources, Part A: Recovery, Utilization, and Environmental Effects*, 42(20), pp.2564-2575.

Morgan, T., Santillan-Jimenez, E., Harman-Ware, A. E., Ji, Y., Grubb, D., & Crocker, M. (2012). Catalytic deoxygenation of triglycerides to hydrocarbons over supported nickel catalysts. *Chemical Engineering Journal, 189*, 346-355.

Pandit, P. and Fulekar, M., 2017. Egg shell waste as heterogeneous nanocatalyst for biodiesel production: Optimized by response surface methodology. *Journal of Environmental Management*, 198, pp.319-329.

Qader SA, and Hill GR, 1969. Hydrocracking of Petroleum and Coal Oils. *Ind Eng Chem Process Des Dev;* 8:462–9.

Sikonia, John G, 1985. Arsenic Management in Shale Oil Upgrading. *Environmental Geochemistry and Health*, 7(2), , pp. 64–68, 10.1007/bf01771340.

Tan, Y., Abdullah, M., Nolasco-Hipolito, C. and Ahmad Zauzi, N., 2017. Application of RSM and Taguchi methods for optimizing the transesterification of waste cooking oil catalyzed by solid ostrich and chicken-eggshell derived CaO. *Renewable Energy*, 114, pp.437-447.

Wang, H., Rogers, K., Zhang, H., Li, G., Pu, J., Zheng, H., Lin, H., Zheng, Y. and Ng, S., 2019. The Effects of Catalyst Support and Temperature on the Hydrotreating of Waste Cooking Oil (WCO) over CoMo Sulfided Catalysts. *Catalysts*, 9(8), p.689-700.

Yotsomnuk, P. and Skolpap, W., 2018. Effect of Process Parameters on Yield of Biofuel Production from Waste Virgin Coconut Oil. *Engineering Journal*, 22(6), pp.21-35.

Zaher, Ferial and Sayed, Hussien and Heakal, Hassan and Hamed, and Said, 2015. Potential of Castor Oil as a Feedstock for the Production of Bio-fuel via Catalytic Hydro- Cracking. *Current Science International*. 4. 443-449.

Zhang, Z., Wang, Q. and Zhang, X., 2019. Hydroconversion of Waste Cooking Oil into Biojet Fuel over NiMo/SBUY-MCM-41. *Catalysts*, 9(5), p.466-755.

Chapter 6: Conclusions and recommendations

6.1. Conclusions

Castor oil was successfully extracted from castor seeds by using solvent extraction method and using hexane as solvent. Based on studies reported by researchers, the conditions at which the castor plants are grown and the operating conditions at which the oil was extracted affect the final oil yield. It is very important to control the extraction conditions to maximise oil yield. Extraction temperature extraction time, and seed/solvent ratio were found to be the operating conditions that highly affect the oil yield during solvent extraction. The effect of extraction temperature, extraction time, and seed/solvent ratio on the oil yield was studied by varying extraction temperature, extraction time, and seed/solvent ratio within the range of 55-7 5^{o}C, 1-7 h, and 0.02-1 g/ml, respectively. The maximum oil yield was found to be 46.01 wt. % at extraction temperature, extraction time, seed/solvent ratio of 70^{o}C, 4 h, and 0.06 g/ml. These operating conditions were further optimised using RSM from Design Expert version 11.0.4 software. . The maximum oil yield of 44.57 % was obtained after optimization at optimal extraction temperature, extraction time, and seed/solvent ratio of 63.28^{o}C, 3.6 h, ad 0.03 g/ml, respectively. The extracted castor oil was characterized using GC-MS analysis and based on the results obtained it was observed that the castor oil produced has the potential in producing biofuel due to the fatty acids present and the physiochemical characteristics of the oil are within the ASTM standard range.

Ni/C dots catalysts was synthesised for the hydrocracking process of castor oil to produce biofuel. The catalyst was synthesised through successive impregnation of Ni nanoparticles over C dots. The effect of Ni-loading was studied by varying Ni-loading within the range of 5-25 wt. %. 5 wt. % Ni-loading catalyst showed highest thermal stability and BET surface area of 71.6940 m^2/g. TEM and SEM images for 5 wt. % Ni-loading catalyst showed high dispersion of nickel nanoparticles and more spherical particles compared to other Ni-loading catalysts. All the catalyst exhibited the same trend on the characteristics of the stretching vibrations absorption band and the peaks became more sharpener with the increase in Ni-loading. The band at 3286 cm-1, 1603 cm-1,, and 1172 cm-1 are the characteristics of the stretching of –OH, C=C, and C-O-C groups on the surface of the catalyst. The XRD peaks increased with the increase in Ni-loading and this means that more nickel particles were detected as Ni-loading is increased.

5 wt. % Ni-loading catalyst was further calcined within the range of 350-750^{o}C to study the effect of calcination temperatures on the characteristics of the catalysts. The catalyst calcined at 350^{o}C showed the highest BET surface area of 71.6940 m^2/g and highest thermal stability. The TEM images revealed that the increase in calcination temperature caused the catalyst to lose its spherical shape and the catalyst became more agglomerated. The FTIR spectra of all the catalyst at different calcination temperature exhibited the same trend on the characteristics of the stretching vibrations absorption band however, the peaks became less sharpener with the increase in Ni-loading. The XRD spectra showed the increase in number of peaks and the peaks became more sharpener with the increase in calcination temperature.

The effects of operating conditions on the hydrocracking process of castor oil was studied. The effect of Ni-loading, calcination temperature, extraction time extraction temperature, and catalyst/oil ratio on the production of biojet and biogasoline. The maximum production yield of biojet was obtained to be 56 wt. % at 5wt. % Ni-loading catalyst calcined at 350^{o}C, reaction temperature of 250^{o}C, reaction time of 1.5 h, and catalyst/oil ratio of 0.005 g/ml and the maximum production yield of biogasoline was obtained to be 36 wt. % at 5wt. % Ni-loading catalyst calcined 350^{o}C, reaction time of 350^{o}C, reaction time of 1.5 h, and catalyst/ oil ratio of 0.003 g/ml. . The overall order of the reaction for the biojet and biogasoline production was investigated from 0 to 4th order and was found to be not fitting to any reaction order. The reaction order was then investigated from 0-1.5 h and from 1.5-2.5 h, the reverse process yield of biofuel reduced was assumed. Second order rate plots best fitted for both biojet and biogasoline production. The rate constant (k) was obtained from the slope of the plots. The rate constants for biojet production from 0.5-1.5 h and 1.5-2.5 h is 0.0326 and 0.007, respectively. The rate constants for biogasoline production from 0.5-1.5 h and 1.5-2.5 h is 0.0294 and 0.0206, respectively RSM from Design Expert version 11.0.4 software was used to determine the optimum process conditions for the hydrocracking of castor oil. The optimal reaction temperature, reaction time, and catalyst/oil ratio were found to be 350^{o}C, 1.5 h, and 0.002 g/ml and produces the maximum production of 50.51 wt. % and 33.57 wt. % of biojet and biogasoline, respectively.

6.2. Recommendations

The possible future work that can be done on this projects include:

- C dots is highly unstable at temperatures above 300^{o}C. Therefore, another carbon material can be used as catalyst support such as carbon onions (Conions).

- The percentage Ni-loadings were found to be slightly lesser than the actual Ni loaded. The standard error should be considered in future.
- Proper hydrocracking set-up should be constructed such as using stainless steel reactor for high reaction temperature and pressure.
- Other methods of synthesizing catalyst should be explored to investigate the effect of Ni-loading.
- The gas phase product should be collected and analysed to confirm whether some of the hydrocracked products went to the gas phase
- Economic evaluation of this project should be done to check how economically feasible this project is.

Appendices

Appendix A: Castor oil extraction

A.1: Effect of operating conditions on the oil yield

The following experimental data was obtained on the study of the effect of extraction time, extraction temperature, and seed/solvent ratio on the oil yield.

Table A. 1. Effect of extraction temperature on the oil yield.

Temperature (ºC)	Oil yield (%)
55	31.82
60	35.1
65	43.5
70	46.01
75	41.22

Table A. 2. Effect of extraction time on the oil yield.

Time (h)	Oil yield (%)
1	37.2
2	42.5
4	45.7
6	40.4
7	35.7

Table A. 3. Effect of seed/solvent ratio on the oil yield.

Seed/solvent ratio (g/mL)	Oil yield (%)
0.02	46.1
0.04	45.2
0.06	44.7
0.08	43.8
1	39.8

A.2: GC-MS analysis of extracted castor oil

The following GC-MS analysis spectra was obtained for the extracted castor oil.

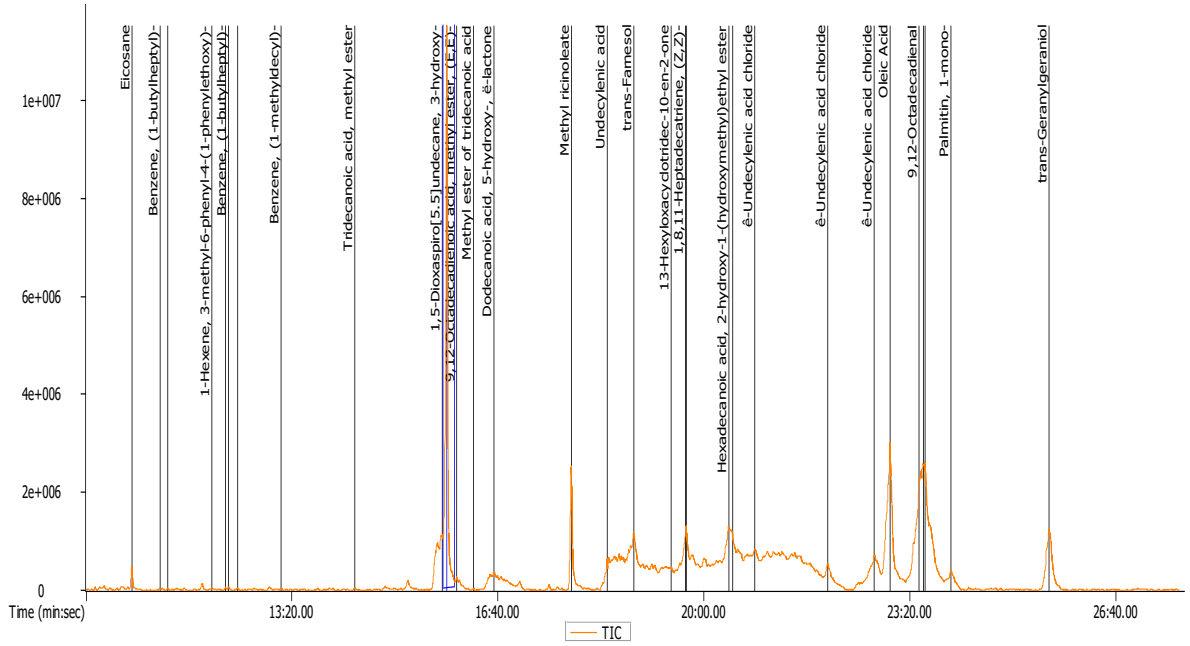


Figure A. 1. GC-MS analysis spectra for the extracted castor oil.

Table A. 4. Full results data obtained from GC-MS analysis.

Peak #	Name	R.T. (min:sec)	S/N	Area	Area %	Weight	Formula
12	9,12-Octadecadienoic acid, methyl ester, (E,E)-	16:00.1	99.738	2486106	0.18458	294	C19H34O2
16	Undecylenic acid	18:25.8	63.056	9622645	0.71443	184	C11H20O2
9	Tridecanoic acid, methyl ester	14:21.2	558.69	840475	0.062401	228	C14H28O2
21	Palmitic acid á-monoglyceride	20:24.0	1080.3	35542422	2.6388	330	C19H38O4
26	Oleic Acid	23:00.5	1398	177986786	13.215	282	C18H34O2
15	Methyl ricinoleate	17:51.2	6032	69307315	5.1457	312	C19H36O3
29	(E)-13-Docosenoic acid	23:34.3	471.7	99227218	7.3671	338	C22H42O2
1	Eicosane	10:44.4	1307.4	9502563	0.70551	282	C20H42
3	Benzene, (1-propyloctyl)-	11:19.6	608.4	584293	0.043381	232	C17H28
2	Benzene, (1-butylheptyl)-	11:11.8	152.89	455226	0.033798	232	C17H28

4	1-Hexene, 3-methyl-6-phenyl-4-(1-phenylethoxy)-	12:02.4	677	962990	0.071497	294	C21H26O
5	Benzene, (1-pentylheptyl)-	12:15.4	767.41	892958	0.066297	246	C18H30
7	Benzene, (1-propylheptyl)-	12:27.5	583.25	685844	0.05092	218	C16H26
6	Benzene, (1-butylheptyl)-	12:18.6	820.21	1051902	0.078098	232	C17H28
8	Benzene, (1-methyldecyl)-	13:09.7	784.75	772546	0.057357	232	C17H28
10	1,5-Dioxaspiro[5.5]undecane, 3-hydroxy-	15:46.0	79.936	35198465	2.6133	172	C9H16O3
11	13-Hexyloxacyclotridec-10-en-2-one	15:50.4	10682	285673193	21.21	280	C18H32O2
13	Methyl ester of tridecanoic acid	16:16.5	542.94	449854	0.033399	228	C14H28O2
14	Dodecanoic acid, 5-hydroxy-, ë-lactone	16:36.3	591.19	10639775	0.78995	198	C12H22O2
17	trans-Farnesol	18:51.7	3488.1	49537885	3.6779	222	C15H26O
20	Cyclohexanecarboxylic acid, hexyl ester	19:42.8	555.36	40069417	2.9749	212	C13H24O2
18	13-Hexyloxacyclotridec-10-en-2-one	19:27.8	71.551	2610201	0.19379	280	C18H32O2
19	1,8,11-Heptadecatriene, (Z,Z)-	19:42.4	314.55	40104213	2.9775	234	C17H30
23	ê-Undecylenic acid chloride	20:49.4	97.575	10074763	0.748	202	C11H19ClO
22	Phthalic acid, isobutyl 2-propylpentyl ester	20:27.7	3235	25734368	1.9106	334	C20H30O4
24	ê-Undecylenic acid chloride	22:00.1	304.12	17656178	1.3109	202	C11H19ClO
25	ê-Undecylenic acid chloride	22:45.3	278.74	68006237	5.0491	202	C11H19ClO
27	9,12-Octadecadienal	23:29.1	679.19	103009926	7.6479	264	C18H32O
28	9,12-Octadecadienoyl chloride, (Z,Z)-	23:33.3	845.47	145602808	10.81	298	C18H31ClO
30	Palmitin, 1-mono-	23:59.8	998.03	16854682	1.2514	330	C19H38O4

31	trans-Geranylgeraniol	25:35.1	5772	85754254	6.3668	290	C20H34O

Appendix B: Catalyst synthesis

Table B. 1. Raw data from AAS analysis

Sample	Experiment Ni-loading (wt. %)	Concentration (ppm)	Actual Ni-loading (wt. %)
5% Ni-loading	5	45101	4.51
10% Ni-loading	10	91221	9.12
15% Ni-loading	15	14443	14.44
20% Ni-loading	20	19622	19.61
25% Ni-loading	25	24714	24.70

Appendix C: Hydrocracking process

C.1: ANOVA analysis

Table C. 1. ANOVA analysis table for Biojet production

Source	Sum of Squares	df	Mean Square	F-value	p-value	
Model	3710,15	9	412,24	14,18	0,0001	significant
A-Temperature	243,27	1	243,27	8,37	0,0160	
B-Time	309,25	1	309,25	10,63	0,0086	
C-Catalyst/oil ratio	409,60	1	409,60	14,09	0,0038	
AB	1,12	1	1,12	0,0387	0,8480	
AC	3,83	1	3,83	0,1319	0,7241	
BC	140,25	1	140,25	4,82	0,0528	
A^2	27,84	1	27,84	0,9574	0,3509	
B^2	633,84	1	633,84	21,80	0,0009	
C^2	257,07	1	257,07	8,84	0,0140	
Residual	290,80	10	29,08			
Lack of Fit	285,30	5	57,06	51,87	0,0003	significant
Pure Error	5,50	5	1,10			

Cor Total	4000,95	19				

The **Model F-value** of 14,18 implies the model is significant. There is only a 0,01% chance that an F-value this large could occur due to noise.

P-values less than 0,0500 indicate model terms are significant. In this case A, B, C, B^2, C^2 are significant model terms. Values greater than 0.1000 indicate the model terms are not significant. If there are many insignificant model terms (not counting those required to support hierarchy), model reduction may improve your model.

The **Lack of Fit F-value** of 51,87 implies the Lack of Fit is significant. There is only a 0,03% chance that a Lack of Fit F-value this large could occur due to noise. Significant lack of fit is bad -- we want the model to fit.

Table C. 2. ANOVA analysis table for Biogasoline production

Source	**Sum of Squares**	**df**	**Mean Square**	**F-value**	**p-value**	
Model	1763,33	9	195,93	16,26	< 0.0001	significant
A-Temperature	198,01	1	198,01	16,44	0,0023	
B-Time	95,11	1	95,11	7,90	0,0185	
C-Catalyst/oil ratio	152,10	1	152,10	12,63	0,0052	
AB	0,0000	1	0,0000	0,0000	1.0000	
AC	7,06	1	7,06	0,5863	0,4615	
BC	68,11	1	68,11	5,65	0,0388	
A^2	19,11	1	19,11	1,59	0,2364	
B^2	341,05	1	341,05	28,31	0,0003	
C^2	78,86	1	78,86	6,55	0,0284	
Residual	120,47	10	12,05			
Lack of Fit	116,47	5	23,29	29,12	0,0011	significant
Pure Error	4,00	5	0,8000			
Cor Total	1883,80	19				

The **Model F-value** of 16,26 implies the model is significant. There is only a 0,01% chance that an F-value this large could occur due to noise.

P-values less than 0,0500 indicate model terms are significant. In this case A, B, C, BC, B^2, C^2 are significant model terms. Values greater than 0.1000 indicate the model terms are not significant. If there are many insignificant model terms (not counting those required to support hierarchy), model reduction may improve your model.

The **Lack of Fit F-value** of 29,12 implies the Lack of Fit is significant. There is only a 0,11% chance that a Lack of Fit F-value this large could occur due to noise. Significant lack of fit is bad -- we want the model to fit.

C.2: GC-MS analysis for hydrocracked product

Table C. 3. GC-MS results table for hydrocracked products

Name	R.T. (min:sec)	S/N	Area %	Weight	Formula
Oxirane, 2-methyl-2-phenyl-	02:02,9	1972,5	0,000235	134	C9H10O
Undecane	02:06,7	135,75	2,363	156	C11H24
Benzene, 1-methyl-3-(1-methylethyl)-	02:08,8	452,21	2,2189	134	C10H14
Benzene, 4-ethyl-1,2-dimethyl-	02:16,1	685,11	0,078677	134	C10H14
Benzene, 1,2,3,4-tetramethyl-	02:21,5	396,74	1,9114	134	C10H14
Bicyclo[2.2.2]oct-5-en-2-ol	02:28,3	706,03	0,082032	124	C8H12O
Benzene, 1-methyl-4-(2-propenyl)-	02:30,4	456,26	0,2541	132	C10H12
Benzene, 1,2,3,4-tetramethyl-	02:33,5	1571,3	0,77104	134	C10H14
1H-Indene, 2,3-dihydro-4-methyl-	02:33,9	711,99	0,77104	132	C10H12
Benzene, 1-methyl-4-(1-methylpropyl)-	02:38,5	105,94	0,025134	148	C11H16
Dodecane	02:40,4	815,75	4,8321	170	C12H26
Decane, 2,3,4-trimethyl-	02:47,4	282,56	0,40027	184	C13H28
Naphthalene	02:51,8	6091,3	0,56791	128	C10H8
Benzene, 1,3-bis(1,1-dimethylethyl)-	03:02,7	26904	5,6691	190	C14H22
Hexyl,1,1-dimethyl-5-phenyl	03:04,6	2592,1	0,61395	189	C14H21
Dodecane, 2,7,10-trimethyl-	03:06,5	489,44	4,5196	212	C15H32
Hexadecane	03:55,2	2166,8	9,5836	226	C16H34
1,2-Butoxypropanol	04:05,7	8737	1,8141	264	C14H32O4

Pentadecane	04:26,0	626,59	6,8708	212	C15H32
Heneicosane	04:43,0	381,98	5,5296	296	C21H44
2,4-Di-tert-butylphenol	04:43,2	23959	5,5296	206	C14H22O
Octadecanedioic acid	05:02,9	6978,4	1,1668	314	C18H3404
Heptadecane	05:08,5	2168,3	10,534	240	C17H36
Eicosane	05:40,5	606,96	5,9218	282	C20H42
2-methylpentane;octane	05:52,8	5658,9	1,7096	200	C14H32
Heneicosane	06:16,1	959,14	5,2213	296	C21H44
2-methoxyethanol	06:37,1	3539,9	0,99997	250	C13H30O4
Tetracosane	06:47,9	139,58	4,2909	338	C24H50
Methyl 8-methyl-nonanoate	06:58,2	1591,8	0,92792	186	C11H22O2
n-Hexadecanoic acid	07:12,5	65,823	0,40368	256	C16H32O2
Dibutyl phthalate	07:16,0	585,41	0,42002	278	C16H22O4
Tetracosane	07:17,5	1126,8	2,3016	338	C24H50
2-octoxyethanol	07:53,8	1483,1	0,39963	250	C13H30O4
2-octoxyethanol	08:27,5	1158,2	0,25671	250	C13H30O4
Benzaldehyde, 2-hydroxy-4-methoxy-3,6-dimethyl-	08:34,4	2479,2	0,24868	180	C10H12O3
Phenol, 4,4'-(1-methylethylidene)bis-	08:36,7	1079,1	1,0257	228	C15H16O2
Roughanic acid	08:54,0	6262,2	0,56327	250	C16H26O2
2-octaxyethanol	08:59,8	408,19	0,039403	250	C13H30O4
Hexanedioic acid, mono(2-ethylhexyl)ester	09:09,2	4115,9	1,684	258	C14H26O4
B-nonylglucoside	09:31,0	1228	0,9756	306	C5H30O6
1,1-Dibutoxybutane	10:26,6	792,04	1,9393	202	C12H26O2
1,2,3,4-Tetrahydro-3-(phenylacetamido)quinoline	10:29,8	1213	1,6772	266	C17H18N2O
9-Octadenoicacid	10:57,6	575,34	0,34354	283	C18H32O2
1-Ethoxyhexane-1-propoxyhexane	11:47,2	1624,4	0,98007	275	C17H38O2
1-Ethoxyhexane-1-propoxyhexane	11:53,5	577,09	1,5631	275	C17H38O2